FUNCTIONALIZATION AND CARBONIZATION OF CELLULOSE NANOFIBRILS AS HIGH-PERFORMANCE FIBER MATERIALS AND THEIR APPLICATIONS

A Dissertation
Presented to
The Academic Faculty

by

Arie Mulyadi

In Partial Fulfillment
of the Requirements for the Degree
Doctor of Philosophy

School of Chemical and Biomolecular Engineering

Georgia Institute of Technology

December 2016

FUNCTIONALIZATION AND CARBONIZATION OF CELLULOSE NANOFIBRILS AS HIGH-PERFORMANCE FIBER MATERIALS AND THEIR APPLICATIONS

Approved by:

Dr. Yulin Deng, Advisor
School of Chemical & Biomolecular Engineering
Georgia Institute of Technology

Dr. F. Joseph Schork
School of Chemical & Biomolecular Engineering
Georgia Institute of Technology

Dr. Sven H. Behrens
School of Chemical & Biomolecular Engineering
Georgia Institute of Technology

Dr. Martha A. Grover
School of Chemical & Biomolecular Engineering
Georgia Institute of Technology

Dr. Preet M. Singh
School of Materials Science and Engineering
Georgia Institute of Technology

Date Approved: October 31, 2016

ACKNOWLEDGEMENTS

First and foremost I would like to express my sincere gratitude to my research advisor, Dr. Yulin Deng, who provided me with instruction to start this project, freedom in exploring different ideas, wise guidance whenever I needed it over the course of my research study, and continuous support to help me move forward. I am really fortunate to have him as my inspiration and mentor. I would also like to extend my thanks for all of my Thesis committee members. Dr. Schork, Dr. Behrens, Dr. Grover, and Dr. Singh gave me an invaluable source of advice, supported my research, and kept my science sound.

I would like to thank the faculty, staff, and fellow students in Renewable Bioproducts Institute for the assistance during my study. I am also grateful for the fellowship provided by Renewable Bioproducts Institute that helps me with the financial support for my research project and professional development through conference meeting.

Next, I would like to thank the help and discussion from my colleagues at Georgia Institute of Technology: Zhe Zhang, Sudhir Sharma, Xiaodan Zhang, Wei Mu, Xu Du, Vincent Li, Wei Liu, Michael Dutzer, Chunjae Yoo, Emily Fitzharris, Clive Liu, Feifei Sun, Dong Ho Kim, Le Yang, Jian Gong, Albert Lee, Junli Zhou, Zhaoyun Lin, and everyone I am missing. I enjoy sharing our research efforts and spending time together as collaborators and friends.

Last but not the least, I would like to express my deepest gratitude to my parents for the unwavering support and encouragement they have shown me throughout my Ph.D. study. Without them, I would not have been able to complete my study and this dissertation.

TABLE OF CONTENTS

LIST OF TABLES

Page

LIST OF FIGURES

LIST OF SYMBOLS AND ABBREVIATIONS

ATRP	Atom transfer radical polymerization
ATR-FTIR	Attenuated total reflectance-Fourier transform infrared spectroscopy
BA	n-butyl acrylate
BET	Braunauer, Emmett, and Teller
CA	Contact angle
C_{dl}	Electrochemical capacitive double layer
CNFs	Cellulose nanofibrils
CV	Cyclic voltammetry
DMSO	Dimethyl sulfoxide
DTGA	First derivative thermogravimetric analysis
EDMA	Ethylene dimethacrylate
EDS	Energy dispersive X-ray spectroscopy
HER	Hydrogen evolution reaction
H_2	Hydrogen gas
J_0	Exchange current density
KPS	Potassium persulfate
L/D	Length over diameter
LSV	Linear sweep voltammetry
FE-SEM	Field emission scanning electron microscopy
MA-SEBS	Maleic anhydride-styrene ethylene butyl styrene coupling agent
MPA	Melamine-phytic acid complex particles
N	Nitrogen atom

nm	nanometer
NMP	Nitroxide mediated polymerization
NSC	N,S-doped carbon nanofibers derived from CNFs
N_2	Nitrogen gas
ORR	Oxygen reduction reaction
O_2	Oxygen gas
P	Phosphor atom
PS	Polystyrene
RAFT	Reversible addition-fragmentation chain transfer
RH	Relative humidity
RHE	Reversible hydrogen electrode
S	Sulfur atom
SCE	Saturated calomel electrode
T	Temperature
TGA	Thermogravimetric analysis
THF	Tetrahydrofuran
UV	Ultraviolet
wt	weight
XPS	X-ray photoelectron spectroscopy
XRD	X-ray diffraction
3D	3 dimensional
µm	micrometer

SUMMARY

Cellulose is a structural component of plant cell walls that serve as most abundant organic polymer on Earth. The latest study indicated that cellulose as renewable and sustainable resources is produced 1.5×10^{12} tons annually and could be considered an almost inexhaustible source of raw material. With the primary occurrence in the form of lignocellulosic material in forests, commercialization of cellulose has been utilized for extensive applications in various industries, primarily as paper and cardboard. In the past decade, a new field of nanoscale cellulose fibers (nanocellulose) has garnered increasing attentions as promising bio-based fibers that can deliver environmentally friendly, high-performance material with additional unique properties. Many scientists believe that nanocellulose can be developed as the next generation of materials. Nanocellulose has the potential to be the basis platform of sustainable building blocks that can compete and substitute some of the markets dominated by petroleum-based feedstock.

Cellulose nanofibrils (CNFs) as nanocelluloses with typical fiber dimension of 5-100 nm in diameter and up to several microns in length give the smallest structural fiber of cellulose with high aspect ratios (L/D). The material can be prepared by breaking down the hierarchical structure of the cellulose fiber from the wood pulp using mechanical disintegration. The wood pulp could be obtained either with or without chemical/enzymatic pretreatment. Owing to the individualized fibrous form, CNFs yield materials with a high surface area, crystallinity, and aspect-ratio-fiber. These properties would potentially allow CNFs as suitable material for various applications such as bio-filler reinforcement, bioabsorbent, and “green” electrocatalyst.

Although the nanosize dimensions of CNFs possess unique properties to expand their functionality toward new application platform, the inherent chemical structure of cellulose would still limit its functionality. CNFs, as straight chain polymers consisted of D-glucose units, have strong hydrophilic tendency due to the present of polar hydroxyl groups and weak hydrophobic nature due to less exposed surface of hydrophobic –CH moieties. In addition, CNFs are intrinsically electric insulators without catalytic property. Therefore, the focus of this dissertation is to promote CNFs functionalities by studying modification approaches aimed to fabricate hydrophobic/oleophilic surface and electrocatalytically-active nanofibers via thermochemical treatment of cellulose. There are three major components of this dissertation:

(1) Water-free grafting of hydrophobic polymer via coupling agent

In the first part, surface hydrophobization of CNFs using coupling agent consisting of the well-defined hydrophobic polymer backbone and reactive anhydride group was applied. The impact of surface hydrophobization treatment via coupling agents on CNFs properties were evaluated. The effect of the modified CNFs as reinforcing filler on the mechanical properties of polystyrene (PS) composite films was tested and compared to that of neat CNFs. The results ascertained the enhancement in mechanical properties of hard, brittle thermoplastic polymer by utilizing CNFs as fillers and the role of surface hydrophobization to optimize the mechanical performance of polymer composites.

(2) *In-situ* hydrophobic polymer grafting in aqueous medium

In the second part of this study, an approach to prepared surface hydrophobized CNFs in aqueous solution was achieved. The grafting of hydrophobic polymer on the surface of CNFs based on dropwise suspension polymerization was applied to the well-dispersed CNFs suspension in water. The properties of hydrophobic CNFs were confirmed, and the reaction

mechanism of polymer grafting was proposed. The hydrophobic CNFs was further utilized to form hydrophobic CNFs aerogels. The characteristics of the hydrophobic CNFs aerogels as effective oil absorbent materials was demonstrated.

(3) CNFs-derived carbocatalyst

The third part of this study focused on the transformation of CNFs as a precursor material for carbon electrode. The fabrication of metal-free carbon electrocatalyst toward oxygen reduction and hydrogen evolution reaction by a combination of heteroatoms-doping, complex particle recombination, and high-temperature annealing was adopted. Carbonization of CNFs easily yielded 3D interconnected carbon nanofibers with high mesopores and good conductivity. The inclusion of heteroatoms on the aromatic carbon structures induced good electrocatalytic activities toward oxygen reduction reaction. To further upgrade carbon nanofiber functionality toward hydrogen evolution reaction, recombination of N,P-doped carbon shell layer on the surface of the N,S-doped CNFs-derived carbon nanofibers was investigated. The results indicated that the hybrid carbon nanofibers obtained by a mixture of heteroatoms-doped CNFs-derived carbon and complex particles of melamine-phytic acid could enhance the electrocatalytic performance of the carbon electrocatalysts toward both oxygen reduction reaction and hydrogen evolution reaction.

CHAPTER I

INTRODUCTION

Cellulose as a naturally occurring polymer produced primarily by plants, algae, and some bacteria is one of the most important sustainable materials. For millennia, this organic polymer has been part of human civilization in the form of wood and plant fiber as an energy source, construction material, and textile. Today, the use of cellulose-based materials continues as raw materials for a broad spectrum of applications in various industries, primarily as paper and cardboard materials. As the most abundant natural polymer, cellulose is a linear homopolymer composed of D-gluco-pyranose units linked by β-1,4-glycosidic bonds shown in Figure 1.1.[1] The degree of polymerization of cellulose varies depending on its source with a range between few hundred and up to 20,000.[1, 2]

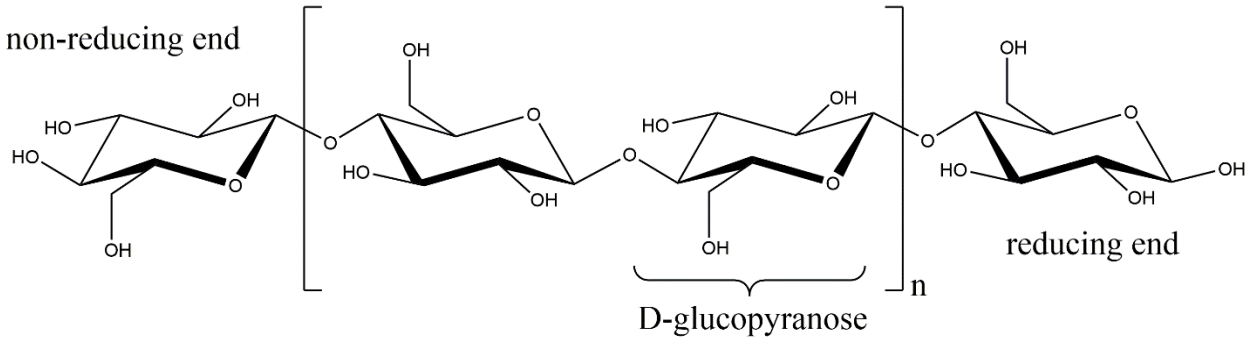

Figure 1.1 Molecular structure of cellulose

The linear chain of the cellulose molecular structure along with the numerous surface hydroxyl groups and its tightly packed arrangement leads to the formation of semicrystalline fiber morphology. The cellulose fibril, which is originated from flat sheets being held together by van der Waals forces and strong intra- and intermolecular hydrogen bonding,[3, 4] is the main cause of its outstanding physical properties, such as high tensile strength and elastic modulus, low density,

good thermal stability, and excellent solvent resistance. A recent study showed that the mechanical and thermal properties of the crystalline domain of cellulose are comparable or even better than some reinforcement materials.[5] Table 1.1 presents the summary of physical properties of some reinforcement materials, including the crystalline domain of cellulose.

Table 1.1 Physical properties of some reinforcement materials. Adapted from Moon et al.[5] with permission of The Royal Society of Chemistry

Material	Density ($g \cdot cm^{-3}$)	Tensile Strength (GPa)	Axial Elastic Modulus (GPa)	Coefficient of Thermal Expansion ($ppm \cdot K^{-1}$)
Kevlar-49 fiber	1.4	3.5	124-130	-2.7
Carbon fiber	1.8	1.5-5.5	150-500	-0.1
Steel Wire	7.8	4.1	210	11.1
Carbon Nanotubes	-	11-63	270-950	-
Boron Nanowhiskers	-	2-8	250-360	-
Crystalline Cellulose	1.6	7.5-7.7	110-220	0.1

Given its abundance availability and outstanding inherent properties, cellulose-based materials have been continuously developed in various forms, including cellulose esters, cellulose ethers, and regenerated cellulose, to provide new functionalities and extend its application range. Recently, the development of cellulose based materials focuses mainly toward a novel form of cellulose called nanocellulose. Nanocellulose is a nanosize dimension of cellulose that can be produced by either top-down approach via delamination of the hierarchical structure of plants or bottom-up approach via cellulose growth from glucose by the assistance of a bacteria. In essence, nanocellulose combines the intrinsic characteristics of cellulose with unique features of a significantly higher surface area, less defect, and higher crystallinity compared to those of traditional wood cellulose fibers. This next generation of cellulose-based materials has the ability to impart diverse functionalities that are suitable as a building block for high-performance engineering applications.

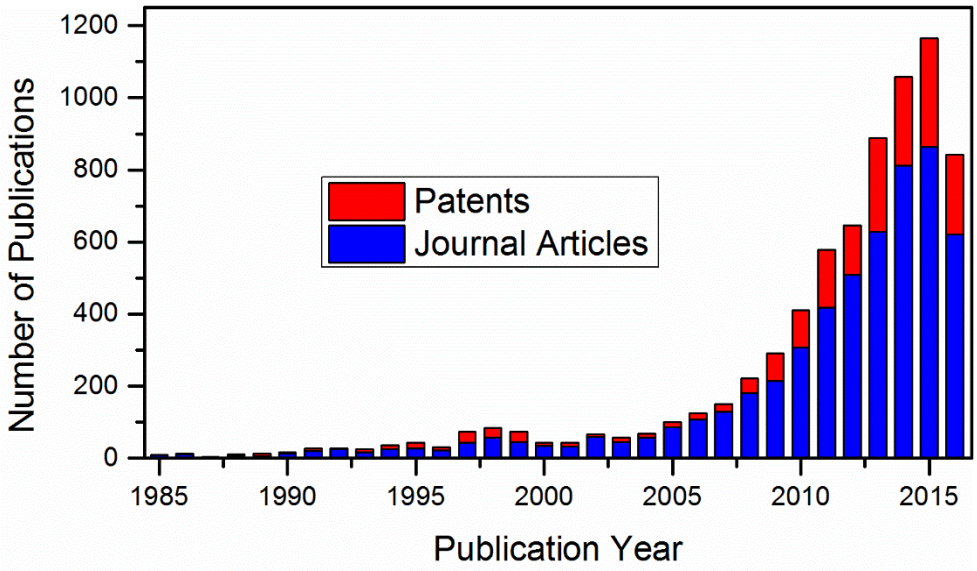

Figure 1.2 The annual number of scientific publications and patents in the field of nanocelluloses. Data analysis completed using SciFinder on August 2016 using combined search term: cellulose nanofibril, cellulose nanocrystal, cellulose microfibril, cellulose whisker, bacterial cellulose, nanocellulose, cellulose nanoparticle, cellulose nanofiber.

The isolation of microfibrillated cellulose as nanocellulose was first published in 1983.[6] However, the interest toward nanocellulose technology has only been established in the last decade as illustrated in Figure 1.2. With the high expectation of commercial nanocellulose products in the near future, the current stage of research and development on nanocellulose technology is still relatively immature, and there is a numerous opportunity available for scientists to explore. While there has been an extensive on-going research related to the nanocellulose processing method and the fundamental properties of nanocellulose, the designing of nanocellulose-based material for high-performance applications remains uncovered adequately. Therefore, in this dissertation, we focus on not only the technological possibilities in nanocellulose modification approaches but also the development of nanocellulose-based material as a sustainable platform for diverse engineering applications.

The outline of this work is organized as the following: Chapter II provides a brief review of the state-of-the-art of nanocellulose modification approaches and applications, focusing primarily on cellulose nanofibrils (CNFs). Chapter III describes the specific objectives of this research. The approaches to achieve these specific objectives are determined, and some crucial issues are listed. Chapter IV contains the study of surface modification via coupling agent polymer to introduce hydrophobic surface. It focuses on the characteristics of the modified CNFs and its influence on mechanical properties of polystyrene (PS) composite. In Chapter V, the surface hydrophobization approach is extended toward aqueous solution modification, in which *in-situ* grafting polymerization is introduced. The creation of hydrophobic CNFs is further employed to form aerogels, which have the capabilities as an effective oil bio-absorbent for oil−water separation. In Chapter VI, a study on the versatility of CNFs as carbon precursors for electrocatalyst application is explored. The feasibility of doping heteroatoms to CNFs-derived carbon toward oxygen reduction reaction is demonstrated. Furthermore, the benefits of CNFs structural morphology and porosity as a template is utilized via recombination with different carbon catalyst to exhibit superior hydrogen evolution reaction. Finally, Chapter VII gives the overall conclusion and the possible future works of this research.

CHAPTER II

LITERATURE REVIEW

2.1 Nanocellulose

In general, nanocellulose can be classified into two different kinds based on their dimension and composition, cellulose nanocrystals (CNCs) and cellulose nanofibrils (CNFs). CNCs, also previously known as cellulose whiskers, are generated by removal of the amorphous domain of cellulose microfibrils by acid hydrolysis and have the rod-like shape. The geometrical dimension of CNCs varies with their cellulose source and isolation method, but typically they display a diameter ranging from 5 to 10 nm and length of 50-300 nm.[5, 7, 8] On the other hand, CNFs are long and fibrous cellulose fibrils composed of both amorphous and crystalline domains with a typical dimension of 5-100 nm in width and up to several micrometers in length.[7-10] The geometrical dimension of CNFs leads to nanofiber with high aspect ratio (L/D) and highly entangled network that exhibits gel-like characteristics in water suspension. CNFs can be produced by either biosynthetic extrusion from bacteria yielding pure native cellulose with high crystallinity[11-13] or defibrillation of wood pulp with the aid of chemical[14-18] or enzymatic treatment[19, 20] and/or mechanical disintegration[21, 22]. However, given the accessibility of wood cellulose as raw material provided by forest product industry, bleached kraft pulp and sulfite pulp are often used as the starting material for CNFs production. The delamination process of the hierarchical structure of wood cellulose and their respective CNCs and CNFs products are illustrated in Figure 2.1. In this dissertation, the focus of the work will only cover CNFs material obtained primarily from wood pulp defibrillation.

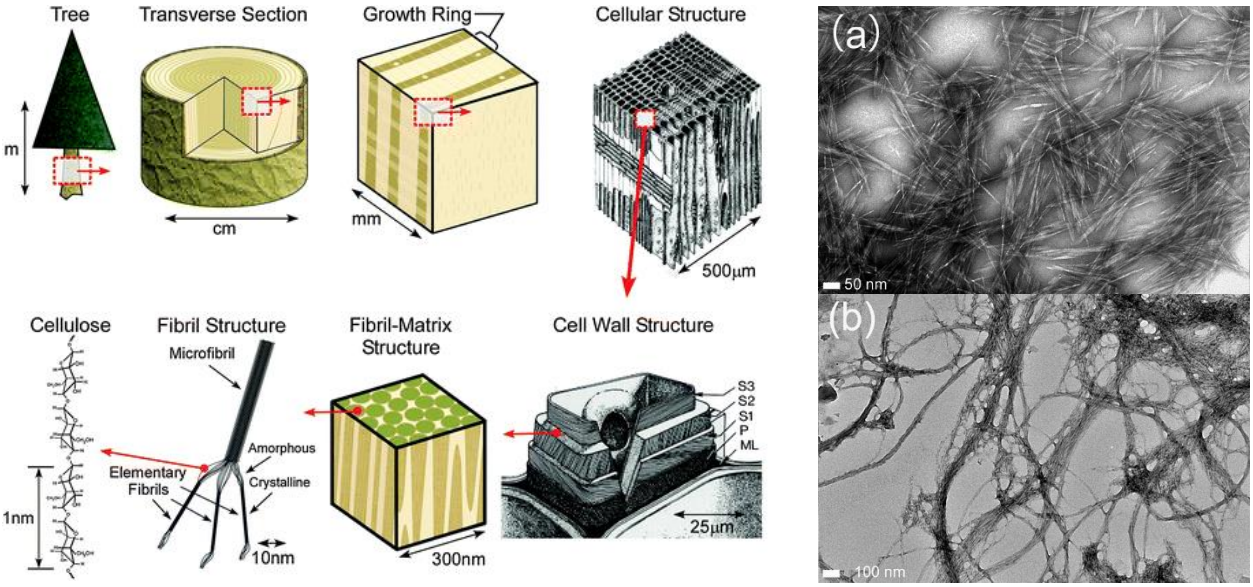

Figure 2.1 Hierarchical structure of nanocellulose along with representative images of (a) CNCs and (b) CNFs. Reprinted with permission from Postek et al.[23] and Xu et al.[24] Copyright 2016 American Chemical Society.

2.2 Modification of cellulose nanofibrils

As CNFs are essentially designed to have nanoparticle morphology and structure while maintaining their cellulose molecular structures, modification of CNFs is one of the important steps to further tailor the properties of this material to meet the specific demand in their utilization for high-performance applications. Furthermore, due to their large specific surface area, it is expected that the modification of CNFs not only provides more challenges during its preparation but also produces more significant impact than that of traditional wood cellulose fiber. In general, there are two common CNFs modification approaches (Figure 2.2): surface functionalization and chemical/physical transformation.

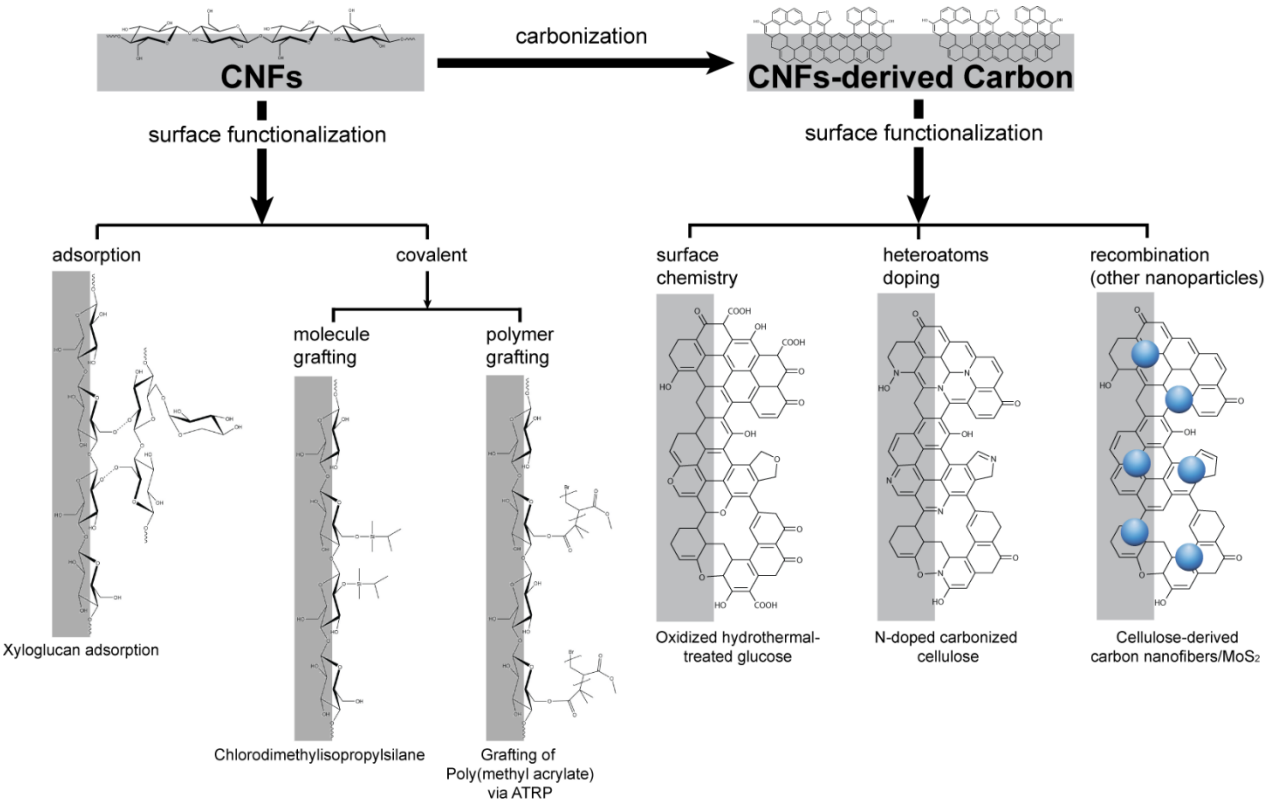

Figure 2.2 General route for CNFs modification approaches. Examples of surface functionalized cellulose-based fibers: xyloglucan adsorption[25], chlorodimethylisopropylsilane[26], and poly(methyl acrylate) via ATRP[27]. Examples of surface functionalized carbohydrate-derived carbon: oxidized hydrothermal-treated glucose[28], N-doped carbonized cellulose[29, 30], and carbon nanofibers/MoS_2 recombination[31]

2.2.1 Surface functionalization

Surface functionalization is targeted to modify the surface of either individual CNFs in their dispersed state or bulk material of aggregated CNFs (i.e. film or aerogel) and can be performed through chemical and physical treatment. The surface of the nanofibrils is composed of a periodical distribution of surface hydroxyl groups. These high number of hydroxyl groups lead to two effects that may not be desirable: strong hydrogen interactions between two nanofibrils and highly polar nanomaterial. Some chemical and physical treatments involving lower hydroxyl groups have been reported. Physical treatment is performed with the aid of electric discharge such as cold plasma[32, 33] and laser[34]. In this study, no physical treatment was applied, and only topochemical surface

functionalization is covered. Moreover, direct surface chemistry of CNFs such as TEMPO-oxidation, sulfonation, etc. is not included as part of surface functionalization step.

There are two main strategies for chemical surface functionalization of CNFs: physical adsorption and covalent bonding. In the physical adsorption method, weak chemical bonds are employed through hydrogen or ionic bonds. The adsorption phenomena of xyloglucan onto cellulose via hydrogen bonding has been successfully studied.[25, 35] Meanwhile, surfactants and polyelectrolytes are utilized to facilitate ionic interaction.[36-41] The negative surface charge of cellulose (arising from either oxidative bleaching of cellulose during pulping process or additional oxidative pretreatment process) could provide electrostatic adsorption with the positive ammonium of cationic surfactants/polycations as the counterions. Different types of polymer chains in the cationic surfactants and polyelectrolytes have been successfully deposited to render different functionality, i.e. lower surface adhesion[39], multilayer polyelectrolyte deposition[17], and nanoparticle binder[42]. However, it is expected that migration of the adsorbed moieties can occur easily through extensive mixing. Furthermore, the presence of excess surfactants or polyelectrolytes may also induce undesirable property such as lower mechanical performance for nanocomposite.[43]

In comparison to the physical adsorption, covalent bonding method creates a chemical interaction that results in a more stable form. A wide range of these methods has been demonstrated. In most cases, the reaction involves a heterogeneous system, in which CNFs would be insoluble nanoparticles and the reacting agent would be soluble in the reaction medium. Generally, there are two types of covalent bonding approach depending on the size of attached molecules: molecule chemical grafting and polymer grafting. Some notable molecule chemical grafting of cellulose involve silylation[44-47], esterification via carboxylic acid[48], anhydride[49-52],

or acyl chloride[53], isocyanate[54-56], and ring opening reaction of epoxide group[57-59]. In the silylation approach, chlorosilane is often used as the reacting agent and the silyl group (R_3-Si) replaces the hydroxyl group of the cellulose structure. Esterification is another common reaction, in which an ester functional group is introduced onto the surface hydroxyl group of the cellulose structure by condensation mechanism. Carboxylic acid, anhydride, and acyl chloride as reacting agents to induce esterification for nanocellulose have been reported in the literature. Depending on the reaction conditions, it has been found that esterification could proceed effectively not just on the surface of nanofibers but also inside the core of the crystalline region of nanofibers[53, 60]. Both silylation and esterification approach often result in the generation of acid by-products. Carbanilation using isocyanate as reaction agents serve as the alternative approach that eliminates this issue. The isocyanate acts as the electrophile that can easily react with the hydroxyl group of cellulose to form a urethane linkage. Nevertheless, all the reported approaches based on silylation, esterification, and carbanilation require water-free condition, which often makes the preparation step for CNFs more complex. In this regards, the ring opening reaction of epoxide group onto cellulose has been performed to graft molecules in the aqueous medium. In this reaction, the hydroxyl group of cellulose is alkali activated by adding sufficient amount of base solution.

Given the limited amount of substituted molecules could have on the CNFs surface, the changes on surface properties of nanofibrils may not be apparent. In this regards, polymer grafting is often desired in order to integrate new surface functionality more sufficiently. Depending on the formation of the polymer chain, general route of polymer grafting involves either “grafting from” or “grafting to” approach. “Grafting to” approach considers attaching pre-formed polymer chains onto cellulose backbone, while “grafting from” approach proceeds by growing polymer chains from the active sites of cellulose backbone.

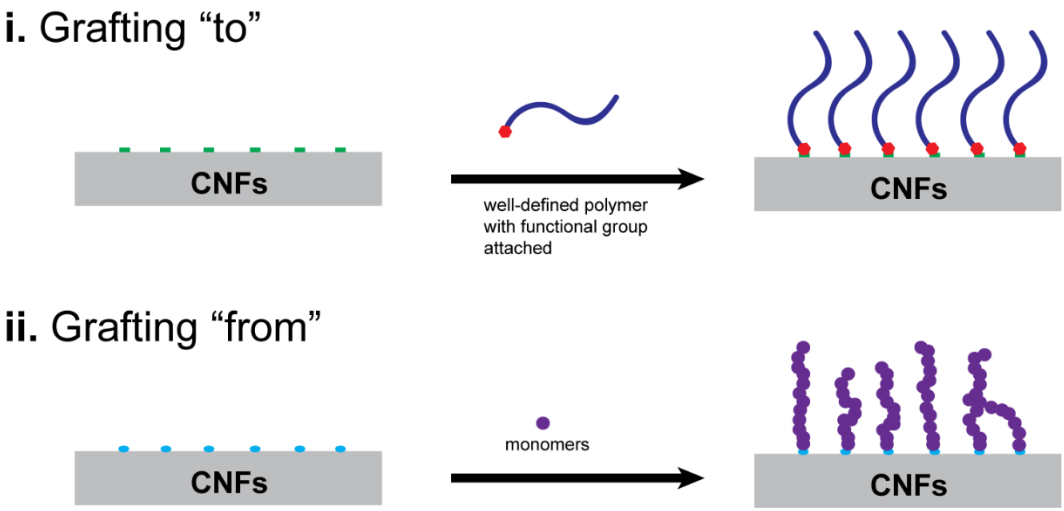

Figure 2.3 Schematic illustration of (i) “grafting to” and (ii) “grafting from” approach

There are only a few methods regarding “grafting to” approach. Polymers consisting of a functional species that are capable of esterification[61, 62], forming carbodiimides coupling[63], terminating living polymer cation[64], inducing “click chemistry”[65-68], are typically required to mediate a linkage to attach the high molecular weight polymer. Although the attached polymer has a well-defined characteristic, the grafting density for this approach is often low due to the steric hindrance of the long polymer chain.[69] Thus, the “grafting to” approach may not be the effective strategy to ensure good grafting coverage.

In comparison to “grafting to” approach, “grafting from” approach can achieve relatively high grafting density with varying degree of control on polydispersity. Various methods have been reported as representation of this approach, such as conventional free-radical polymerization[70-73], direct oxidation on cellulose backbone[74-76], ionic graft polymerization[77-79], ring opening polymerization[80-84], atom transfer radical polymerization (ATRP)[27, 67, 85-87], nitroxide mediated polymerization (NMP)[88], and reversible addition-fragmentation chain transfer (RAFT)[89, 90].

Among all the polymerization methods, polymer grafting on cellulose via free-radical initiation is the most popular choice. The attractiveness of this method originates from the diverse

monomers applicability, the unlimited copolymer formation, the high tolerance of reaction condition, and the technological feasibility in terms of a large-scale process.[91] Grafting via conventional free-radical polymerization method can be performed using typical free-radical initiators such as dibenzoyl peroxide (BPO), Azobis(isobutyronitrile) (AIBN), potassium persulfate (KPS), potassium permanganate, and Fenton's reagent. In this method, free-radical could initiate on either cellulose structure or monomer. Thus, the generation of ungrafted polymer (homopolymer) would be unavoidable. In this regards, grafting via free-radical exclusively on cellulose structure or direct oxidation on cellulose is found as an alternative solution. However, relatively expensive transition metal ions such as ceric ammonium nitrate are required as the initiator. Moreover, the ceric ammonium nitrate is known to be active only in a very acidic condition (i.e. pH of the medium is 1), in which a severe damage on the nanofibers could be expected for this reaction medium. Nonetheless, the two methods would still have an issue with regards to controlling the polydispersity of grafted polymer.

Ionic graft polymerization and ring-opening polymerization serve as the alternative methods to use a different mechanism other than free-radical. There are, however, only limited amount of studies performed. It has been noted that ionic graft polymerization will be difficult to implement given the high-demanding reaction conditions (anhydrous and high purity reagents).[91] On the other hand, ring-opening polymerization is only limited to certain monomers, such as ε-caprolactone and L-lactic acid.

In the recent advance of polymerization techniques, living polymerizations have been explored as grafting method. Szwarc first defined "living polymerization" in 1956 as chain polymerization growth in the absence of chain breaking reaction (i.e. chain transfer or irreversible termination steps).[92] Such mechanism would generate the polymers with controlled composition,

molecular weight distribution, and architecture. In combination with a radical process, the concept of living radical polymerization (LRP) was introduced as a versatile approach that gives precisely controlled polymers for a wide range of monomers and reaction conditions.[93] Moreover, in grafting process, the large amount of homopolymer formation could be easily avoided. Atom transfer radical polymerization (ATRP), nitroxide mediated polymerization (NMP), and reversible addition-fragmentation chain transfer (RAFT) are the three major methods representing LRP mechanism. Nevertheless, these methods are still not widely used for industrial-scale, and their applicability would strongly depend on the practical application of the end-products.

2.2.2 Surface hydrophobization

Among various properties that are desired to obtain, tuning the surface wetting properties of CNFs is one of the most common objectives for surface functionalization. Neat CNFs are amphiphilic materials that are composed of hydrophilic and hydrophobic sites.[94, 95] Although the inherent amphiphilicity of CNFs has been taken advantages as dispersant agent[94], surface hydrophobization of CNFs is often desired and has been proven to contribute significantly to various aspect of field, such as to maintain barrier and mechanical properties of CNFs films in the environment with high relative humidity[96], to produce a stable colloidal suspension in various organic solvents[26, 83], to be utilized as stabilizer for formation of water-in-oil (w/o) Pickering emulsion[97, 98], to improve surface compatibility with hydrophobic polymer matrices[47, 81, 99], and to induce oil/water separation property[100, 101].

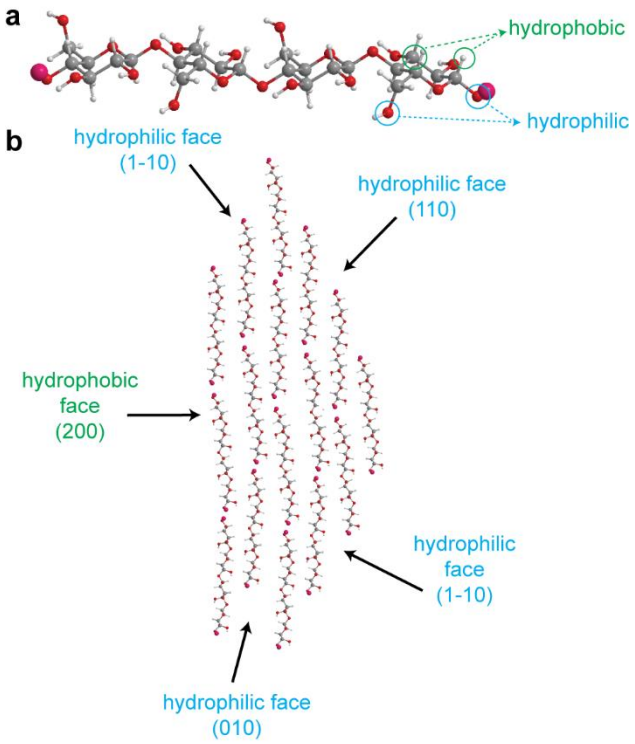

Figure 2.4 (a) 3D molecular structure of cellulose. (b) Schematic model of cellulose crystal in the elementary fibrils with the representation of both hydrophobic and hydrophilic face[94, 102]

Various attempts have been reported in either introducing hydrophobic compound or lowering accessible hydroxyl groups. Using fluorosurfactant, Aulin et al. could reduce the high dispersive surface energy of cellulose at 54.5 mN/m to ~12 mN/m.[41] Rodionova et al. performed gas-phase esterification of nanocellulose films using trifluoroacetic acid anhydride and acetic acid to render esterified film with a contact angle of 79.2°.[48] The same group also used acetylation reaction to obtain acetylated films with a contact angle of 82.7°.[96] Using the similar acetylation reaction, Jonoobi et al. were able to achieve higher contact angle of 115°.[60] Yoshida et al.[52] and Missoum et al.[103] utilized AKD as a sizing agent using solvent-free condition and nanoemulsion, respectively. In both methods, contact angle value around 100° was observed. Tome et al. tested surface hydrophobization of bacterial cellulose using several anhydrides (acetic, butyric, hexanoic, and alkenyl succinic anhydride) and hexanoyl chloride in an ionic liquid. Contact angle values in

the range of 80-104° were obtained. Surface silylation of nanocellulose using chlorodimethylisopropylsilane was able to generate modified nanocellulose with water contact angle between 111-146°.[104] Lu et al. could attain hydrophobic microfibrillated cellulose that gave a water contact angle value of 110° using a titanate coupling agent (Lica 38).[47] Recently, a commercial-scale hydrophobic nanocellulose with contact angle around 90° was available developed by American Process Inc. through the American Value Added Pulping (AVAP)® technology.[105]

2.2.3 Carbonization and its surface functionalization

Aside from surface functionalization, in which the molecular structure and physical properties of CNFs backbone remain unaltered, chemical/physical transformation of CNFs is another type of modification approach. The transformation of CNFs is aimed to convert either the molecular structure or physical morphology of CNFs. Some examples of cellulose transformation are dissolving pulp and carbonization. In this thesis work, only carbonization of CNFs is considered.

In general, the term "carbonization" refers to the thermal transformation of organic molecules into inorganic solid carbon. During the carbonization, thermochemical process causes the organic molecules of material to be broken down into volatile matter, non-volatile matter, and ash.[106, 107] The volatile matter can be categorized into two products: the condensed liquid fraction called bio-oil and the non-condensable gas called syngas. The volatile matter is often the major products of carbonization process. The non-volatile matter of carbonized cellulose is a carbon-rich material composed of a complex mixture of polycyclic aromatic carbon sheets.[108, 109] When obtaining the carbonaceous material, a small amount of inorganic residue may present. The term used for this inorganic residue is called ash.

Common methods of preparing carbonized cellulosic materials are pyrolysis (slow, fast, or flash), flash carbonization, gasification, hydrothermal treatment, or a combination thereof.[106, 107, 110-113] Depending on the carbonization method, the yield of carbonaceous material may vary. In the slow pyrolysis process, slow heating rate (5-7 °C/min), relatively long vapor residence time (>1 h), and a wide temperature range (300-800 °C) was executed. The main product of this process is the carbonaceous solid, which is accounted for a relatively high yield range of 35-50 wt%. The fast pyrolysis is characterized by fast heating rate (300-800 °C/min) and relatively shorter vapor residence time (0.5-10 s). The process typically operates in the temperature range of 400-600 °C and generates a high yield of bio-oil with only 15-25 wt% of bio-carbon. The flash pyrolysis use even faster heating rate (~1000 °C/min) and relatively shorter vapor residence time (<2 s). Only 10-20 wt% of carbon solid could be produced with syngas as the main product. Unlike pyrolysis, flash carbonization uses air flow and elevated pressure reaction condition. No liquid product was reported to be found using this method.[113] Gasification is another process that involves partial combustion as a controlled oxygen gas is included in the reaction condition. The method is designated to produce syngas as the main product with some carbon solid as by-products. Hydrothermal carbonization is another different process that involves wet feedstock. The method requires elevated temperature and pressure to transform the feedstock material into the carbon-rich material. The resultant carbon from this method would contain a high amount of oxygen (~20 wt%).[114] Regardless the discrepancy in the carbonization methods, the main mechanism associated with the carbon network formation often does not change. There are three main reactions involved: dehydration, decarboxylation, and polycondensation.[106, 109, 114, 115]

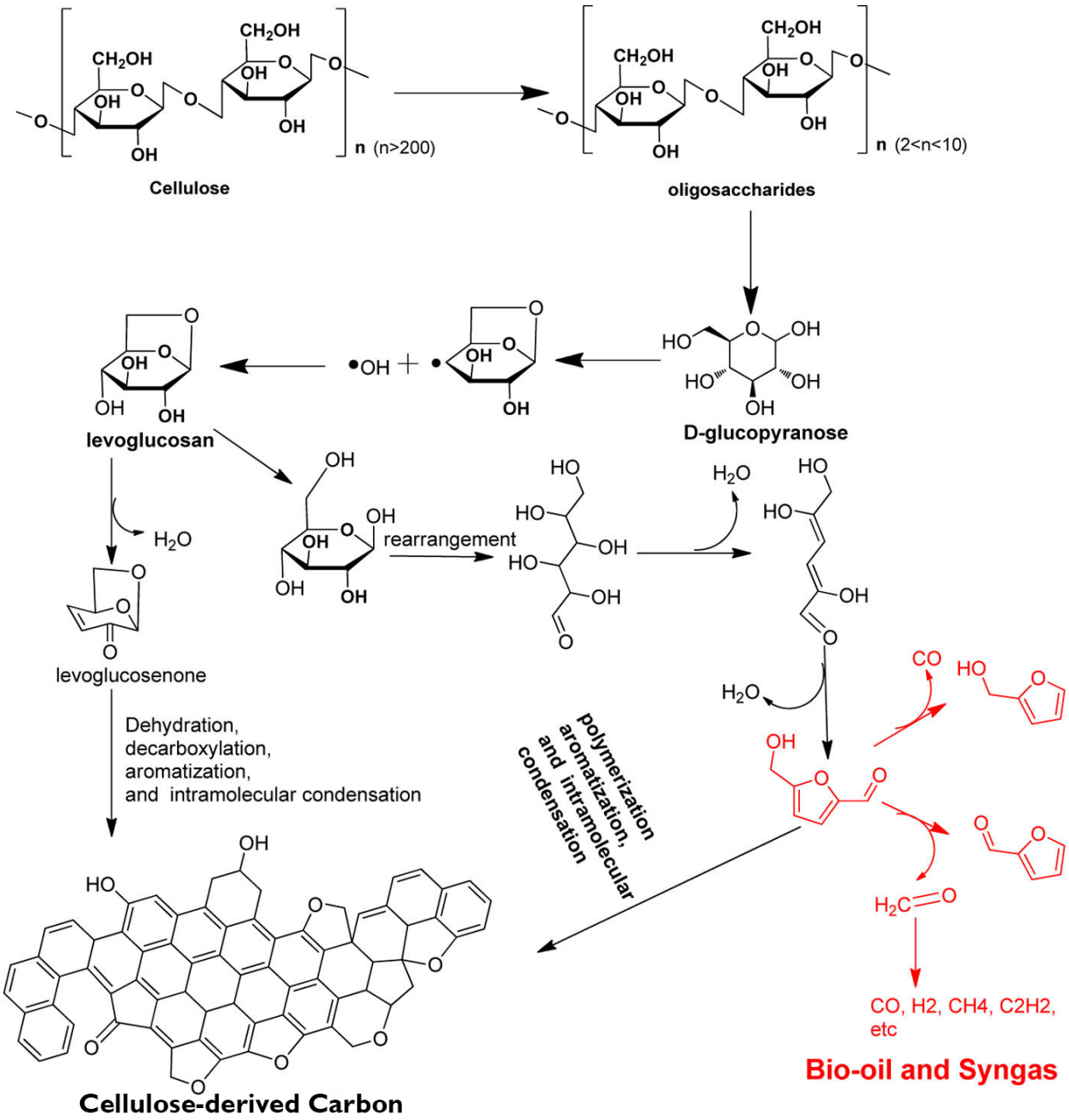

Figure 2.5 Example of cellulose pyrolysis mechanism. Three products are produced: cellulose-derived carbon, bio-oil, and syngas. Adapted with permission from Liu et al.[106] Copyright 2016 American Chemical Society.

The obtained carbonaceous material from cellulose is often referred as bio-carbon. The predominant aim for the development of bio-carbon is stemmed from the desire to create sustainable carbon nanomaterials. With the increasing attention for nanocarbon, such as carbon

nanotube (CNT) and graphene as illustrated in Figure 2.6, toward high-performance applications, it would not be surprising that bio-carbon products could also be utilized as the substitute for some of the petroleum-based nanocarbon. The main interest in nanocarbon lies in their excellent intrinsic properties. Nanocarbons have shown to exhibit excellent mechanical properties (up to 130 GPa for tensile strength and 1 TPa for Young's modulus), high surface area (up to ~1300 m^2/g), outstanding electrical properties (10^2-10^5 S/cm), low optical absorption, chemical inertness, superhydrophobic property, and good thermal stability.[116-120]

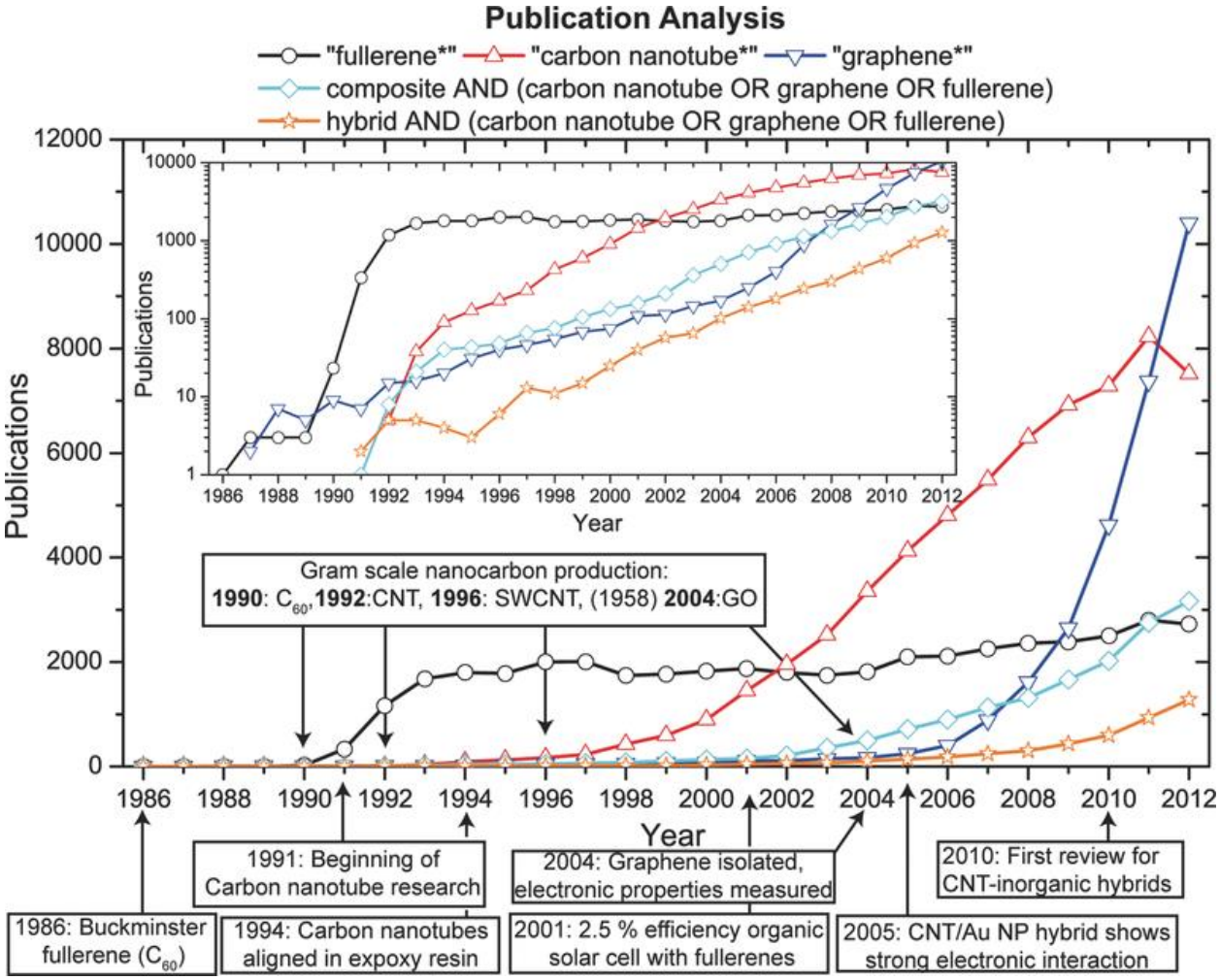

Figure 2.6 Development of nanocarbon research based on publication analysis. Reprinted from Shearer et al.[116] with permission of John Wiley and Sons.

In order to compete with the petroleum-based nanocarbon, it is important that the synthesized bio-carbon have comparable properties. The properties of bio-carbon are influenced by the precursor properties of cellulosic materials and treatment condition. Carbonization of cellulose typically would yield a hard carbon, which is a non-graphitizable carbon class.[112] However, the graphitization capability for cellulose-derived carbon could be achieved to a certain extend for some high purity cellulose with very high crystallinity.[112] Aside from the source of feedstock, carbonization temperature is another important aspect that greatly affects the properties of bio-carbon. The difference in carbonization temperature would change the composition of aromatic arene-like network[112, 115], the growth of carbon crystallite[121], electronic properties[112, 121, 122], and surface area[106, 122]. In general, the graphite-like layers would not start to form until the temperature reach 350 °C, in which large amount of furanic-group is expected. As the temperature increases up to 900 °C, aromatic arene-like network dominates the structure of bio-carbon and form semi-ordered carbon crystallite. Above 900 °C, the obtained bio-carbon is subjected to graphitization, in which more ordered carbon crystallite and increasing crystalline thickness are expected (Figure 2.7).

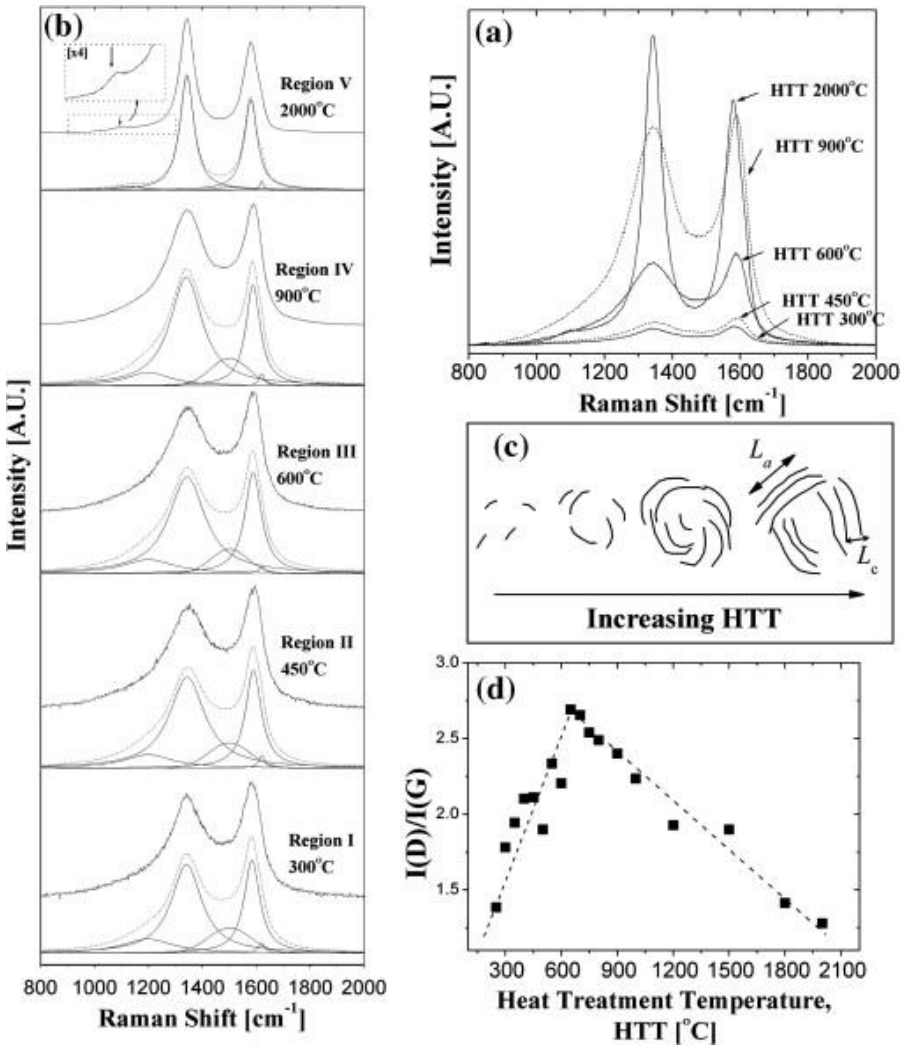

Figure 2.7 (a) Observable changes in Raman spectra for carbonization of microcrystalline cellulose using various heat treatment temperature (HTT). (b) Deconvolution of each Raman spectrum. (c) Schematic illustration of crystalline carbon growth. (d) Intensity ratio of D band and G band derived from Raman spectra. Reprinted from Rhim et al.[121], with permission from Elsevier.

The bio-carbon with low defect carbon-rich structure would allow the material to have more favorable electrical properties. The electrical conductivity of cellulose is 10^{-8} S/cm.[112] The effect of carbonization temperature on the electrical properties of cellulose-derived carbon has been studied by Rhim et al.[121], as shown in Figure 2.8. As cellulose was carbonized at the temperature of 350 °C, the electrical conductivity of carbonaceous material could increase up to 10^{-5} S/cm. Cellulose-derived carbon prepared at 600 °C would have electrical conductivity around 10^{-3} S/cm.

A further increase in the temperature up to 1000 °C would improve the electrical conductivity to reach 10^2 S/cm. However, no significant change was detected while increasing the temperature up to 2000 °C. The average electrical conductivity of 33 S/cm has been reported for various carbonized CNFs.[118] It should be noted that the inherent electrical conductivity of cellulose-derived nanocarbon would always be inferior compared to the typical petroleum-based nanocarbon.

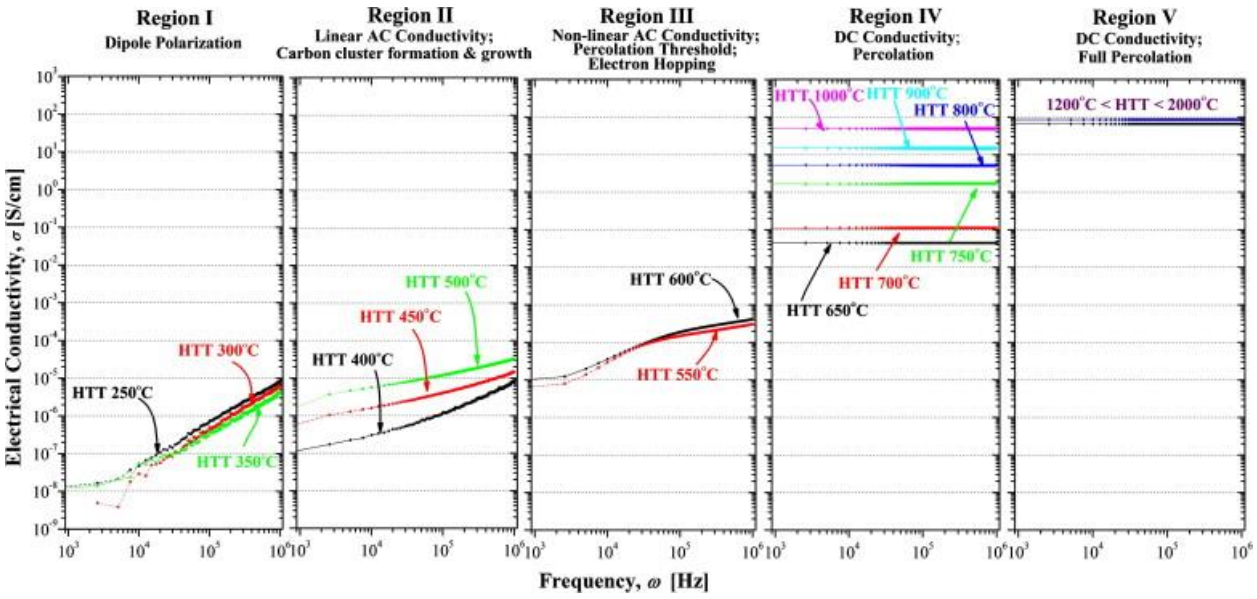

Figure 2.8 Electrical conductivity measurement for carbonized microcrystalline cellulose at various heat treatment temperature (HTT). Reprinted from Rhim et al.[121], with permission from Elsevier.

The effect of carbonization temperature on the development of the surface area and pore structure for bio-carbon have been studied by Brown et al.[122] At carbonization temperature of 450 °C, the surface area of the obtained bio-carbon showed less than 10 m^2/g. With increasing temperature to 750 °C, the surface area of bio-carbon increased sharply to reach 400 m^2/g. A lower surface area is then expected at 1000 °C because of the microstructural arrangement at high temperature. In comparison to the surface area for petroleum-based nanocarbon, the surface area

of bio-based carbon is still comparable. Additionally, even though the surface area of the material is expected to be slightly lower, CNFs-derived carbon nanofiber may have better interconnected nanocarbon structure that could facilitate better carbon network continuity.

Since carbonization of cellulosic material could lead to a carbon-rich material with O/C ratio of 95%[121], only limited surface functionality is inherently present. In this regard, surface functionalization methods used for petroleum-based nanocarbon can also be performed for bio-carbon to give the similar surface functionality. There are three typical routes for the surface functionalization of bio-carbon: surface chemistry, heteroatoms doping, and surface recombination.[106, 116] Surface chemistry, such as oxidation, amination, and sulfonation, is a process of introducing new surface functional groups. This method is often used as a preliminary step for further chemical grafting, the same step used to surface engineer CNFs. In addition to surface chemistry, heteroatoms doping is another functionalization by incorporating non-carbon atoms to replace some carbon atoms in the carbon network. Several heteroatoms dopants, such as nitrogen, phosphor, sulfur, and boron, are used to induce chemical heterogeneity that would affect the electronegativity of aromatic carbon atoms.[123] Surface recombination is the other surface functionalization step. In surface recombination, other nanoparticles from different materials, i.e. metals, semiconductors, or oxides, or similar nanomaterials with different nanostructure are imparted on the bio-carbon template to introduce new functionality, nanostructure, or a combination of both.

2.3 Applications of cellulose nanofibrils

2.3.1 Cellulose nanofibrils-based applications

As sustainable nanomaterial with a potential of industrial-size production, the physiochemical, thermal, and mechanical properties of CNFs have been found useful as

reinforcing fibers in commodity polymers and concretes, aerogels and foams, colloid particles, and films. The combination of excellent strength originated from the crystalline region, the high aspect ratio of nanofiber, and surface compatibility with various hydrophilic polymers (i.e. chitosan[124], polyethylene oxide[24], and polyvinyl alcohol[125]), has shown to improve the overall mechanical properties of the nanocomposite. Moreover, the surface modified CNFs can be used to reinforce some hydrophobic polymers such as natural rubbers[126], polylactic acid[127], polypropylene[128], and polyethylene[129]. Similarly, the addition of CNFs to the cement paste could facilitate an increase in fracture toughness.[130]

CNFs-based foams and aerogels could be prepared from drying water/air emulsion stabilized by CNFs and octylamine[131] and freeze-drying CNFs suspension[132, 133], respectively. The resultant aerogels or foams could have low density with a highly porous structure, which is suitable as porous templates for scaffolding[132], liquid or gas absorbent[134-137], and conductive material[138]. In addition, the good dimensional stability of neat CNFs offers a potential advantage as thermal insulations.[139]

Owing to their unique nanofiber morphology, CNFs, as colloid particles, can be used as thickeners and suspension stabilizer in various emulsion products. CNFs have been tested to stabilize salad dressing[140], fracturing fluids of oil recovery[140], and water-based paint[141].

Films prepared from neat CNFs showed high intrinsic oxygen barrier[8, 142] and oil resistance capabilities[142]. Moreover, the films can act as selective permeation of hydrogen gas filtration membrane.[143]

2.3.2 Cellulose nanofibrils-derived carbon-based applications

CNFs-derived carbon nanofibers have been found useful as pollutant adsorption, energy storage material, electrical component, and catalyst. As pollutant adsorption, the carbonized CNFs possess high surface area and hydrophobicity to provide excellent adsorption capacity and selectivity for oils, dyes, and heavy ions removal.[144, 145] In addition to the high surface area, the obtained CNFs-derived carbon can be tuned during the carbonization process to enhance their specific capacitance performance and increase the amount of energy stored in the supercapacitor.[146] The CNFs-derived carbon nanofiber composites could also provide better electromechanical stability than conventional CNT- or graphene-based composites, which make the material suitable for a stretchable electrical conductor.[147] Moreover, the functionalized CNFs-derived carbon nanofibers showed promising potential as lithium ion battery anodes[118, 148], catalyst (i.e. electrocatalyst for oxygen reduction reaction and hydrogen evolution reaction)[29-31], and supercapacitor[149-151]

CHAPTER III

PROBLEM ANALYSIS AND OBJECTIVES

As reviewed in chapter II, CNFs as nanocellulose are one of promising next generation sustainable building block due to their inherent physio-chemical-mechanical properties. Furthermore, the material can easily undergo modification that will further expand their potential applications. Although extensive investigations on nanocellulose process and characteristics have been reported, developing economical and environmentally-friendly modification technologies for CNFs are still a great challenge that limits the practical feasibilities in diverse engineering applications. In this thesis, we seek various functionalization approaches to introduce hydrophobic surface for each individual nanofiber and demonstrate their applicability as effective bio-fillers and bioabsorbent. The synthesis method and the impact of each modification on the material properties were extensively studied. In addition, we investigated the thermochemical transformation of CNFs and exploited the utilization of CNFs as potential renewable nanocarbon resources. Thus, the objectives of this research work are:

- to synthesize hydrophobic CNFs using coupling agent polymer and ascertain the reinforcing ability of surface functionalized CNFs on mechanical properties of hard, brittle thermoplastic polymer
- to synthesize hydrophobic CNFs in an aqueous medium, elucidate the mechanism of *in situ* modification approach, and comprehend the impacts of surface functionalized CNFs on the characteristics of aerogels

- to synthesize CNFs-derived carbon nanofibers, exploit different carbon surface functionalization methods, and ascertain the implication of surface functionalized CNFs-derived carbon nanofibers toward effective electrocatalyst material

3.1 Objectives

3.1.1 The synthesis of hydrophobic CNFs using coupling agent polymer and the reinforcing ability of surface functionalized CNFs on mechanical properties of hard polymer

In the fabrication of nanocomposite, excellent filler dispersion and surface compatibility between the filler and the matrix are the key aspects of producing outstanding mechanical properties. As reinforcing bio-fillers for hydrophobic polymers, neat CNFs possess a high number of surface hydroxyl groups that lead to the incompatible filler-matrix surface interaction and self-aggregation tendency. While surface hydrophobization of CNFs is one of the approaches taken to solve this issue, most of the reported methods in literature aimed toward hydrophobization of aggregated CNFs or adding compatibilizer agent simultaneously with polymer processing. In this regard, comprehensive investigations on facile hydrophobization method of individual nanofibrils, characterization of hydrophobic CNFs, and the role of hydrophobic CNFs toward the mechanical properties of nanocomposite are important. Moreover, the excellent reinforcing capability of CNFs should be ascertained by reinforcing hard polymer.

3.1.2 The synthesis of hydrophobic CNFs in aqueous medium, the mechanism of in situ modification approach, and the impacts of surface functionalized CNFs on the characteristics of aerogels

Following up on the reported hydrophobization method for CNFs, an organic solvent often used as the dispersion medium. Because CNFs are often prepared as a suspension in water to

prevent the aggregation of their nanofiber, preparing CNFs as a suspension in the organic solvent requires energy extensive method (i.e. through drying process to remove all water) or excess usage of solvent (i.e. through repetitive solvent-exchange). In most cases, the method causes nanostructure change due to unavoidable aggregation. Furthermore, it has been reported that some solvent could disrupt the crystalline region of CNFs. In this regard, finding an economical, non-toxic surface hydrophobization approach using aqueous medium is important. In addition, the method should also be optimized to accommodate minimal changes in terms of nanofiber morphology. The investigation on the properties of surface modified CNFs should be elucidated in form of low density material, such as aerogel. The use of aerogel could easily magnify the modification impact on overall CNFs properties.

3.1.3 The synthesis of CNFs-derived carbon nanofibers, the exploration of different carbon surface functionalization methods, and the implication of surface functionalized CNFs-derived carbon nanofibers toward effective electrocatalyst material

As a sustainable and inexpensive material, CNFs can be designed as bio-carbon nanofiber. The information available on carbonization method and the resultant properties of CNFs-derived carbon nanofibers are still very limited. Moreover, the pyrolysis and gasification method requires dry CNFs, which often generate CNFs aggregated form that could induce material heterogeneity during carbonization. On the other hand, hydrothermal CNFs would change the morphology of CNFs into aggregated sphere nanoparticles. Thus, it is necessary to find an alternative method that can produce carbon nanofibers from CNFs to satisfy this requirement. Additionally, investigating functionalization methods for CNFs-derived carbon nanofibers that would allow the material to compete with the traditional nanocarbon (i.e. graphene-based) is of particular interest. With the recent interest toward metal-free carbon electrocatalyst in the progress of fuel cell and hydrogen

gas generation, surveying the potential usage of CNFs-derived carbon nanofibers in this field is significant.

3.2 Approach determination

3.2.1 Surface hydrophobization

In order to achieve hydrophobic CNFs with high water repellency, the covalent interaction via grafting of the hydrophobic polymer is the preferred method to minimize the probability of wet leaching. While grafting of hydrophobic molecules can reduce the accessible hydroxyl group of CNFs surface, the presence of long carbon chain in the hydrophobic polymer will ensure that the introduction of non-polar entities can adequately block the surface hydroxyl groups of CNFs. In addition, the amount of grafting should be low enough to have lower surface energy without significantly affecting the morphology and mechanical properties of CNFs. Ideally, it is desirable to have uniform grafting across individual fibers. While more complex methods such as ATRP (atom transfer radical polymerization), NMP (nitroxide mediated polymerization), and RAFT (reversible addition-fragmentation chain transfer) could provide a robust control on the grafted polymer, the use of these methods often does not substantiate an economical benefit of the end-products. On the other hand, conventional methods such as free-radical polymerization is readily available in the larger-scale.

Because the homogeneity of hydrophobic CNFs is another important aspect, optimization of grafting preparation/procedure is often necessary. In order to mitigate any heterogeneity during functionalization step, a homogeneous mixture should always be prepared through adequate mixing or with the aid of rotor/stator homogenizer. In addition, multiple replications should be conducted to minimize any possible discrepancy. Good isolation of the modified CNFs after the synthesis is also important to eliminate the effect of excess impurities or unreacted reactants.

Repetitive steps of centrifugation, filtration, or Soxhlet extraction were used in all experimental work and could satisfy a good isolation method of the product.

3.2.1 Carbonization

Carbonization methods of CNFs would use two-step approaches: solvothermal (wet state condition) and pyrolysis (dry state condition). First, the solvothermal method was utilized to produce dispersed carbonized CNFs and avoid morphology change associated with hydrothermal. As the carbonized CNFs would solve nanofiber hornification issue, the dry carbonized CNFs could be easily dispersed to undergo pyrolysis. The pyrolysis was aimed to improve the inherent electrical property and surface area of CNFs-derived carbon.

In order to generate additional functionality to the CNFs-derived carbon, various surface functionalization methods were tested. Heteroatoms-doping, such as N, S, and P-doping, has been found as an effective method to improve the electrochemical properties of carbon material. Simultaneous doping and carbonization in the solvothermal method were adapted to avoid excess use of a doping agent that is commonly needed using pyrolysis method. Furthermore, surface recombination was also used to enhance the material effectiveness of carbon materials further as an electrocatalyst.

CHAPTER IV

WATER-FREE GRAFTING OF HYDROPHOBIC POLYMER VIA COUPLING AGENT

4.1 Introduction

In the recent developments of renewable and sustainable resources, cellulose nanofibrils (CNFs) have received major attentions because of their properties as high-performance biomaterials. Owing to their excellent mechanical strength, biodegradability, and low density,[152, 153] CNFs are attractive as potential nanoparticle reinforcement fillers in composite and often comparable to the conventional reinforcement fillers, such as aramids and glass fibers. CNFs commonly produced by mechanical disintegration of cellulose fibers are composed of both crystalline and amorphous regions and have typical dimensions of 20-40 nm in width and several micrometers in length.[8] CNFs dimensions display relatively high length-to-diameter aspect ratios with averaged value of 100.[152, 153] CNFs' high aspect ratio could significantly improve the mechanical properties of the composite at very low contents.[154] Yet, one of the challenges in the current development lays in the limited performance of CNFs as filler reinforcement in hydrophobic polymeric matrices due to CNFs' self-aggregation tendency and incompatible matrix-CNFs interfacial interaction.

Surface modification of CNFs has been an essential technique for engineering composite materials. Grafting the designed polymer onto CNFs surface is an effective and straightforward method to improve CNFs properties without affecting its biodegradability. The addition of a long

This chapter has been modified from the following publication: Surface Modification of Cellulose Nanofibrils by Maleated Styrene Block Copolymer and Their Composite Reinforcement Application, Cellulose, 2016, vol. 23, nb. 1, p.519

chain of the hydrophobic polymer would help in masking accessible hydroxyl groups of CNFs and limiting irreversible agglomeration of fibers upon drying.[155, 156] In addition, reducing the degree of hydrophilicity will lead a better interfacial adhesion with hydrophobic polymer matrix. Surface modification with polymer could be achieved by esterification of the coupling agent. One of the most common coupling agents reported in the literature is anhydride-modified copolymers such as maleated styrene block copolymer.[157] Maleic anhydride-grafted styrene–ethylene/butylene–styrene (MA-SEBS) is one of the convenient maleated styrene block copolymers that displays balanced elasticity, excellent processability, and good thermal stability due to the properties of the SEBS thermoplastic elastomer. The anhydride group of this coupling agent reacts rapidly when in contact with the surface hydroxyl group of CNFs at elevated temperature. Thus, grafting coupling agent onto CNFs can be performed in their solid-state mixture, which has the main advantage of a very rapid process on the minute time scale compared to the typical solution grafting method, which requires hours or even days.[158] Blending the coupling agent together with fillers and matrix polymer/monomer in a master batch is a common strategy of using coupling agent.[159, 160] To our knowledge, no attention has been devoted to determine CNFs functionalized by anhydride-modified copolymer prior to final composite processing. In this work, the modification process involving solvent treatment followed by coupling polymer agent grafting is subjected to chemical, physical and thermal characterizations. Furthermore, the work provides a mechanical evaluation of using both solvent-treated and surface-modified CNFs as reinforcement fillers for brittle-hard polymers such as polystyrene (PS).

4.2 Experimental Section

4.2.1 Materials

Cellulose nanofibrils (CNFs) prepared from mechanically refined bleached softwood kraft pulp were purchased from the University of Maine Process Development Center. Maleic anhydride-grafted polystyrene-*block*-poly(ethylene-*ran*-butylene)-block-polystyrene (MA-SEBS) containing approximately 2 wt% maleic anhydride and polystyrene pellets with average molecular weight of 230,000 were obtained from Sigma-Aldrich. The 99 % Tetrahydrofuran (THF) containing BHT as inhibitor was supplied by Alfa Aesar.

4.2.2 Grafting procedure

Modified CNFs were prepared from a solid mixture of CNFs and coupling polymer agent. In this study, a 0.35 wt% CNFs suspension in THF was prepared using solvent exchange method by successive centrifugation-redispersion steps. Maleated styrene block copolymer, MA-SEBS, added to the 0.35 wt% CNFs/THF suspension at a weight ratio of MA-SEBS to CNFs of 4:1 and mixed using mechanical stirring until completely dissolved. The mixture was dried by casting and evaporating all the solvent at room temperature. The completely dry solid was then cured to undergo grafting reaction at 150 °C over a 15-min period. The grafting chemistry followed the esterification mechanism as shown in Figure 4.1. The resulting cured solid was dispersed and homogenized in THF solution, followed by washing with THF to extract free polymer. After successive washing, a small amount of the modified CNFs/MA-SEBS in THF suspension sample was dried for characterization and the rest was stored for composite preparation.

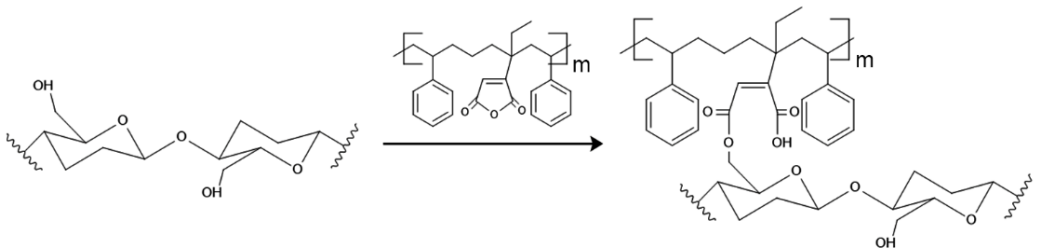

Figure 4.1 Esterification reaction between CNFs and maleated styrene block copolymer coupling agent

4.2.3 Characterization of the grafted cellulose nanofibrils

A quantitative amount of polymer after grafting was measured by gravimetric method. The chemical structures of neat CNFs, THF treated CNFs and grafted CNFs were identified using Bruker Vertex 80 V attenuated total reflectance-Fourier transform infrared spectroscopy (ATR-FTIR). The scan range was 4000 to 400 cm^{-1} with a resolution 4 cm^{-1}. Surface morphology of samples was imaged with a LEO 1530 thermally assisted field emission scanning electron microscope (FE-SEM) in which all samples were gold-sputtered. Sessile drop contact angle measurement of film samples was captured using FTÅ200 Dynamic Contact Angle Analyzer (First Ten Ångstroms). Thermogravimetric analysis (TGA) and its first derivative were operated to assess moisture absorption, thermal degradation profile, and amount of grafted polymer using the PerkinElmer STA 6000. A 20 mg portion of the sample was heated from 35 to 600 °C at a rate of 10 °C/min under a flowing nitrogen atmosphere. X-ray diffraction analysis performed by scanning angular range (2θ) from 5° to 35° at a step size of 0.02° on the X'Pert PRO X-ray diffractometer (PANalytical) was applied to estimate the percent crystallinity (% Cr) of samples. The resulting diffraction patterns were deconvoluted using curve-fitting software (Fityk 0.9.8) based on Voigt functions to separate amorphous and crystalline contributions. The crystalline contribution of cellulose was fitted according to five peaks [(1-10, 110, 102, 200, and 004)] with the position of the maximum peak at 14.8°, 16.7°, 20.8°, 22.8°, 34.5°, respectively.[161] Percent crystallinity was calculated as the ratio of the sum of non-overlapping areas of crystalline peaks to the total area of the crystalline peaks and the amorphous region, with a minimum value of intensity at 2θ of 18°, as indicated in Equation (4.1) [162-164]

$$\%Cr = \frac{A_{101} + A_{10\bar{1}} + A_{021} + A_{002} + A_{040}}{A_{101} + A_{10\bar{1}} + A_{amp} + A_{021} + A_{002} + A_{040}} \qquad (4.1)$$

Colorimetric titration was used to measure the amount of unesterified anhydride and its isomeric acid form. A small amount (0.175 g) of dried samples was dispersed in 75 mL of xylene at room temperature. 15 mL of 0.05 N potassium hydroxide solution in methanol was added and the mixture was agitated for 1 h at room temperature. The formed mixture was back titrated with 0.05 N sulfuric acid solution in methanol using methyl red as an indicator. The acid number was calculated as:

$$\text{Acid Number} = AN = \frac{(A-B)N \times 56.1}{W} \qquad (4.2)$$

where A is the volume (in milliliter) of the acid solution used to titrate the blank, B is the volume (in milliliter) of the acid solution used to titrate the sample, N is the normality of the acid solution, W is the weight (in gram) of the sample. The hydrolysis effect in this procedure was validated as commercial cellulose acetate showed only 3 wt% mass loss.

4.2.4 Composite film and characterization

Polystyrene pellets were mixed with the desired amount of CNFs suspension in THF at room temperature (0−2.0 wt% filler composite). The mixture was adjusted to 7.5 wt% solid content by adding THF and magnetically stirred for 1−2 h until all polystyrene pellets were dissolved. The polymer mixture was homogenized for 1 min and casted on an aluminum pan. Dry composite films were obtained after solvent evaporation overnight at room temperature. Sample films were placed in an oven for 60 min at 50 °C to ensure complete solvent removal.

Uniaxial tensile testing of composite films was carried out using Instron 5566 equipped with a 10 kN load cell. Strip specimens were prepared by cutting films into 100 mm × 10 mm strips with 0.12 mm average thickness. Sample conditioning and testing were prepared according to ASTM D882-12. Strip specimens were exposed in a temperature- and humidity-controlled

chamber (23 °C and 50 % RH) for at least 48 h prior to the test. The speed of testing was 5 mm/min. Sample break within the grip area was mitigated by lining a Kapton tape. A minimum of four samples was tested for each composite film and the average values were reported.

4.3 Results and Discussion

4.3.1 Effect of grafting on cellulose nanofibrils

The average weight of samples was found to increase by 33.7% gravimetrically after the grafting reaction, and the total polymer fraction of modified CNFs was estimated around 25.2 wt%. This value was relatively consistent with the value determined by the percent area of two consecutive peaks in the rate of mass loss curves from TGA. The peak area above 380 °C, which corresponded to polymer chain scission, showed 29.6 wt% polymer content.

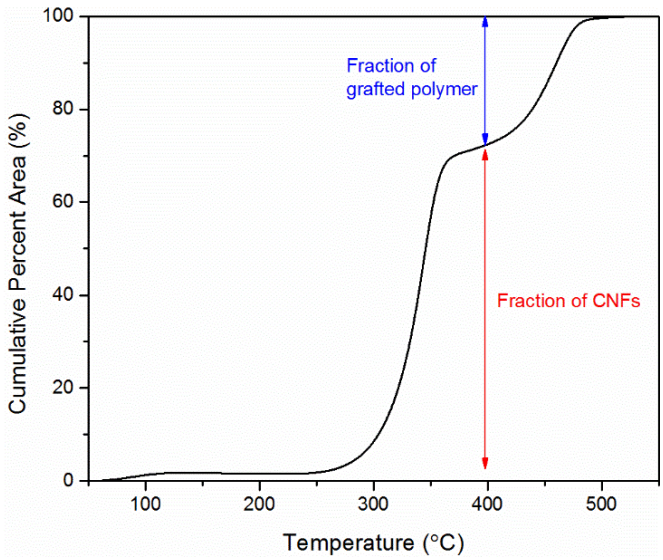

Figure 4.2 Estimated polymer fraction from thermal decomposition analysis for the modified cellulose nanofibrils

To assess the changes in chemical structure due to polymer grafting, ATR-FTIR spectra were measured for each step of the grafting treatment. Figure 4.3 shows the ATR-FTIR spectra of neat CNFs from water suspension, THF pretreated CNFs, and polymer modified CNFs. All CNFs

features were observed in the three spectra: notably, a broad band of hydroxyl groups stretching at 3327 cm^{-1}, ─CH stretching at 2885 cm^{-1}, ─CH_2 bending at 1427 cm^{-1} and wagging at 1315 cm^{-1}, C─O─C stretching of glycosidic linkage at 1161 cm^{-1}, C─O stretching in the 1000−1100 cm^{-1} range, and anomeric C_1─H deformation at 895 cm^{-1}.[165-170] A slight change in band intensity was observed after solvent treatment, notably, at 986 cm^{-1} associated with C(6)─O(6) stretching in the crystalline region of cellulose.[165, 167, 169] In the case of the polymer modified CNFs sample, the additional absorption bands at 1700−1750 cm^{-1} was identified as the monoester functional group.[171, 172] In addition, significant changes in the frequency of C─O stretching in the 1000−1100 cm^{-1} interval confirmed that esterification occurred. Reduction in peak intensity at 1034 cm^{-1} corresponding to C(6)─O(6) stretching may suggest that the new ester linkages arise from the primary alcohol. There was, however, no reduction of band intensity for hydroxyl groups stretching observed. It is possible that the unchanged hydroxyl group peaks originated from isomeric acid groups of anhydride from the coupling polymer agent. The characteristics of the grafted polymer could be witnessed through new absorption peaks of polystyrene aromatic ring deformation at 698 and 756 cm^{-1}, C=C stretching ring vibration at 1583 and 1601 cm^{-1}, and ─CH_2 asymmetric and symmetric stretching at 2922 and 2852 cm^{-1}.[173] Thus, these infrared spectra provided supporting evidence of a grafting reaction that occurred between cellulose and the coupling polymer agent.

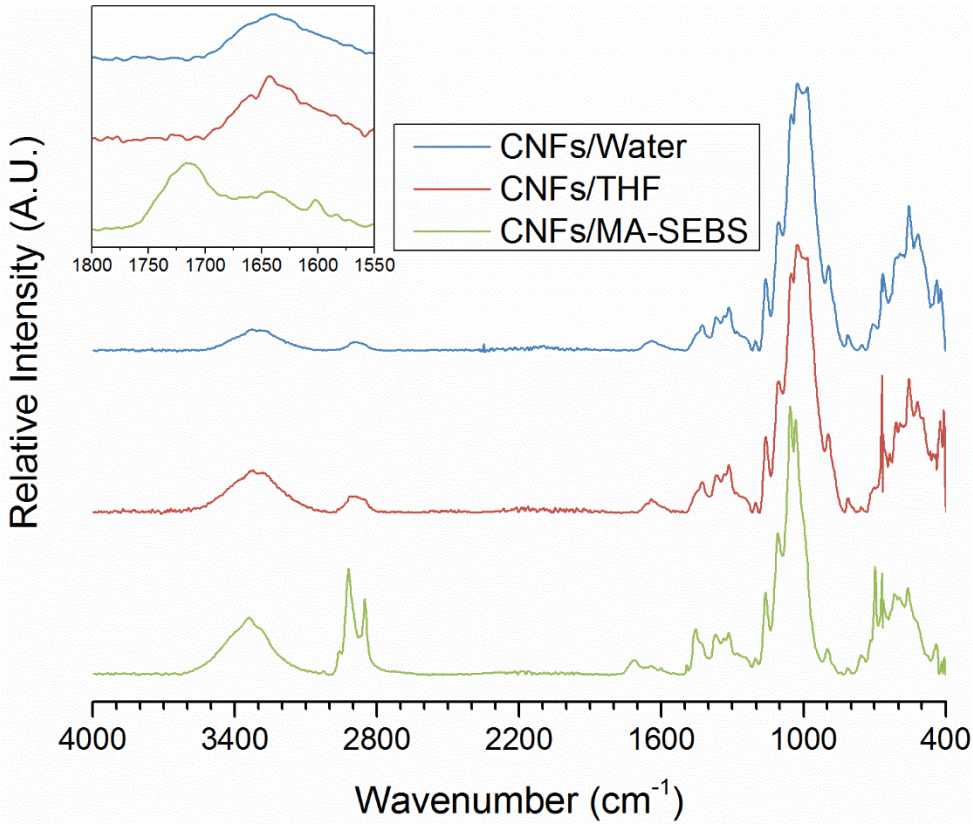

Figure 4.3 ATR-FTIR of neat CNFs, THF-pretreated CNFs, and polymer-modified CNFs.

Further information on the reaction between the hydroxyl group of cellulose and anhydride group of the coupling agent was inferred from acid number using colorimetric titration. The acid number (AN) values for THF-pretreated CNFs, pure coupling polymer agent, and polymer modified CNFs were 3.23, 19.32, and 13.78, respectively. The higher value of acid number value given by the coupling polymer agent suggested the presence of anhydride group and/or its isomeric acid, while a low acid number value for THF pretreated CNFs indicated that the presence of CNFs has little or no significant effect on acid-base reaction. For modified CNFs, the acid number value was closer to that of the neat coupling polymer agent than that of THF-pretreated CNFs. The trend concluded that only a small amount of maleic anhydride moieties from the polymer was actually grafted onto CNFs, while most of the non-grafted maleic anhydride moieties were transformed to their isomeric acids.

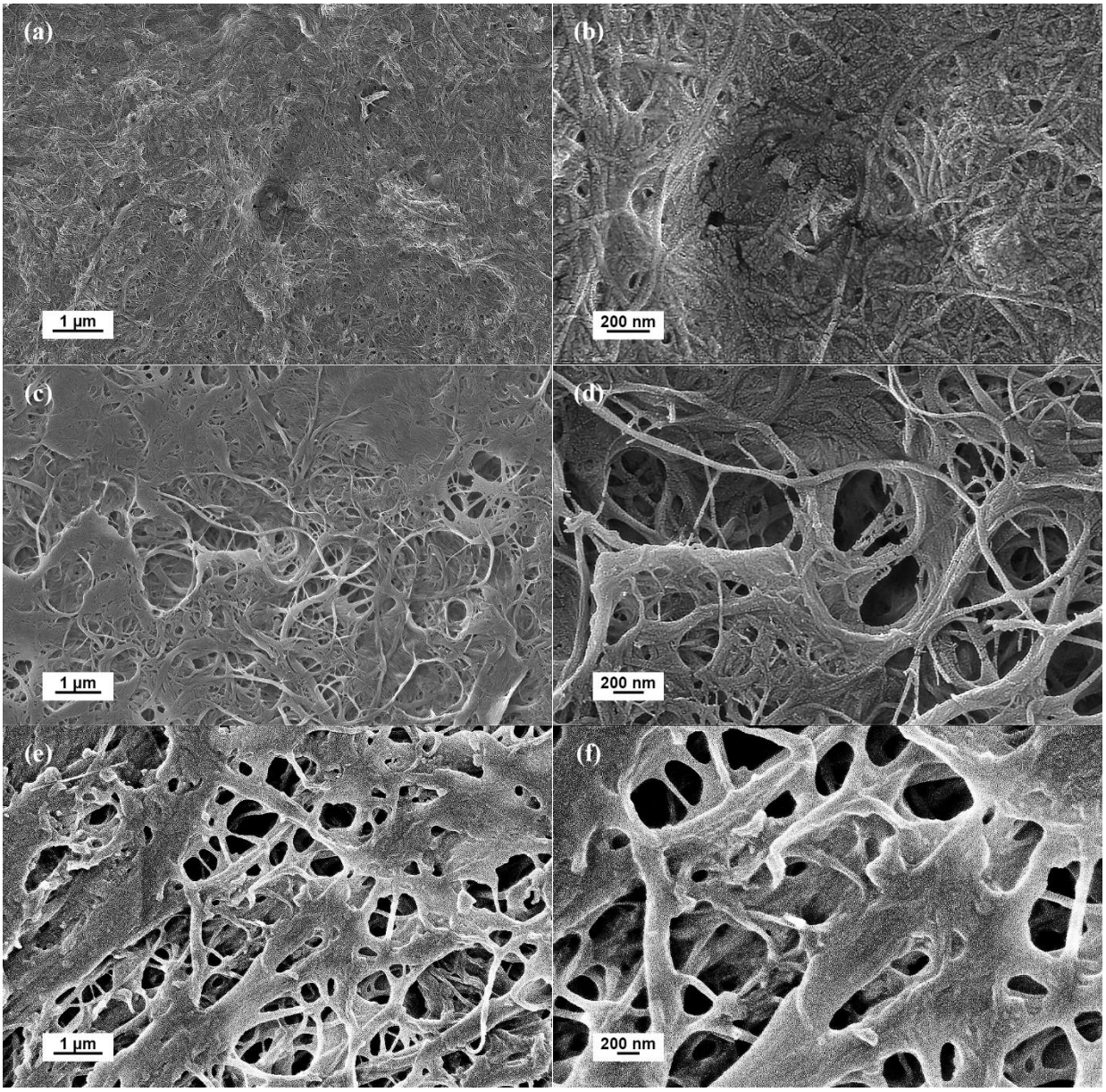

Figure 4.4 FE-SEM images of (a,b) neat CNFs, (c,d) THF-pretreated CNFs, and (e,f) polymer-modified CNFs at two different magnification

Scanning electron micrographs revealed the surface morphology of neat CNFs, THF-pretreated CNFs, and modified CNFs. Figure 4.4 highlights the distinction of between cellulose and polymer surface. The characteristics of the cellulose surface can be observed by the entanglement of nanofibrils as they agglomerate as indicated in Figure 4.4a,b. Figure 4.4c,d shows that the surface morphology of solvent-treated CNFs remains the same as that of neat CNFs. In

comparison to the surface morphology of neat CNFs and THF-pretreated CNFs, the polymer surface on modified CNFs depicted on Figure 4.4e,f has a smoother surface as they entangle.

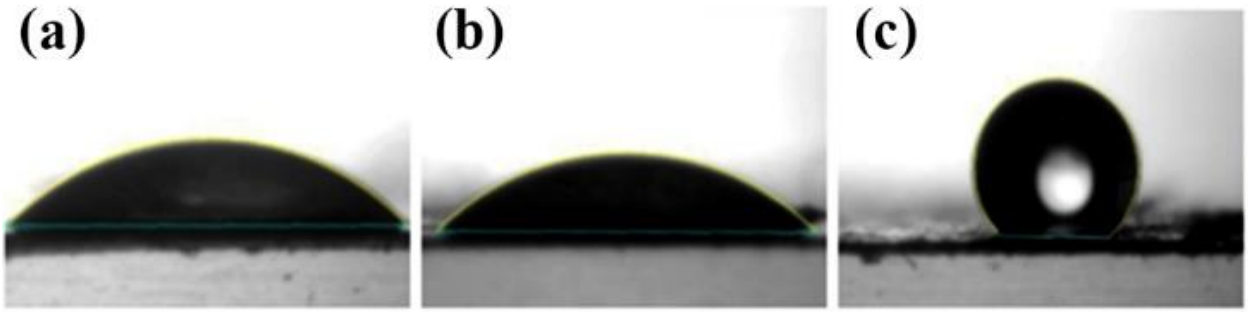

Figure 4.5 Contact angle images of (a) neat CNFs, (b) THF-pretreated CNFs, and (c) polymer-modified CNF film

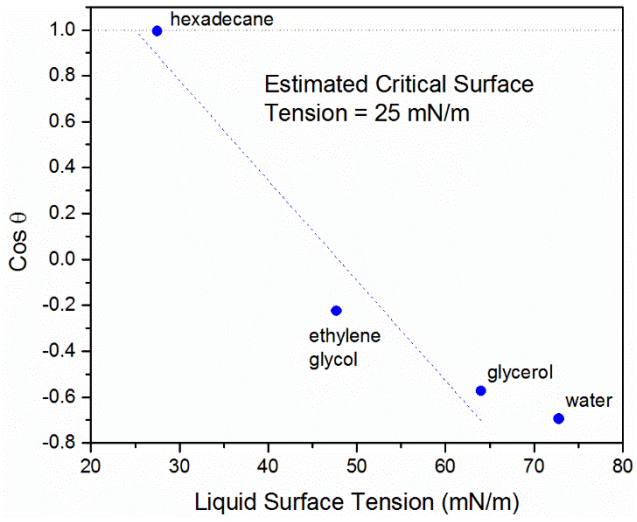

Figure 4.6 Estimation of critical surface tension for modified CNFs film using Zisman plot

Surface wetting of CNFs samples was assessed using the sessile drop contact angle method. Figure 4.5 shows the captured images as water droplet was in contact with CNFs samples. As expected from neat CNFs and THF-pretreated CNFs film, the hydrophilic surface showed averaged contact angles of 48.2° and 46.4°, respectively. In comparison, the presence of grafted polymer on CNFs surface exhibited a hydrophobic property given the maximum contact angle of 130°. The hydrophobic property of the modified CNFs was also indicated by the low surface

energy of the material. Figure 4.6 shows the estimated critical surface tension of 25 mN m^{-1} for modified CNFs film samples using Zisman plot.

The moisture content of CNFs film before and after modification was also measured. The values indicated that polymer-modified CNFs contained 60% less water than neat CNFs. The decrease in moisture content was consistent with the higher contact angle value, in which hydrophobic polymer surface of modified CNFs can block the access of water to the hydrophilic part of CNFs. It is also found that moisture content of THF-pretreated CNFs was 28% lower than that of neat CNFs. Considering surface wetting characteristic was unchanged and a more highly porous film structure was obtained because of the lower capillary force acting on the cellulose nanofibrils,[174] the smaller amount of adsorbed moisture indicated that THF was successfully replaced water after the solvent-exchange, which corresponds to the assumption that the organic molecules introduced during solvent-exchange step are retained and included on drying [175].

Table 4.1 Sessile drop contact angle values, moisture absorption, onset temperature, and temperature at maximum weight loss rate from TGA, and crystallinity from XRD pattern.

	Contact angle (°)	Moisture absorption (%)	Onset temperature, T_o (°C)	Temperature at maximum weight loss rate, T_m (°C)	Crystallinity (%)
CNFs/Water	48.2 ± 2.8	5.0 ± 0.9	296.2 ± 7.3	332.7 ± 9.0	62%
CNFs/THF	46.4 ± 5.6	3.6 ± 0.9	305.4 ± 5.5	340.7 ± 8.7	55%
CNFs/MA-SEBS	130.0 ± 4.1	2.0 ± 0.4	314.7 ± 2.2	348.8 ± 4.6	42%

Figure 4.7a,b shows the TGA data on weight loss (Figure 4.7a) and the first derivative of weight loss (Figure 4.7b) as a function of temperature. The decomposition onset temperature (T_o) and temperature at maximum weight loss rate (T_m) are given in Table 4.1. The weight loss curve showed that the characteristics shape of the curve was unchanged after organic solvent treatment.

Treatment of CNFs with an organic solvent, however, showed an increase in both the onset temperature and the temperature at maximum weight loss rate. For polymer-modified CNFs, a two-step degradation curve was observed, in which the first step corresponded to the decomposition of CNFs and the second step corresponds to the decomposition of grafted polymer. A further increase in both the onset temperature and the temperature at maximum weight loss rate was found for polymer-modified CNFs. Furthermore, a higher temperature at the maximum weight loss rate for grafted polymer at 461.0 °C was achieved in comparison to that of the neat coupling polymer agent at 442.0 °C.

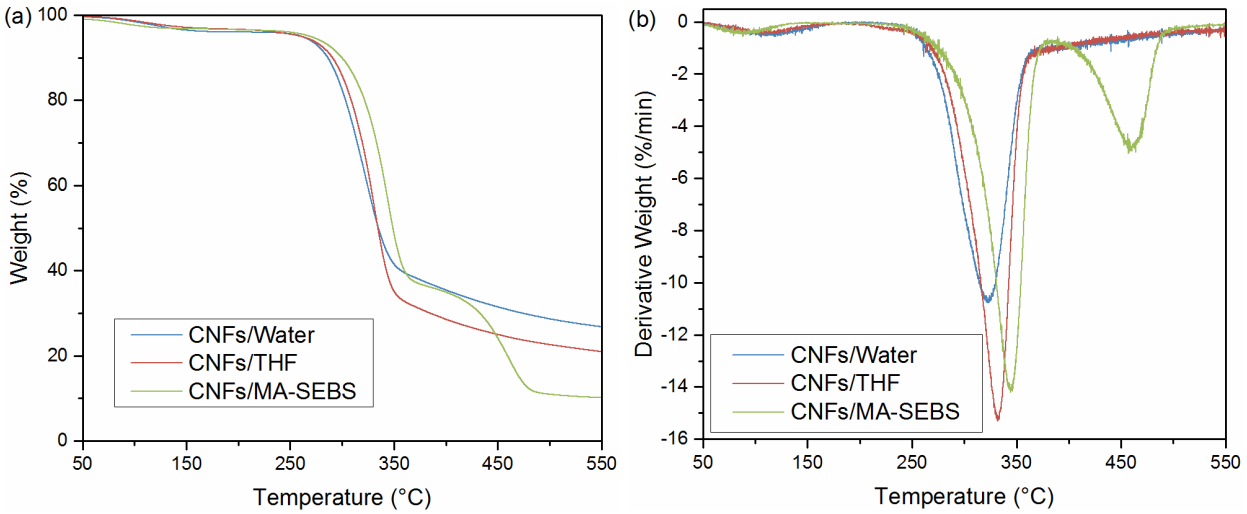

Figure 4.7 Thermogravimetric analysis: (a) weight loss curve and (b) the rate of weight loss curve for neat CNFs, THF-pretreated CNFs, and polymer-modified CNFs

Figure 4.8 shows the XRD pattern for neat CNFs, THF-pretreated CNFs, and polymer-modified CNFs. The spectra revealed a similar pattern for all samples, which suggests that original crystalline structures of CNFs could be well preserved after modification. Table 4.1 presents the calculated crystallinity for each CNFs film. A reduction in crystallinity was observed after exposure with THF and grafting with the polymer. The decrease in crystallinity after organic solvent treatment suggested that the solvent-exchanged process with THF was capable of

disrupting the ordering of cellulose crystal.[176] A further crystallinity decrease after polymer grafting was also observed. However, instead of a disruption of the cellulose crystalline region, the decrease in the ratio of crystallinity was caused primarily because of an increase in the amorphous region originating from the grafted polymer.

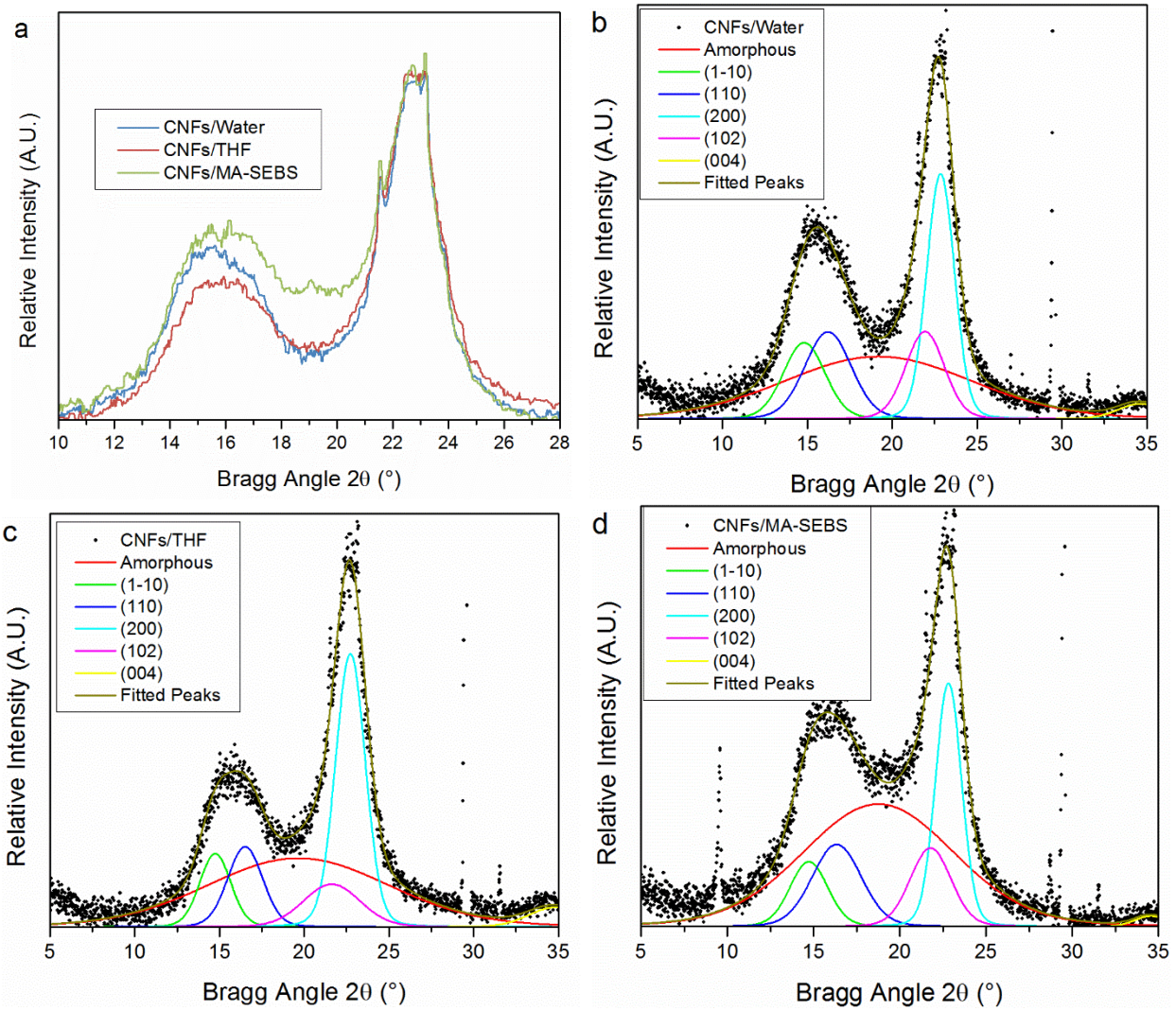

Figure 4.8 (a) XRD pattern for neat CNFs, THF-pretreated CNFs, and polymer-modified CNFs film. Deconvoluted of XRD pattern for: (b) neat CNFs, (c) THF-pretreated CNFs, and (d) polymer-modified CNFs.

4.3.2 Reinforcing effect of modified cellulose nanofibrils

Mechanical properties of polystyrene reinforced with CNFs was assessed using uniaxial tensile testing. Figure 4.9 and Table 4.2 show typical tensile stress-strain curves of brittle-hard polymer films and their measured tensile strength, Young's modulus, and elongation at break for all the composites. The tensile strength, Young's modulus, and elongation at break for control polystyrene film were 20.6 MPa, 1,764 MPa, and 1.32%. Significant improvement in the tensile strength and elongation at break for the composite at lower loadings of 0.5 wt% was observed. The composite showed a tensile strength of 27.5 MPa and elongation at break of 1.77%, which are 33 and 34 % higher than those of neat PS film, respectively. The improvements in both tensile strength and elongation at break are attributed to the high mechanical properties of CNFs and the ability of CNFs to bridge numerous crazes induced by the tensile stress.[177] However, as a higher concentration of CNFs filler was added, a lower tensile strength and elongation at break of composites were observed. This behavior can be attributed to extensive fiber-fiber entanglement and self-agglomeration tendency of CNFs.

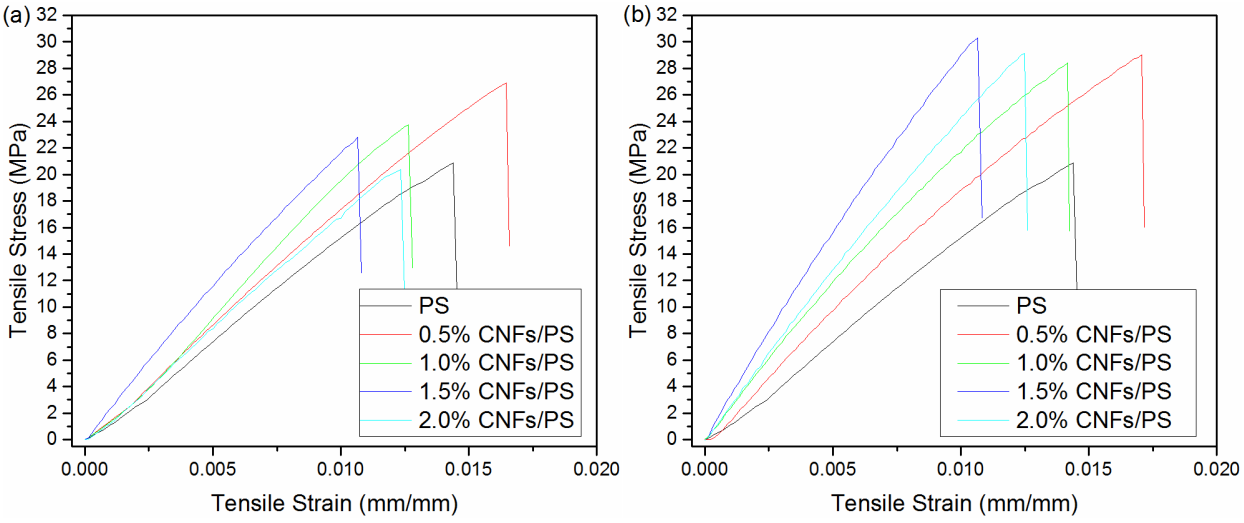

Figure 4.9 Representative tensile stress-strain curves for neat PS and composite films with (a) THF-pretreated CNFs and (b) polymer-modified CNFs.

The mechanical percolation effect of CNFs fillers was demonstrated by the measured Young's modulus. It has been previously reported that cellulose nanoparticle would form a rigid continuous three-dimensional network linked through hydrogen bonding above the percolation threshold.[178] The percolation threshold based on the volume fraction for the filler can be estimated by the following Equation (4.3) [177, 178]

$$\varphi_C = \frac{0.7}{(L/D)} \quad (4.3)$$

where L and D are length and diameter of fillers respectively. In this manner, a CNFs percolation threshold of 1.0 wt% was obtained when using CNFs L/D of 100 and density values of 1.59 and 1.05 g cm^{-3} for CNFs and PS, respectively. The experimental percolation threshold as shown in Table 2 was captured by a large increase in Young's modulus of composite comprising 1.5 wt% CNFs to 2,717 MPa compared to those of the composite comprising 0.5 and 1.0 wt% CNFs at 1,864 and 1,993 MPa, respectively.

Table 4.2 Tensile Strength, Young's Modulus, and Elongation at Break of the PS composite at various loadings.

Filler Content (wt%)	Filler	Tensile Strength (MPa)	Young's Modulus (MPa)	Elongation at Break (%)
0		20.6 ± 1.4	1,764 ± 49	1.32 ± 0.04
0.5	CNFs/THF	27.5 ± 0.3	1,864 ± 29	1.77 ± 0.10
	CNFs/MA-SEBS	29.5 ± 0.7	2,150 ± 29	1.69 ± 0.03
1.0	CNFs/THF	25.9 ± 2.1	1,993 ± 73	1.49 ± 0.14
	CNFs/MA-SEBS	30.2 ± 1.7	2,421 ± 96	1.50 ± 0.03
1.5	CNFs/THF	23.3 ± 1.0	2,717 ± 82	1.10 ± 0.04
	CNFs/MA-SEBS	26.2 ± 1.6	3,060 ± 166	1.00 ± 0.03
2.0	CNFs/THF	20.4 ± 1.4	2,003 ± 124	1.17 ± 0.03
	CNFs/MA-SEBS	27.6 ± 0.9	2,781 ± 91	1.16 ± 0.07

The high improvement of tensile strength and elongation at break for the PS composite reinforced with modified CNFs was found to be relatively the same as that with unmodified CNFs at 0.5 wt%. This result suggested that the optimal reinforcing effect of CNFs filler could be achieved for 0.5 wt% loading without surface modification in PS matrices. The behavior, however, deviated as modified CNFs fillers loading increased above 0.5 wt%. In comparison to the unmodified CNFs suspension, polymer-modified CNFs fillers show a better-reinforcing effect as they could consistently maintain the strength of composite films in between 26.2 and 30.2 MPa. It can be inferred that the difference in tensile strength is attributed to the stronger filler-matrix interaction. In contrast, Young's modulus and elongation at break of PS composite reinforced with surface-modified CNFs exhibit the similar trend as those with unmodified CNFs, in which a large jump of modulus is observed at 1.5 wt% CNFs and the highest elongation at break is obtained at 0.5 wt% CNFs. The result suggested that surface modified CNFs has little effect on Young's modulus and elongation at break. It could also be inferred that fiber-fiber entanglement leading to a percolation network highlighted the changes in Young's modulus and elongation at break for brittle-hard polymer reinforced with CNFs. The slight differences in both Young's modulus and elongation at break for composites with the same amount of filler content could possibly be attributed to the introduction of some fiber aggregates during surface modification method leading to changes in the CNFs dimension.

4.4 Conclusions

Surface modification of CNFs through a solvent-exchanged followed by grafting of a maleated block copolymer coupling agent is reported. SEM showed a distinct difference in CNFs surface morphology before and after polymer grafting. The presence of the grafted polymer promoted the hydrophobic surface and better thermal stability. A decrease in the crystalline phase of CNFs was

found after organic solvent treatment, but no further significant reduction of CNFs crystals was observed during grafting. As a reinforcement filler of a brittle-hard polystyrene matrix, the addition of high-aspect-ratio CNFs at 0.5 wt% exhibited the best mechanical properties among those tried as portrayed by the higher tensile strength, Young's modulus, and elongation at break. Surface-modified CNFs for higher filler loading supported the assertion that stronger interfacial compatibility between the CNFs and hydrophobic polymer matrix contribute to greater strength, while fiber-fiber interaction in the polymer matrix contributes more significantly to the changes in Young's modulus and elongation at break.

CHAPTER V

IN-SITU HYDROPHOBIC POLYMER GRAFTING IN AQUEOUS MEDIUM

5.1 Introduction

With increasing environmental and ecological concerns to reduce water pollutants from organic contaminants frequently occurring from industrial wastewater and oil spills,[135, 179-182] there is a growing demand for more efficient, economical, and environmentally conscious methods to remove oil contaminants or improve oil−water separation. The use of 3D porous sorbent materials that possess outstanding absorption capacity, high oil−water selectivity, and low density appears as a promising approach.

Aerogels, defined as a class of light-weight nanoporous materials,[183-185] show appropriate characteristics in liquid absorption applications. Various types of aerogels as sorbent materials such as carbon nanofiber,[179] carbon nanotube,[180, 186] graphene,[180, 187] silica,[188, 189] cellulose nanofibrils,[95, 136, 190] polymers,[191, 192] and any combination of these with other polymers have been recently reported in the literature. Among these newly developed aerogels, the one based on cellulose nanofibrils (CNFs) provides advantages from an environmental and economical perspective as CNFs are the most abundant renewable resources and their aerogel fabrication requires neither solvent involvement nor complex processes. In addition, it has been well-documented that cellulosic-based aerogels are capable of absorbing a variety of organic solvents.[95, 145] Unfortunately, neat CNFs aerogels exhibit a poor tendency for oil/solvent pick up

This chapter has been modified from the following publication: Fluorine-Free Oil Absorbents Made from Cellulose Nanofibril Aerogels, ACS Applied Materials & Interfaces, 2016, vol. 8, nb. 4, p.2732

from water as abundant free hydroxyls on the CNFs surface can easily be saturated with water. Thus, modification of CNFs into the hydrophobic material is necessary.

Hydrophobic CNFs aerogels have been demonstrated to improve oil/solvent absorption from the water.[95, 135, 136, 182] Most literature reported methods for fabricating hydrophobic CNFs aerogels involve surface hydrophobization after freeze-drying by chemical vapor deposition.[95, 136, 182] This process often requires relatively expensive and toxic fluorine chemicals. Furthermore, the treatment may be a diffusion-limited process such that nonuniform functionalization between the outer layer and inner layer may occur for thick aerogel. For aerogel as an oil absorbent, it is necessary to functionalize the whole aerogel. Mechanical action may be applied to the aerogel, and the deformation of aerogel may occur (such as squeezing) during the application process. As it occurs, the exerted pressure could cause the water to penetrate the hydrophobic outer layer, and the hydrophobic inner layer would prevent water from being stored inside. Another possible approach for improving CNFs hydrophobicity is chemical grafting methods. Although a large variety of chemical grafting methods has been reported,[193] almost all available approaches require an organic solvent medium such as chlorosilane in toluene.[26, 104] Such a process will make aerogel fabrication more complex. In addition, the aerogel would contain inorganic species, Si, which could become an environmental concern upon chemical incineration for product disposal. Surface modification based on adsorption has also been widely used. However, in a comparison to a covalent bond, physical or ionic absorption is reversible, and hydrophobicity could be easily lost due to desorption of the modifiers. Thus, the more environmentally friendly method for CNFs surface modification directly in water to produce hydrophobic aerogel upon freeze-drying remains a challenge. In this study, we report an *in situ* surface modification method that can convert hydrophilic CNFs to hydrophobic species in aqueous medium directly, which has many advantages

compared to an organic solvent or vapor deposition methods. Furthermore, our method does not use expensive and toxic fluorine chemical or inorganic Si, which is an environmentally friendly method to convert hydrophilic cellulose surface to hydrophobic material *in situ*.

Practically, one pot surface modification of CNFs using hydrophobic styrene-acrylic monomer was conducted in an aqueous medium. Hydrophobic aerogels are prepared by freeze-drying of modified CNFs dispersion. The objective is to improve aerogel uptake of oil/solvent from water using nontoxic, less expensive materials and noncomplex equipment. The physical properties of aerogels, such as their low density, highly porous structure, large specific surface area, and excellent elastic property, are also maintained.

5.2 Experimental Section

5.2.1 Materials

Never dried cellulose nanofibrils prepared from mechanically refined bleached softwood kraft pulp were purchased from the University of Maine Process Development Center. The CNFs was mechanically produced without any chemical (carboxymethylation nor TEMPO) pretreatment. The charge density of CNFs is −133 μeq g^{-1}, which was measured by charge titration. Potassium persulfate (KPS), sodium hydrogen carbonate ($NaHCO_3$), pyridine (99.8%, anhydrous), and toluene (99%) were obtained from Sigma-Aldrich. Isopar M Fluid was received from ExxonMobil Chemical. Methanol (HPLC grade) was obtained from Fisher Scientific. Dimethylformamide (DMF) was supplied by EMD Chemicals. Chloroform (99.8%) and dimethly sulfoxide (DMSO) were provided by BDH Chemicals. Styrene (99%) containing TBC inhibitor, n-butyl acrylate (≥98%) stabilized with 4-methoxyphenol, and n-hexane (≥95%) were supplied by Alfa Aesar. Ethylene dimethacrylate (EDMA) was provided by Acros. Kymene™ 920A (a polyamide-epichlorohydrin resin, a cross-linking agent for papermaking) was procured from

Ashland. All chemicals and solvents were used as received without further purification. Deionized water was used in all experiments. See Table 5.1.

5.2.2 Synthesis of hydrophobic CNFs

Polymerization with a monomer dropwise-feeding method was adapted. Specifically, 0.8 wt% CNFs suspension in water was charged into a 250 mL three-necked round-bottom flask connected with a nitrogen gas inlet, a reflux-condenser, and a mechanical stirrer, and mounted in an oil temperature-controlled bath. Nitrogen was bubbled through the suspension under 350 rpm stirring for at least 45 min at 80 °C to remove dissolved and vapor space oxygen. KPS was added as an initiator and the mixture was stirred for 15 min. A 1 mL portion of a monomer mixture containing n-butyl acrylate, styrene, and ethylene dimethacrylate was introduced dropwise over a period of 35 min. During monomer addition, the flask was continuously purged with a nitrogen atmosphere and the stirring rate was kept at 350 rpm. In this condition, monomer drops were presented in emulsion forms in the solution. After monomer addition was completed, the polymerization system was stirred for another 145 min to ensure complete reaction. A buffer was added at the end of the reaction to neutralize pH, and the mixture was allowed to reach room temperature. The suspension was washed with excess water through centrifugation−redispersion for 5 repetitions; 2.3 wt% hydrophobic polymer modified CNFs suspension in water was stored for further use.

Table 5.1 Basic recipe of *in situ* grafting method

Chemicals	Amount (g)
CNFs	1.0
Water	125
KPS	0.156
n-butyl acrylate	0.6 (dropped in)
Styrene	0.25 (dropped in)
EDMA	0.08 (dropped in)
$NaHCO_3$	0.15

5.2.3 Preparation of hydrophobic CNFs aerogel

A 50 mL plastic tube was used as the mold to produce aerogels; 2 wt% kymene with respect to the solid weight of hydrophobic CNFs was added to the suspension. The mixture was stirred under mechanical stirring and transferred into the mold. The hydrophobic CNFs hydrogel was frozen in liquid nitrogen (−196°C) for 5 min. Aerogels were obtained by freeze-drying under 20 mTorr vacuum (VirTis Freezemobile 25EL Sentry 2.0) at room temperature for 4 days. The freeze-dried samples were cured in an oven at 120 °C for 3 h to allow the formation of cross-linked network between kymene and CNFs. The final aerogels were stored in the ambient environment before further use.

5.2.4 Characterization of aerogels

FT-IR spectra of hydrophobic aerogel samples were measured as KBr pellets on a Bruker Vertex 80 V spectrometer in the scan range of 4000−400 cm^{-1} with a resolution 4 cm^{-1}.

Stability of leaching of the surface polymer was evaluated by Soxhlet extraction of aerogel sample using chloroform for 24 h. Samples were dried overnight at room temperature after extraction and subsequently dried under vacuum for 6 h at room temperature. The stability of polymer on CNFs surface to solvent leaching was confirmed by comparing the weight, water contact angle, chemical structure, and thermal decomposition before and after extraction.

Thermogravimetric analysis (TGA) and its first derivative were performed to estimate the amount of polymer on the surface and to assess thermal degradation profile using PerkinElmer STA 6000. A 20 mg portion of the sample was heated from 35 to 600 °C at a rate of 10 °C/min under a flowing nitrogen atmosphere.

Static sessile drop contact angle measurement of aerogel samples was captured using FTÅ200 dynamic contact angle analyzer (First Ten Ångstroms).

Surface morphology of samples was imaged by LEO 1530 thermally assisted field emission scanning electron microscope (FE-SEM), in which all samples were gold-sputtered.

The apparent density of aerogels was calculated by measuring the mass and dimensions using caliper and balance. Porosity of aerogels was evaluated as

$$\text{Porosity}\,(\%) = \left(1 - \frac{\rho_{aerogel}}{\rho_s}\right) \times 100$$

where ρ_{aerogel} is the apparent density of aerogels and ρ_{s} is the bulk density of hydrophobic cellulose, respectively.

The bulk density of hydrophobic cellulose was estimated as a composite of cellulose, polyamide-epichlorohydrin (PAE), and a styrene-acrylic copolymer

$$\rho_s = \frac{1}{\frac{w_{cellulose}}{\rho_{cellulose}} + \frac{w_{PAE}}{\rho_{PAE}} + \frac{w_{copolymer}}{\rho_{copolymer}}}$$

where $w_{\text{cellulose}}$ is the weight fraction of cellulose, w_{PAE} is the weight fraction of kymene, and $w_{\text{copolymer}}$ is the weight fraction of styrene-acrylic copolymer estimated from TGA. The bulk density of cellulose ($\rho_{\text{cellulose}}$) is taken as 1,600 mg·cm^{-3}, while the bulk densities of PAE (ρ_{PAE}) and styrene-acrylic copolymer ($\rho_{\text{copolymer}}$) are assumed 1,150 and 1,080 mg·cm^{-3}, respectively.

Moisture uptake of the hydrophobic CNFs aerogels was evaluated by measuring the total mass change as samples exposed to a temperature- and humidity-controlled chamber for 7 days given by

$$\Delta M(\%) = \left| \frac{W_s - W_b}{W_b} \right| \times 100$$

where W_s is the current mass of aerogels after being exposed to a temperature- and humidity-controlled chamber (23 °C and 50 % RH) and W_b is the baseline mass of aerogels after preconditioning under vacuum for 24 h at room temperature.

BET specific surface area was evaluated from nitrogen adsorption isotherms. Samples were conditioned overnight under vacuum at room temperature. Nitrogen adsorption isotherms were measured at −196 °C using a Quadrasorb EVO system from Quantachrome Instruments. BET analysis was performed in the low relative pressure range between 0.05 and 0.25. Measured BET specific surface area was compared with its theoretical value assuming individual nanofibrils given by

$$BET_{calc}\left(m^2/g\right) = \frac{4}{D \cdot \rho_{cellulose}}$$

where D is nanofibrils width and $\rho_{cellulose}$ is the bulk density of cellulose. The average width of nanofibrils was assumed 37 nm corresponding to image analysis.

Compression tests of hydrophobic CNFs aerogels were performed using Instron 5566 equipped with a 10 kN load cell. Cylinder aerogels were compressed with a speed of 1 mm/min to 80% of its original length.

5.2.5 Oil/Solvent absorption performance

Cylindrical shaped aerogels with a dimension of 20 mm in length and 25 mm in diameter were dried under vacuum at room temperature for a minimum of 24h. Mass of dry aerogels (m_0)

was recorded and immersed in 50 mL of solvent/oil for 1 min. Solvent/oil-saturated aerogels were removed, and excess liquid on the surface was blotted using blotting paper. Mass of wet aerogels (m_w) was measured, and the absorption capacities (C_{abs}) were evaluated as

$$C_{abs}(w/w) = \frac{m_w - m_0}{m_0}$$

Theoretical solvent/oil absorption capacity of aerogels was also calculated on the basis of aerogel pore volume assuming a constant volume of soaked aerogels.

$$C_{calc}(w/w) = \frac{\text{Porosity} \times \rho_{solvent/oil}}{\rho_{aerogel}}$$

Aerogel reusability was evaluated by repetitive cyclic toluene absorption and evaporation sequence. Evaporation of wet aerogels was performed at room temperature overnight and subsequently dried under vacuum for 24 h.

Solvent-induced shape recovery of aerogels was investigated. Aerogels were immersed in an equal volume of pyridine and allowed to be fully saturated. The sample was compressed to 80% of its original length for 10 s and the weight was unloaded. Shape recovery was calculated by the shape change of aerogel measured by the length of cylinder shaped aerogel.

5.3 Results and Discussion

5.3.1 In situ surface hydrophobization of CNFs

The principle of polymer surface modification based on suspension (surfactant-free emulsion) in the heterogeneous systems has been reported for various nanoparticles, such as carbon black,[194] silica,[195-198] and iron oxide.[199] As shown in Figure 5.1, free radical polymerization could occur on the CNFs surface. Specifically, aqueous free radicals initiate polymerization on dissolved monomer to form living oligomers. Although these living oligomers will further grow to form a homopolymer particle in water, in the absence of surfactant, these

living oligomers are unstable[194, 200, 201] and have a tendency to improve their stability through adsorption onto a solid surface such as CNFs. Besides, the free radicals formed in water can also directly attach to the CNFs surface, which causes direct surface initiation of the polymerization. Further growth of the polymer chain on the surface is continued through coagulation of oligomers and polymerization of adsorbed monomers. Both homopolymerization and grafting take place simultaneously in the system and cause competitive reactions. The presence of competitive reactions highlights the importance of controlling the reaction condition to hinder homopolymerization and promote grafting. This was achieved by keeping the concentration of monomer in the reactor relatively low such that aggregation tendency of oligomers was limited. For this reason, a monomer dropwise method was adopted in this study. In addition to free radical formation on monomer, potassium persulfate has also been reported to generate cellulosic radicals.[202-204] It was reported that free radicals could be formed through hydrogen abstraction at C1 or oxidative ring opening at C3.

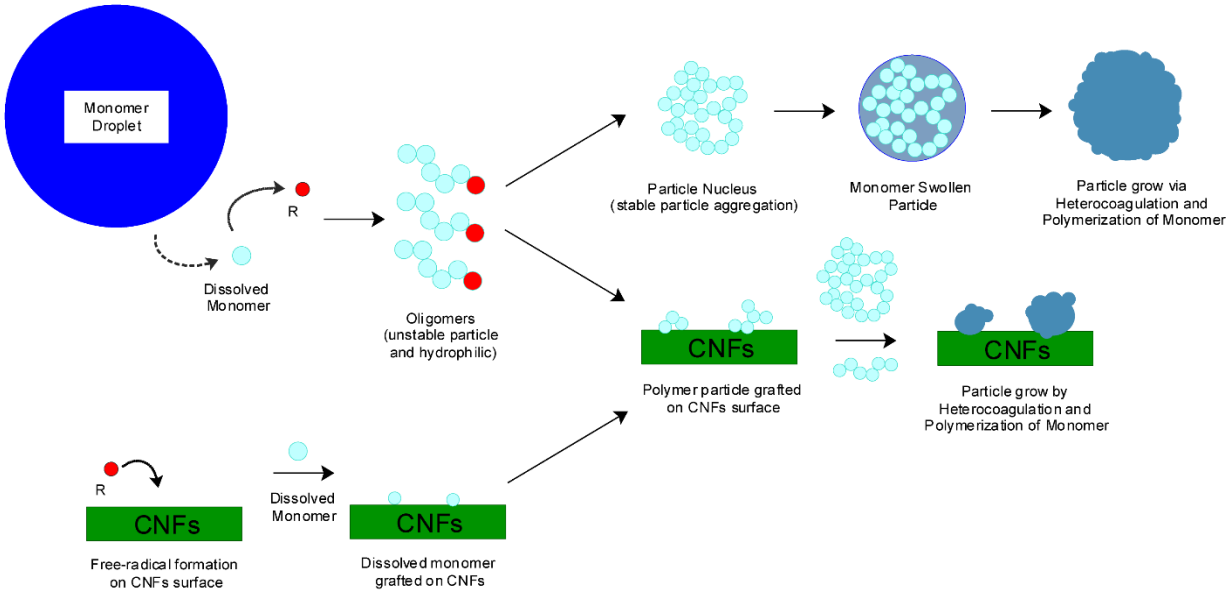

Figure 5.1 Schematic representation of polymer surface modification based on dropwise suspension (surfactant-free emulsion) polymerization.

In the early attempt with n-butyl acrylate and ethylene dimethacrylate, the results showed that some large agglomerates of CNFs were present in the products. This is because self-adhesive characteristics of poly(butyl acrylate)[205, 206] and the cross-linking of ethylene dimethacrylate would lead to bridging effects among fibrils. Reducing the amount of cross-linker is undesirable as the cross-linker promotes resistance toward organic solvent that could dissolve deposited polymer. In order to mitigate the agglomeration problem, a small part of n-butyl acrylate was substituted with styrene. The change in surface wetting of CNFs could be indirectly observed through the sedimentation of CNFs suspension, as reported in similar work using carbon black.[194] Rapid sedimentation of CNFs suspension indicates the presence of high polymer content which completely masks the surface hydroxyl group. However, it is important to have some available hydroxyl groups on CNFs for aerogel preparation. This could be accomplished by controlling the total concentration of styrene-butyl acrylate monomer mixture in the system. Our synthesized surface-modified CNFs suspensions settled slowly after a day.

5.3.2 Hydrophobic CNFs aerogels as bioabsorbent

The as-prepared hydrophobic CNFs aerogels obtained using the styrene-acrylic modified CNFs showed an average density of 23.2 mg cm^{-3}, the porosity of 98.5%, and BET specific surface area of 18.4 $m^2 g^{-1}$. The measured density, porosity, and BET specific surface area are consistent with data reported previously for CNFs aerogel prepared under similar conditions.[136, 183, 185, 190] The lower value of measured BET specific surface area as compared to the theoretical BET surface area for an individual fibril, 67.6 $m^2 g^{-1}$, indicated the presence of CNFs aggregation upon freeze-drying.

The grafting of polymer on the surface of CNFs was identified from ATR-FTIR spectra of hydrophobic CNFs aerogels as shown in Figure 5.2. The pronounced band appearing at 1732 cm^{-1}

together with the less pronounced bands at 1261, 2937, and 2959 cm^{-1} correspond to C=O ester, C─O acrylate, ─CH_2 asymmetric, and ─CH_3 asymmetric stretching of n-butyl acrylate and ethylene dimethacrylate. The peak at 702 cm^{-1} is associated with the presence of the polystyrene aromatic ring. These results suggest that copolymerization of n-butyl acrylate, styrene, and ethylene dimethacrylate is present as attached polymer. The spectra also show that the characteristics of CNFs were maintained as indicated by anomeric C_1─H deformation at 899 cm^{-1}, C─O stretching in 1034−1111 cm^{-1} range, C─O─C stretching of glycosidic linkage at 1161 cm^{-1}, ─CH_2 wagging at 1317 cm^{-1}, ─CH_2 bending at 1429 cm^{-1}, and a broad band of hydroxyl groups stretching at 3339 cm^{-1}.[167, 169, 170, 207, 208]

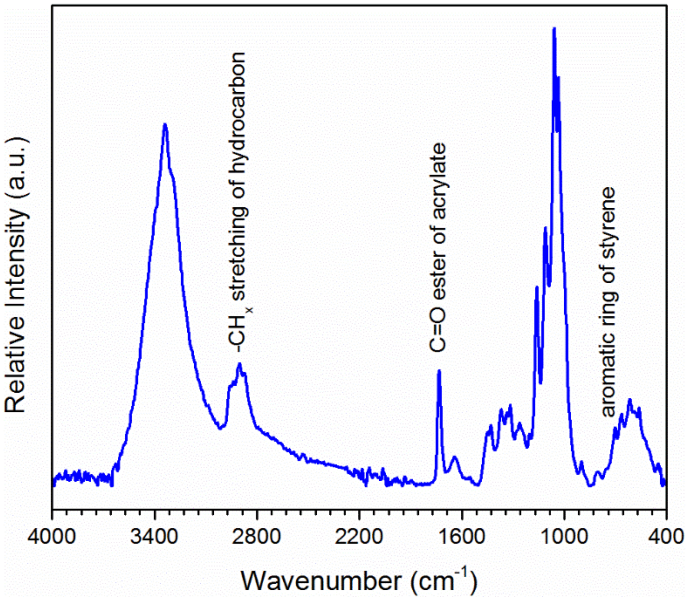

Figure 5.2 ATR-FTIR of hydrophobic CNFs aerogels.

A two-step degradation profile was observed from TGA weight loss curve as indicated in Figure 5.3. The second degradation step starting from 380 °C confirmed the coated polymer chain scission. The amount of polymer deposited on the surface of cellulose nanofibrils was further estimated using the rate of weight loss curves in TGA through the percent area of the second peak.

The as-prepared hydrophobic CNFs aerogels contained 15.3 wt% copolymer located on CNFs surface.

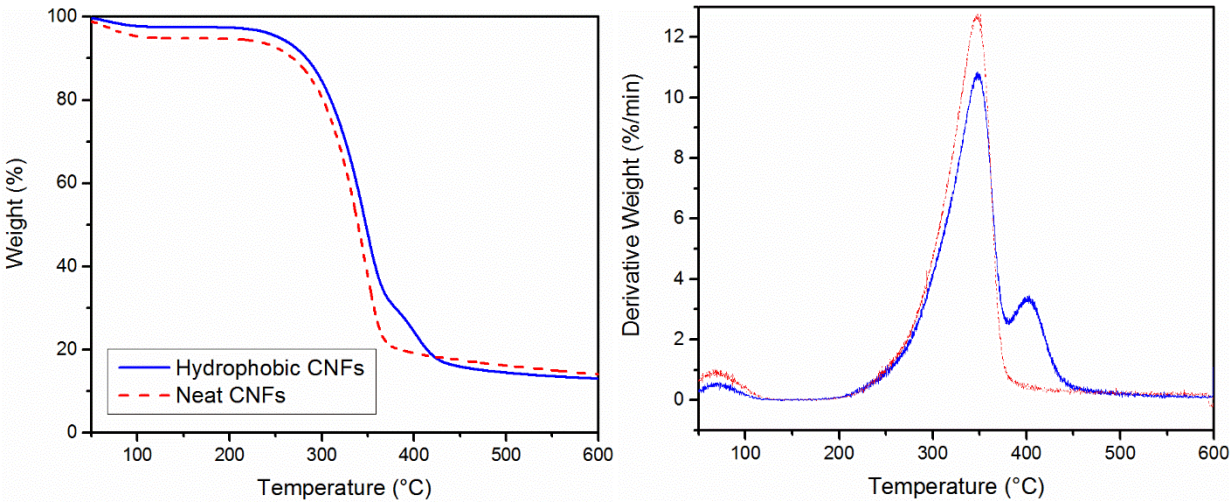

Figure 5.3 Weight loss curve and the rate of weight loss curve as a function of temperature.

The presence of styrene-acrylic copolymer covered on the surface of cellulose nanofibrils would create lower surface energy.[209-212] Furthermore, microporous structure of aerogels can form air pockets that exhibit a Cassie-Baxter wetting state leading to greater surface hydrophobicity. Such hydrophobic CNFs aerogels demonstrated neither water-wettable nor water-absorbing characteristics, as shown by apparent water contact angle of 149° (Figure 5.4a) and aerogel ability to stay afloat on the water surface (Figure 5.4b,c). The hydrophobic CNFs aerogels, however, still allow organic solvent/oil to be absorbed (Figure 5.4d). Excellent oil extraction from water by hydrophobic aerogels was also observed (Figure 5.4e−h). Typical neat CNFs aerogels would be fully wetted as they are in contact with water leading to their inability to pick up chloroform under water. In contrast, hydrophobic CNFs aerogels form water barriers around themselves and only collect chloroform. Similar wetting behavior was also reported in other hydrophobic CNFs aerogels performed using different modification methods.[95, 135, 136, 182, 190] Experiments on water vapor absorption and water uptake upon immersion were conducted for the

as-prepared hydrophobic CNFs aerogels. The aerogels showed 4.1% mass increase after processing for 7 days at 23°C and 50% RH, while their water uptakes were up to 0.5 g/g aerogels. As a comparison, neat CNFs aerogels exhibited 37.3 g water uptake/g aerogels, which is 70 times higher than the hydrophobic CNFs aerogels. These results indicate the aerogels reported in this work have high selectivity in absorbing oil from water.

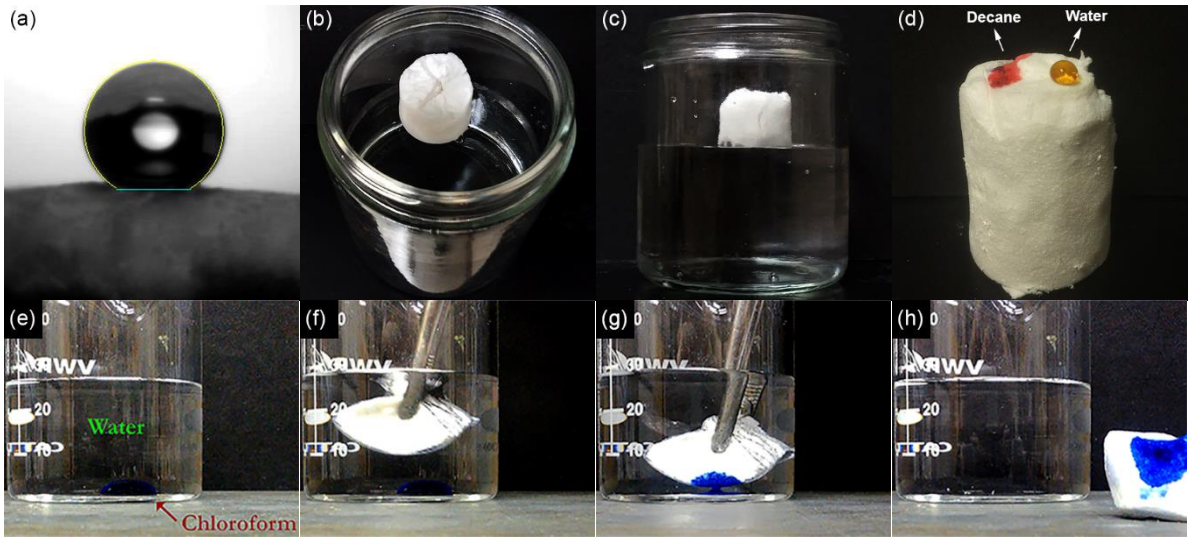

Figure 5.4 Wetting characteristics of hydrophobic CNFs aerogels. (a) Static sessile drop water contact angle of hydrophobic CNFs aerogel. (b,c) Photograph of floating hydrophobic CNFs aerogel on the water surface. (d) Image of the absorbed dodecane droplet (dyed with oil red) and standing water droplet (dyed with methyl orange) on hydrophobic CNFs aerogel. (e─h) Sequential images of chloroform absorption (dyed with oil blue) under water.

The hydrophobic aerogel prepared in this method has hydrophobicity for the whole aerogel and not just for the outermost layer. Although treating just the outermost layer of aerogel would provide the described water barrier characteristic, a small amount of water could still penetrate the aerogel through the presence of large pores. The hydrophobic inner part of aerogel would prevent any water from swelling the fiber.

The stability of a cross-linked polymer layer on the CNFs surface to solvent leaching was verified (Figure 5.5a,b). Overall mass loss of 9.9 wt% was recorded through gravimetric

measurement, while estimated copolymer loss based on the difference in the peak area of polymer scission using TGA is 3.7 wt% (Calculated based on Figure 5.5b). The slight mass loss upon leaching is originated from desorption of ungrafted polymer and non-cross-linked polymer. The reduced amount of coated polymer on the cellulose surface does not significantly affect surface hydrophobicity of the aerogel as shown by the high water contact angle (144°, Figure 5.5d).

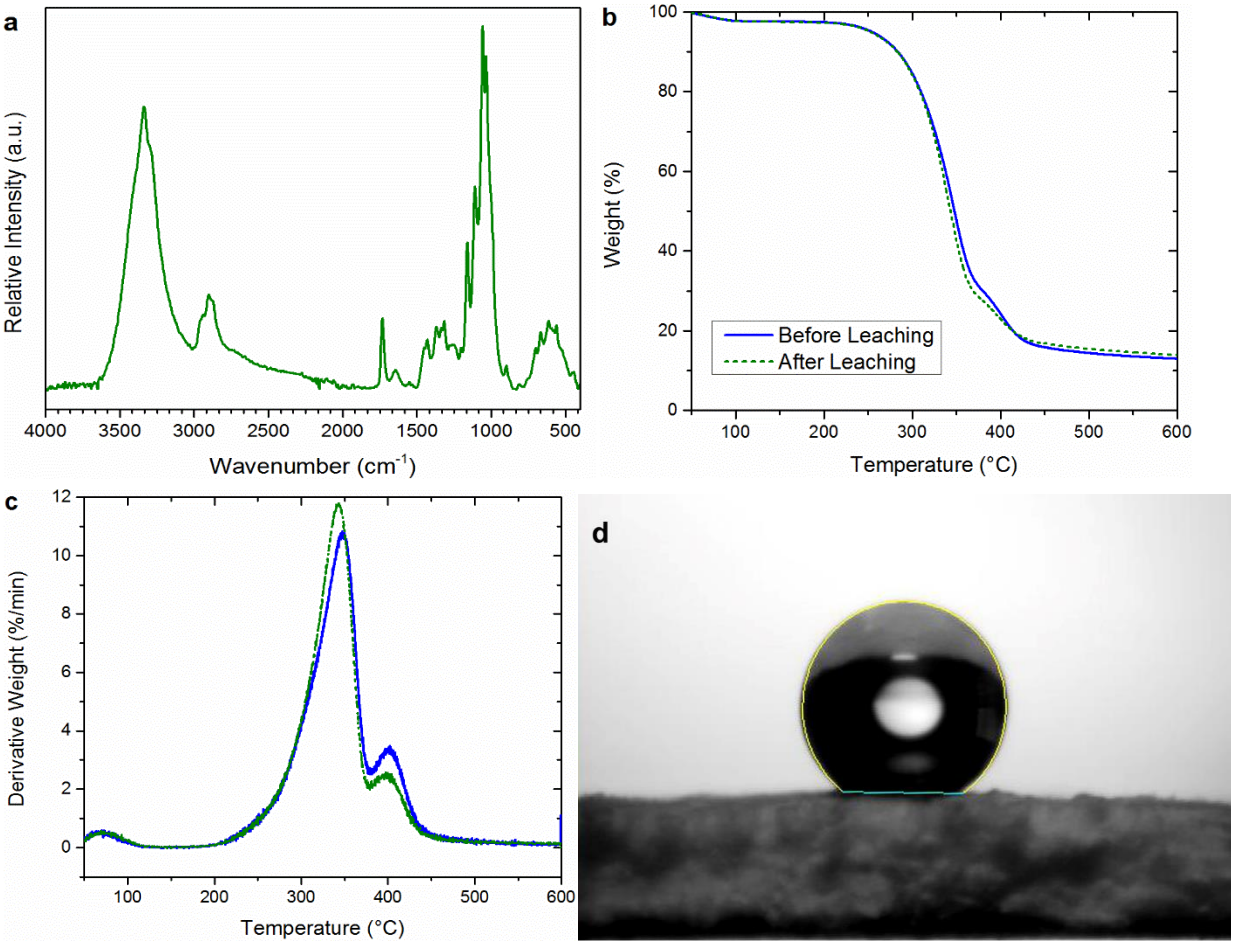

Figure 5.5 (a) ATR-FTIR of the hydrophobic CNFs after chloroform leaching for 24 h. (b) TGA and (c) DTGA for the hydrophobic CNFs before and after leaching test. (d) Water contact angle measurement of the hydrophobic CNFs after leaching test.

The morphology of hydrophobic CNFs aerogels was examined and compared with neat CNFs aerogels using FE-SEM as shown in Figure 5.6a−f. The micrographs of the internal structure of aerogels taken at radial cross-section show a similar macroporous structure for both neat and

hydrophobic CNFs aerogels. All CNFs aerogels exhibited a highly porous open-structured skeleton that comprises sheets formed by CNFs aggregates and interconnected with individual CNFs (Figure 5.6a,b). The same characteristics have also been reported in the previous literature using the same vacuum freeze-drying method.[183, 185, 213] The similarity between parts a and b in Figure 5.6 suggested that the aggregation tendency of nanofibrils in suspension upon chemical modification prepared in this procedure was minimal compared to the aggregation introduced upon freeze-drying. The change in the surface morphology before and after modification was further observed (Figure 5.6e,f). The presence of the deposited polymer layer generates irregular roughness on fiber surface as indicated by the patchy texture of grafted polymer. The masking of surface hydroxyl groups also leads to lower apparent fibrillar joints in the network (Figure 5.6b,d,f). It is expected that the decrease in fibrillary network is caused by less accessible hydrogen bonding on the surface to form covalently bonded interfiber bond entanglement.

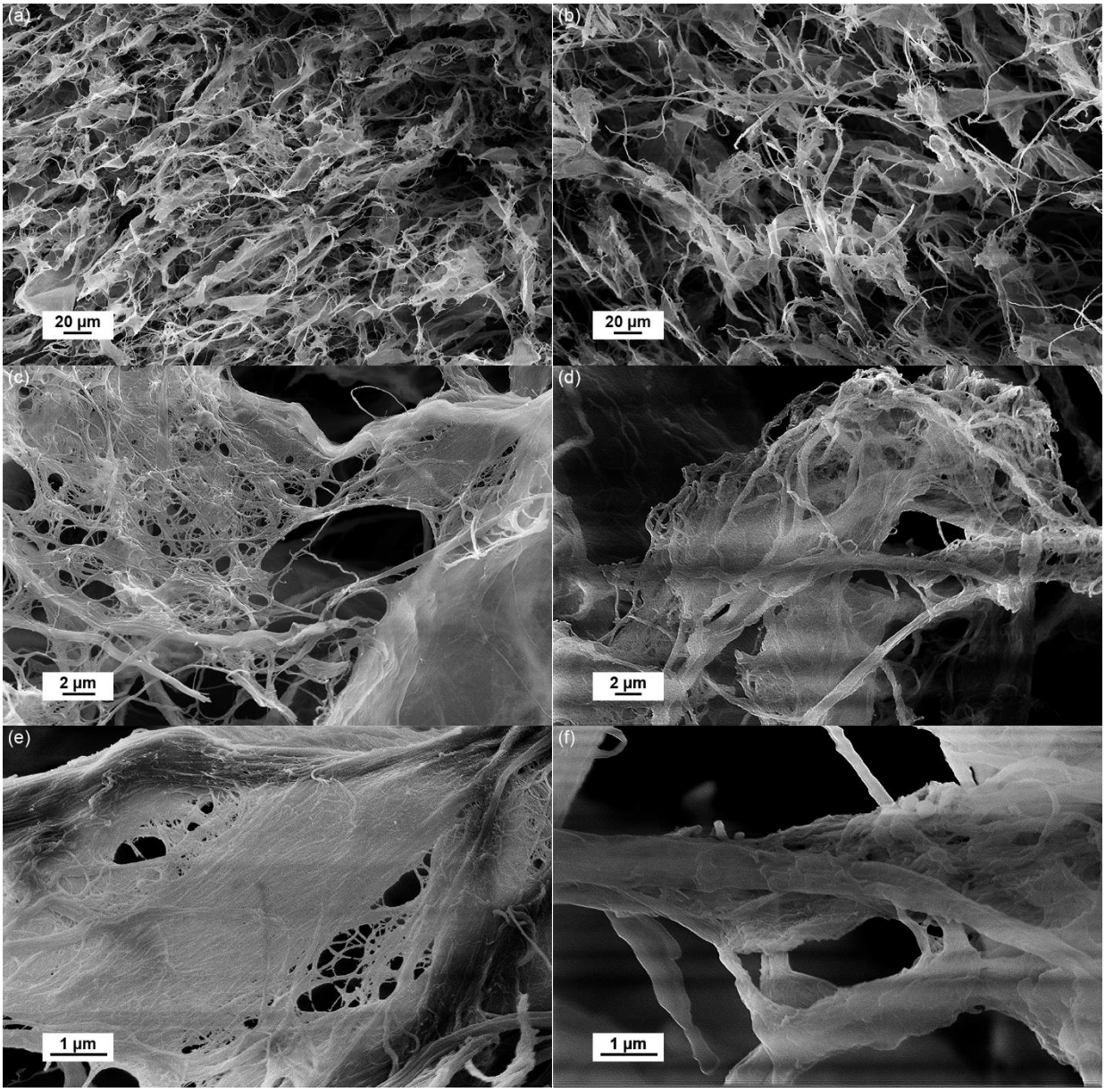

Figure 5.6 FE-SEM images of (a,c,e) neat CNFs aerogels and (b,d,f) hydrophobic CNFs aerogels at different magnification.

Hydrophobic CNFs aerogels are softer than neat CNFs aerogels. Figure 5.7 shows the compressive strain-stress curves for both aerogels of the same density. Neat CNFs aerogels exhibit linear elastic deformation region at low strain below 5% followed by a gradual transition to nonlinear elastic collapse and densification region,[183, 214] while no apparent linear elastic deformation region could be observed for hydrophobic CNFs aerogels. Densification regions for

both CNFs aerogels start gradually above 60% strain. The compressive modulus and maximum stress at 80% strain are significantly reduced for hydrophobic CNFs aerogel. The specific modulus values extracted from a the low strain value for the neat and hydrophobic CNFs aerogels are 2.7 and 0.4 MPa $cm^3 \cdot g^{-1}$, respectively. The maximum compressive stress at 80% strain also decreases from 157 kPa for neat CNFs aerogels to 78 kPa for hydrophobic CNFs aerogels. Lower mechanical properties correspond to the lower both interfiber hydrogen bonding and physical entanglement,[95, 184] which are consistent with previous FE-SEM images.

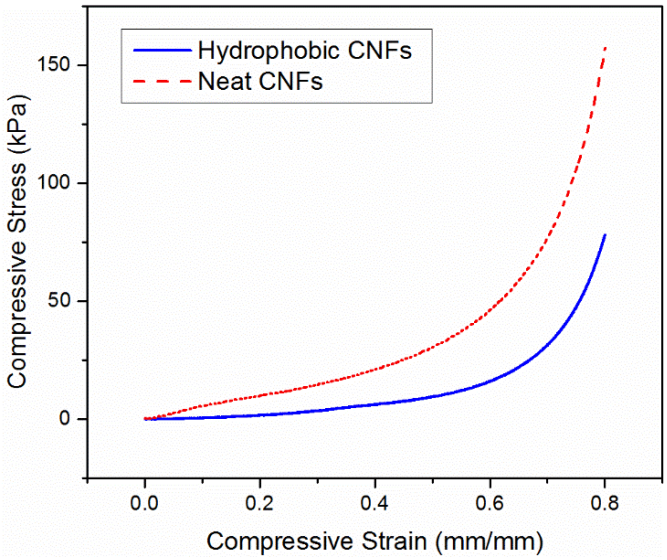

Figure 5.7 Mechanical properties of neat and hydrophobic CNFs aerogels.

The interconnected fibrillar joints for CNFs aerogel framework were estimated from the measured compressive modulus and Clyne et al. modeling approach[184, 215] given by

$$\left(\frac{L}{D}\right)^2 = \frac{9E_{CNF}f}{32E_{aerogel}}$$

E_{CNF} is the modulus of CNFs with a mean width of 37 nm (assumed as 84 GPa), $E_{aerogel}$ is the measured compressive modulus of aerogel, and f is the volume fraction of CNFs in aerogel (given by $\rho_{aerogel}/\rho_s$). The calculated aspect ratios for the interconnected fibrillar joints for both neat and hydrophobic CNFs aerogels are 79.1 and 205.2, respectively. These values suggest that as grafted

polymer masked the free accessible hydroxyl groups of CNFs surface, interfiber hydrogen bonding area formed during freeze-drying for hydrophobic CNFs aerogels was reduced by a factor of 2.6 compared to that of neat CNFs aerogels.

Oil/solvent absorption performance of hydrophobic CNFs aerogels was investigated for various liquids with different polarity, viscosity, and density. Hydrophobic CNFs aerogels exhibit absorption affinity toward both polar and nonpolar liquids as indicated by similar absorption capacities for Isopar M Fluid and methanol at 29.0 and 28.2 $g \cdot g^{-1}$, respectively. In addition, the viscosity difference between those liquids has no influence on the amount of absorbed liquid. Absorption capacities of hydrophobic CNFs aerogels depend strongly on liquid density as indicated in Figure 7. The absorption capacities for toluene with a density of 0.863 $g \cdot mL^{-1}$ and chloroform with a density of 1.49 $g \cdot mL^{-1}$ are 30.0 and 46.6 $g \cdot g^{-1}$, respectively. These values are close to the previously reported hydrophobic nanocellulose aerogels prepared by freeze-drying.[136, 190]

The oil removal capacity of CNFs aerogel is governed primarily by total pore volume of aerogel. Calculated pore volume per gram of hydrophobic CNFs aerogels was 42.4 cm^3. Figure 5.8 indicates that oil uptake of hydrophobic CNFs aerogels could fill approximately 73-84% of theoretical pore volume. The value suggests that at least 16% of total pore volume is inaccessible to the wetting liquid. This is due to the presence of trapped air, which is indicated by the presence of air bubble upon compressing soaked aerogels in the liquid. Also, the lower volume of the maximum absorption compared to the calculated one may be due to the shape change, such as aerogel shrinking, upon removal of wet aerogels from their immersed liquid. The accessibility of pore volume for higher density liquid, such as DMSO and chloroform, was further lowered by 11%. A literature reported the dependence of aerogel density with liquid absorption capacity, in

which denser aerogels held the absorbed liquid better.[95] These results suggest that small pores with relatively thick walls are important parameters for keeping trapped liquid inside and providing high structural strength against pore deformation. Thus, it is believed that the as-prepared aerogels do not have enough small pores to maintain their optimum liquid sorption capacity for heavy oil. The inadequate amount of small pores was in agreement with the presence of CNFs aggregation upon freeze-drying as shown by previous SEM images in Figure 5.6b,d,f. It is expected that even though CNFs aggregation would not change the total pore volume of aerogel, it may shift the pore size distribution toward larger pores.

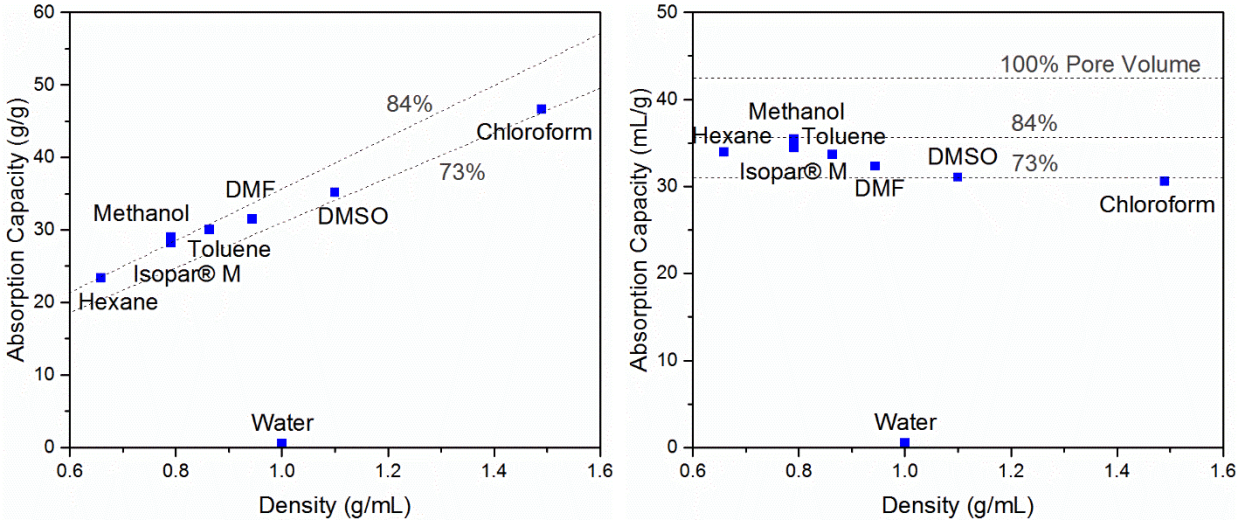

Figure 5.8 Absorption capacities of various oils for hydrophobic CNFs aerogels and their theoretical pore volume capacities.

Reusability of hydrophobic CNFs aerogels as oil/solvent absorbents was investigated by successive absorption-evaporation of toluene as shown in Figure 5.9. During liquid evaporation at room temperature in the first cycle, structural deformation of aerogels occurred as macropores collapsed permanently leading to reduced pore volume. The lower pore volume of dry aerogels for the next repeat cycle leads to lower oil uptake. As a result, a 60% decrease in toluene absorption capacity in the second cycle from the first cycle was detected during solvent uptake. The maximum

absorption capacity, however, was not decreased after second repeat cycle as no further structural deformation was observed.

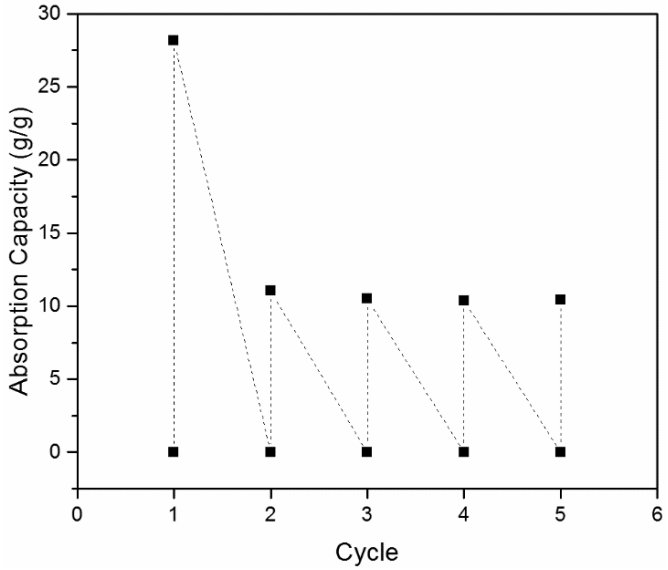

Figure 5.9 Absorbent reusability of hydrophobic CNFs aerogels over five cycles

Neat CNFs aerogels, as shown previously, have a water-induced shape recovery property.[213] As the presence of grafted polymer contributed primarily to alter surface wetting characteristics of aerogels, the solvent-induced shape recovery property of CNFs aerogels could still be retained. However, because the surface modification changes the CNFs' hydrophobicity so the capillary force of aerogel pores as well as the swellability of CNFs, the solvent that could stimulate the shape recovery of the compressed aerogel should be different for modified and unmodified CNFs aerogels. Instead of water that was used in the previous study for neat aerogel shape recovery,[213] it was found that pyridine could stimulate the shape recovery of hydrophobic aerogel as shown in Figure 5.10a─d. The mechanism for pyridine stimulated shape recovery of hydrophobic CNFs aerogels should be similar to that for water stimulated shape recovery of neat CNFs aerogels. Specifically, a solvent with high polarity and moderate surface energy, such as pyridine and DMSO, would penetrate polymer layer and partially swell the cellulose. The swelled cellulose

would expand and create open pore structure, which leads to more liquid penetration. As liquid diffuses into the cellulose network, a hydrodynamic force is introduced allowing the deformed aerogel to expand and recover its shape within several minutes.

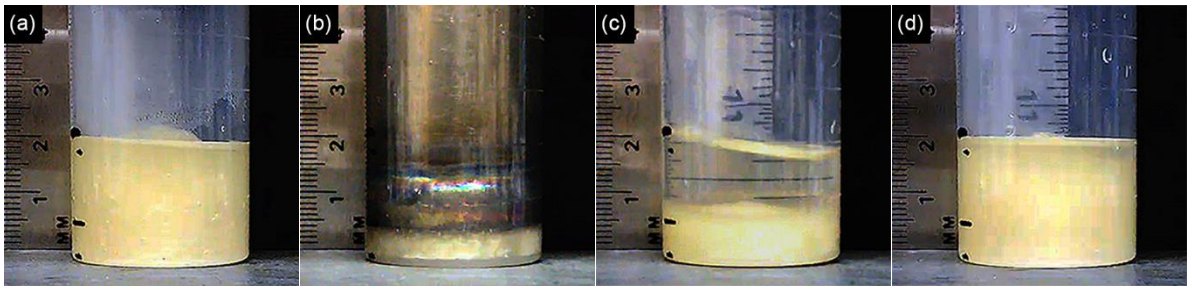

Figure 5.10 Sequential photograph of pyridine-induced shape memory of hydrophobic CNFs aerogel: (a) aerogel initially immersed in equal volume of pyridine, (b) wet aerogel deformation by compressing to 80% its original length, (c) temporary shape upon unloading, (d) shape recovery after 5 min.

5.4 Conclusion

Surface modification of cellulose nanofibrils using styrene-acrylic monomers was successfully obtained in an aqueous medium with a monomer dropwise polymerization method. No fluorine chemical is used in the aerogel and the hydrophobic modification of CNFs was done in water directly rather than in organic solvent. Hydrophobic aerogels were presented using the modified CNFs. The hydrophobic aerogels displayed similar characteristics as those of previously reported CNFs aerogels with fluorine chemical modification, including low density, highly porous structure, and excellent elasticity. The performance of hydrophobic aerogels as absorbents showed high oil removal efficiency from water. The maximum absorption capacities for various oils and solvents are similar to those prepared using chemical vapor deposition method. The hydrophobic aerogels also demonstrated solvent-induced shape recovery ability in several minutes by using pyridine as a solvent.

CHAPTER VI

CELLULOSE NANOFIBRILS-DERIVED CARBOCATALYST

6.1 Introduction

With a growing interest in renewable energy technologies as well as chemical conversion, developing effective and affordable catalysts is extremely important. Although noble-metal based catalysts have a high intrinsic catalytic activity toward sluggish electrochemical reactions, such as oxygen reduction reactions (ORR), oxygen evolution reactions (OER), and hydrogen evolution reactions (HER), they are expensive and often susceptible to the crossover effects.[216, 217] Commercially-viable strategies are proposed by substituting noble-metal catalysts with metal-free catalysts. Among them, carbon-based catalysts have stimulated enormous interest due to their low cost, environmental friendliness, and abundance. Furthermore, both theoretical and experimental studies have shown that functionalizing carbon-based materials with heteroatoms dopants, such as nitrogen, phosphorus, sulfur, and boron, would improve both electrochemical properties and catalytic activities.[123, 217-221] Doped carbon nanomaterials have been successfully prepared as high-performance HER electrocatalysts.[221-227] In particular, co-doping two heteroatoms with different electronegativities (N/P or N/S) on graphene material could boost its electrocatalytic activity attributed to their synergistic effect. However, to the best of our knowledge, most of the reported literature rely on rather expensive carbon materials, such as graphene oxide, and only limited work has been performed using sustainable materials as their carbon precursors.

This chapter has been modified from the paper submitted: Facile Approach for Synthesis of Doped Carbon Electrocatalyst from Cellulose Nanofibrils toward Metal-Free Oxygen Reduction and Hydrogen Evolution

Cellulose nanofibrils (CNFs), as biomass nanomaterials derived from plants, have drawn a great interest as promising raw materials for preparing carbonaceous materials due to their abundant availability, sustainability, biodegradability, inherent nontoxicity, and encouraging potential to be produced in industrial-size quantities.[5, 7, 228] Furthermore, CNFs, owing to its nanoscale diameter and high aspect ratio, can easily form an interconnected three-dimensional network structure, which could facilitate better mass transport and improve electrokinetics in achieving enhanced electrocatalytic performance.[229-231] Recently, N-doped carbon materials derived from nanocellulose have been synthesized and demonstrated experimentally as effective ORR carbocatalysts.[29, 30, 232] The carbocatalysts cannot only promote ORR activity comparable to traditional Pt-based electrocatalysts but also exhibit better electrochemical stability toward methanol contamination. However, there is still no report using N, P, or S-doped nanocellulose based carbon materials as the effective electrocatalysts for HER.

Herein, bifunctional metal-free carbocatalyst toward HER and ORR using N,S-doped carbon nanofibers/N,P-doped graphitic carbon hybrid was synthesized through the deposition of N,P-enriched complex particles onto N,S-doped carbon fiber network. The as-synthesized carbon hybrids showed promising ORR and HER activities, as indicated by their low onset potential and high exchange current density. Thus, this approach is an encouraging method of deriving nanocellulose to construct catalytically active carbon nanofibers toward both HER and ORR.

6.2 Experimental Section

6.2.1 Materials

Never dried cellulose nanofibrils prepared from mechanically refined bleached softwood kraft pulp were purchased from the University of Maine Process Development Center. The CNFs were produced mechanically without any chemical (such as carboxymethylation nor TEMPO)

pretreatment. Tetrahydrofuran (THF) was obtained from EMD. Melamine was provided by BeanTown Chemical. 50 wt% phytic acid was supplied by TCI. Ammonium thiocyanate, 5 wt% Nafion® perfluorinated resin, and potassium hydroxide was procured from Sigma-Aldrich. Reagent alcohol, acetone, and sulfuric acid were received from BDH. Commercial 20 % Pt/C as electrocatalyst reference was purchased from Fuel Cell Store. All chemicals and solvents were used as received without further purification. Deionized water was used in all experiments.

6.2.2 Catalyst preparation

Cellulose nanofibrils suspension in water was solvent exchanged to THF by successive centrifugation-redispersion procedure. 15 g of 1.75 wt% CNFs suspension in THF underwent solvothermal with 0.165 g ammonium thiocyanate at 245 °C for 4.5 h in a 45 mL Parr Teflon-lined stainless steel autoclave. The product was thoroughly washed with acetone followed by DI water to obtain the doped carbon nanofibers.

Table 6.1 Series of carbon hybrids precursors

Sample	NSC (g)	Melamine (g)	Phytic Acid (mL)	MPA:NSC (wt/wt)
1	0.025	0.020	0.08	1
2	0.025	0.075	0.30	5
3	0.025	0.155	0.63	10
4	0.025	0.31	1.25	20

Carbon nanocomposites were prepared by mixing the solvothermal-treated CNFs-derived N,S-doped carbon nanofibers (NSC) with the complex particles of melamine-phytic acid (MPA) according to Table 6.1. For each nanocomposite formulation, 50 wt% phytic acid in water was added into dissolved melamine solution with a molar ratio of 1:1 under stirring for 5 min. The aqueous solution was further cooled down to 5 °C, in which some white precipitates appeared. After at least 2 h, NSC was added and the mixture was further incubated at 5 °C for overnight under static conditions to give the desired NSC/MPA ratio. The solid mixture was separated from

the dissolved excess materials using a centrifuge and further re-dispersed in water. A uniform mixture was obtained under sonication for 30 min. The suspension was allowed to be sedimented before lyophilization under 20 mTorr vacuum (VirTis Freezemobile 25EL Sentry 2.0, USA) at room temperature for 4 days to form the carbon nanocomposite. Pyrolysis of the carbon nanocomposite was performed under nitrogen atmosphere at 400 °C for 2 h followed by another 2 h at 900 °C. The pyrolysis of neat MPA has been tested to yield approximately 2 % solid carbon material.

6.2.3 Characterization of catalyst material

Surface morphology of the samples was imaged by LEO 1530 thermally assisted field emission scanning electron microscope (FE-SEM) coupled with INCA 200 X-Sight de Oxford instruments for energy-dispersive X-ray spectroscopy (EDS) analysis. X-Ray photoelectron spectroscopy (XPS) analysis was performed with a Thermo K-Alpha instrument equipped with monochromatic AlKα radiation at 1486.6 eV X-ray source. Charge neutralization was performed using a low energy flood gun. The samples were supported on Cu substrate. The spectra were calibrated by setting the C1s peak at 284.8 eV. Raman spectroscopy was recorded on a Thermo Nicolet Almega XR instrument with a 488 nm excitation laser beam wavelength. The intensity of the D and G bands was measured from the maximum height of the peaks. X-ray diffraction (XRD) was conducted by scanning angular range (2θ) from 10° to 60° at a scan rate of 1°/min on X'Pert PRO X-ray diffractometer (PANalytical) with CuKα radiation. BET specific surface area was determined from the linear region of the nitrogen adsorption curve in the relative pressure range between 0.05 and 0.25, while the total pore volume was measured at P/P_0 value of 0.99. The samples were conditioned for 20 h under vacuum at 150 °C. N_2 sorption analysis was carried out at -196 °C using a Quadrasorb EVO system equipped with QuadraWIN software to give the

calculated surface area and pore size. Quenched Solid Density Functional Theory (QSDFT) model analysis was used in the evaluation of pore size distribution considering the effects of surface roughness and chemical heterogeneity of carbon.

6.2.4 Electrocatalytic activity

The electrocatalytic activities toward ORR and HER were performed using A CHI 760D electrochemical workstation (CH Instruments) in a three-electrode configuration with a working electrode, a graphite rod as a counter electrode and an SCE reference electrode. A working electrode was fabricated by coating a mirror polished glassy carbon electrode with a suspension of carbon sample. Specifically, the suspension was prepared by dispersing 5 mg of each carbon sample in a solution composed of 350 µL of reagent alcohol, 260 µL of water, and 95 µL of 5 wt% Nafion® binder. A homogeneous suspension was obtained after sonication for 30 min. A 2.5 µL of the as-prepared suspension was dropped onto the glassy carbon electrode with a diameter of 3 mm (0.07065 cm^2 geometric area). The catalyst loading on the electrode was estimated to be 0.25 mg cm^{-2}. The working electrode was dried at 65°C before electrochemical measurement. Linear sweep voltammetry (LSV) and cyclic voltammetry (CV) for ORR tests were conducted in an O_2-saturated 0.1 M KOH electrolyte with a scan rate of 5 and 100 mV s^{-1}, respectively. The electrolyte was bubbled with high-purity oxygen flow for about 20 min before each test and kept constant throughout the whole experiment. The carbon catalyst durability was tested using 1,500 continuous CV cycles and a constant voltage of its maximum cathodic peak. The HER activity was performed in an N_2-saturated 0.5 M H_2SO_4 electrolyte using LSV with a scan rate of 2 mV s^{-1}. The stability of catalyst material was also tested by 1,500 continuous CV cycles from 0 to -0.8 V (*vs.* SCE) and 15,000 s of continuous operation at a constant potential of -0.7 V (*vs.* SCE). All potentials are referenced to the reversible hydrogen electrode (RHE) based on the Nernst equation:

$E_{RHE} = E_{SCE} + 0.059\ pH + 0.2412$. The electrochemical double layer capacitance (C_{dl}) of carbon catalysts was conducted to estimate their effective electrochemical surface area. The measurement was performed by sweeping CV at different rates in the region of 0.15-0.25 V (*vs*. RHE) using a 0.5 M Na_2SO_4 electrolyte. The values of C_{dl} were calculated as half value of the slopes in a linear relationship between the capacitive current ($\Delta J_{|Ja-Jc|}$) at 0.2 V (*vs*. RHE) and the CV scan rates. The calculated electrochemical double layer capacitance was further utilized to normalize the catalyst activities in relation to both their surface area and loading.[222, 226, 233]

6.3 Results and discussion

6.3.1 N,S-doped CNFs carbon nanofibers (NSC)

In the present study, highly porous N,S-doped 3D carbon nanofibers (NSC) was first prepared using *in situ* solvothermal carbonization of CNFs in the presence of ammonium thiocyanate salt. In this step, salt molecules decomposed into reactive N/S species (NH_3, H_2S, and CS_2), in which both nitrogen and sulfur atoms are easily fixed onto the polycyclic aromatic carbon framework formed from the dehydration and polycondensation of cellulose.[234, 235] The average yield of an insoluble solid upon solvothermal carbonization was 55.8 % by gravimetric measurement. An additional weight loss up to 75.3 wt% was observed after high-temperature pyrolysis.

The morphology of the resulting N,S-doped carbon aerogel was characterized by scanning electron microscopy. As shown in Figure 6.1a and 6.1b, the use of solvothermal carbonization followed by pyrolysis could retain the morphology of neat CNFs, in which an interconnected three dimensional porous network is clearly observed. In addition, no agglomerated microsphere is found on the fiber surface, which is different from other reported carbonized cellulose.[114, 118, 236] The interconnected carbon network is beneficial to facilitate efficient long-range transport of

electrons. Composition mappings of pyrolyzed NSC were analyzed using EDS. Figure 6.1d and 6.1e show homogeneous distributions of nitrogen and sulfur heteroatoms across the surface of carbon nanofibers.

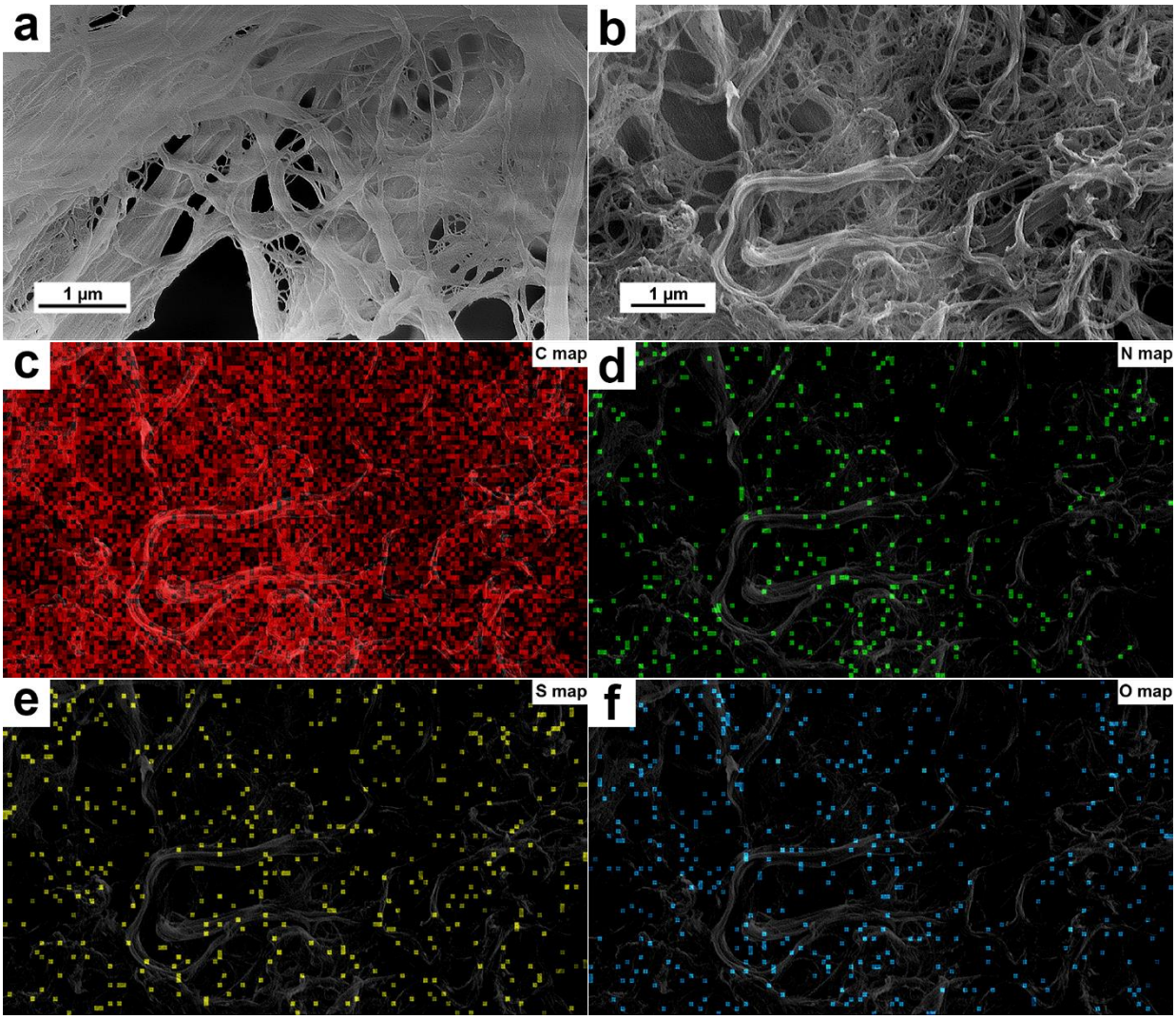

Figure 6.1 (a) SEM image of neat CNFs aerogel. (b) SEM image of carbonized NSC revealing its 3D network nanostructure and the corresponding EDS elemental mapping of (c) carbon (red); (d) nitrogen (green); (e) sulfur (yellow); and (f) oxygen (blue)

The carbon structure, quantitative amount of doping, and chemical state of dopants greatly influence the electrocatalytic performance of carbon-based material.[237] Raman spectroscopy is an important tool to investigate the structural information of carbon-based materials and to give an

insight into the electrochemical properties of the carbon material. As presented in Figure 6.2a, Raman spectra show the characteristic peaks of graphitic layers (G band) at around 1,587 cm^{-1}, disordered carbon at around 1,362 cm^{-1} (D band), and the second order of the D band (2D band) at around 2,830 cm^{-1}. The presence of a broad and weak 2D band indicates the characteristic feature of few-layered graphene lattices in the as-prepared carbon samples. Figure 6.2a also indicates sharper first-order D and G bands with increasing pyrolysis temperature. This trend suggests that NSC undergoes an increase in carbon crystallite size and more graphitic domains with increasing pyrolysis temperature. The same result has also been confirmed in literature.[238] Larger crystallite size, which consists of a highly-ordered carbon structure, is a preferred structural property for carbocatalysts as it would enhance the electron migration into or out of deeper carbon structure. In addition, Figure 6.2a depicts an increasing intensity ratio of the D band and G band (I_D/I_G) with increasing pyrolysis temperature. The Raman I_D/I_G ratio is a good indicator to represent the level of defects in carbon material caused by the integration of heteroatoms species in the carbon framework. Therefore, an increasing I_D/I_G ratio until a pyrolysis temperature of 900 °C may indicate that more in-plane heteroatoms (graphitic-like) exist, which agrees with the results of XPS presented in Table 6.2. Correspondingly, the decrease in I_D/I_G ratio with pyrolysis temperature of a 1,050 °C implies the severe decomposition of in-plane heteroatoms. Thereby, pyrolysis of NSC at 900 °C (NSC900) should be assumed as the most optimal functionalized carbon structure.

Table 6.2 Physiochemical properties of various NSC samples

Sample	Elemental Composition (At. %)				Raman I_D/I_G ratio	BET surface area ($m^2\ g^{-1}$)	Pore volume at $P/P_0 = 0.99$ ($cm^3\ g^{-1}$)
	C	N	S	O			
NSC	68.2	9.4	2.5	19.9	-	-	-
NSC450	78.1	15.5	1.1	5.3	0.76	241	0.61
NSC600	83.4	13.4	0.5	2.6	0.82	289	0.68
NSC750	88.9	7.5	0.4	3.2	0.83	359	1.12
NSC900	91.4	3.4	0.5	4.7	0.88	612	1.26
NSC1050	93.6	1.6	0.5	4.3	0.86	504	0.86

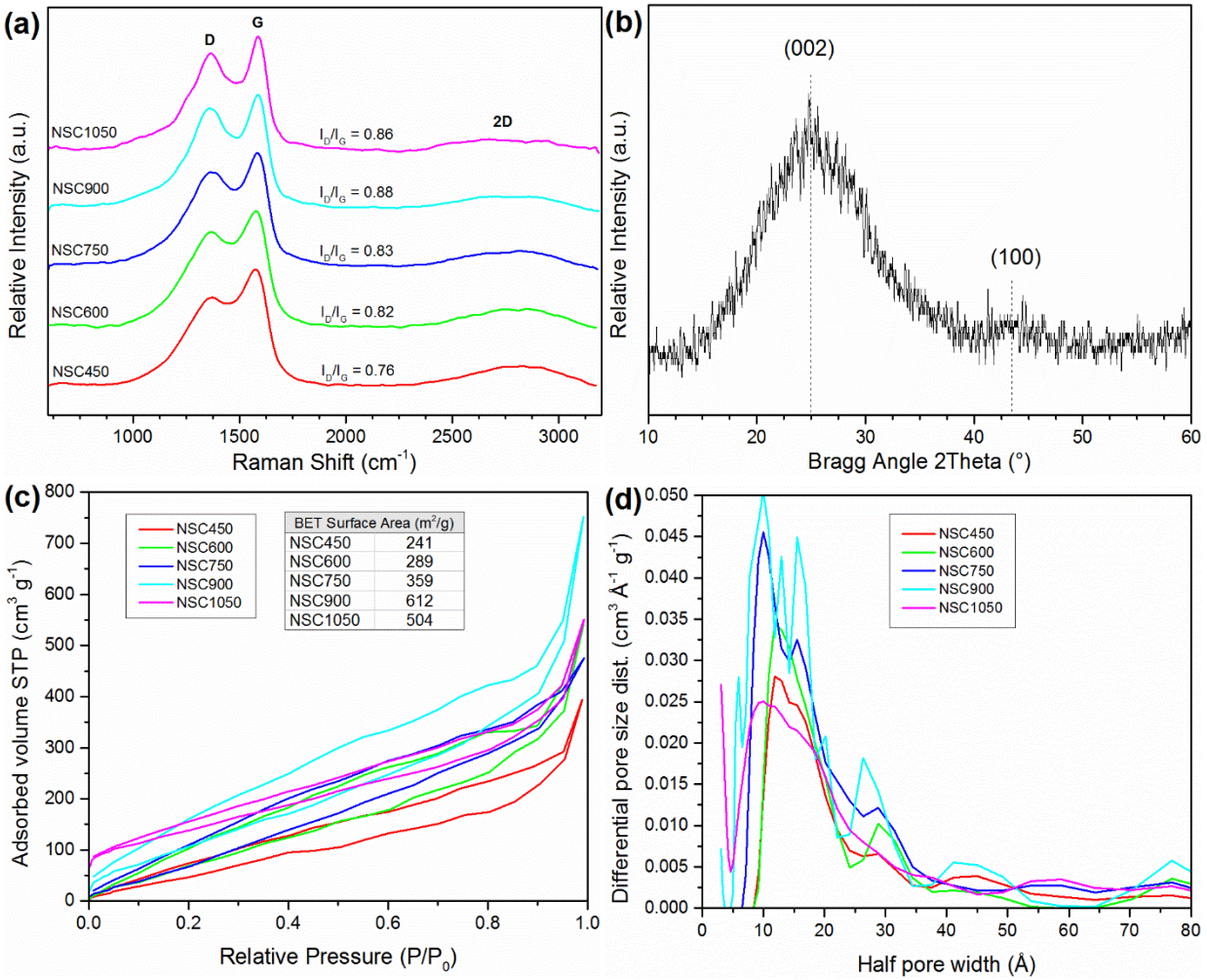

Figure 6.2 (a) Raman spectra of NSC samples pyrolyzed at different temperatures, (b) XRD pattern of NSC900, (c) N_2 physisorption isotherms, and (d) corresponding pore size distribution of NSC samples pyrolyzed at different temperatures

Further structural characterization of carbon material was conducted by XRD. Figure 6.2b indicates that NSC900 exhibits two diffraction peaks at 24.9° and 43.5°. The two broad peaks of the XRD pattern suggest that there are partially disordered carbon structures. The higher graphitic interlayer spacing at 3.53 Å compared to that of perfect graphite at 3.35 Å indicates a turbostratic structure. Based on the Scherrer equation, the crystal thickness of (002) lattice is 7.85Å and the carbon structure could be modeled as 2-3 (averaged at 2.2) layer-stacked sheets, which is in agreement with the previous 2D band of Raman spectra.

Nitrogen adsorption-desorption measurements were performed to quantify the specific surface area. Figure 6.2c shows that the specific surface area of different pyrolyzed NSC varies between 241 and 612 $m^2 g^{-1}$ with pore volume in the range of 0.61 to 1.3 $cm^{-3} g^{-1}$. In addition, the pore size of pyrolyzed NSC is dominated by mesopores with pore radii in the range of 5 to 25 nm, as highlighted in Figure 6.2d. It has been reported that an electrocatalyst with sufficient mesopores would produce an effective electrochemical activity.[239, 240] Increasing specific surface area was also found with increasing pyrolysis temperature with a maximum at 900 °C. The observed trend is supported by the results in the literature.[223, 241] Figure 6.2d further suggests that when the pyrolysis temperature is above 900 °C, decomposition of some carbon structure causes the collapse of mesopores to generate more micro- and macropores. In addition, it may also be possible that a tar-like substance at 1,050 °C would form an intermediate melt that could easily block some pores.

The elemental composition and chemical state of the pyrolyzed NSC were further investigated using XPS. As shown in Figure 6.3a and Table 6.2, the quantitative elemental analysis yields carbon-based material consisted of integrated nitrogen and sulfur atoms. Higher pyrolysis temperatures lead to the reduction of oxygen, nitrogen, and sulfur content, which stipulates the thermal instability of nitrogen and sulfur dopants in the carbonaceous nanofiber. The as-prepared

NSC900 is composed of 3.4 % N, 0.5 % S, and 4.7 % O. The amount of nitrogen atoms has been found to be similar to other nitrogen-doped carbon materials, prepared through different synthetic routes, with the capability to enhance their electrocatalytic performance.[242-245]

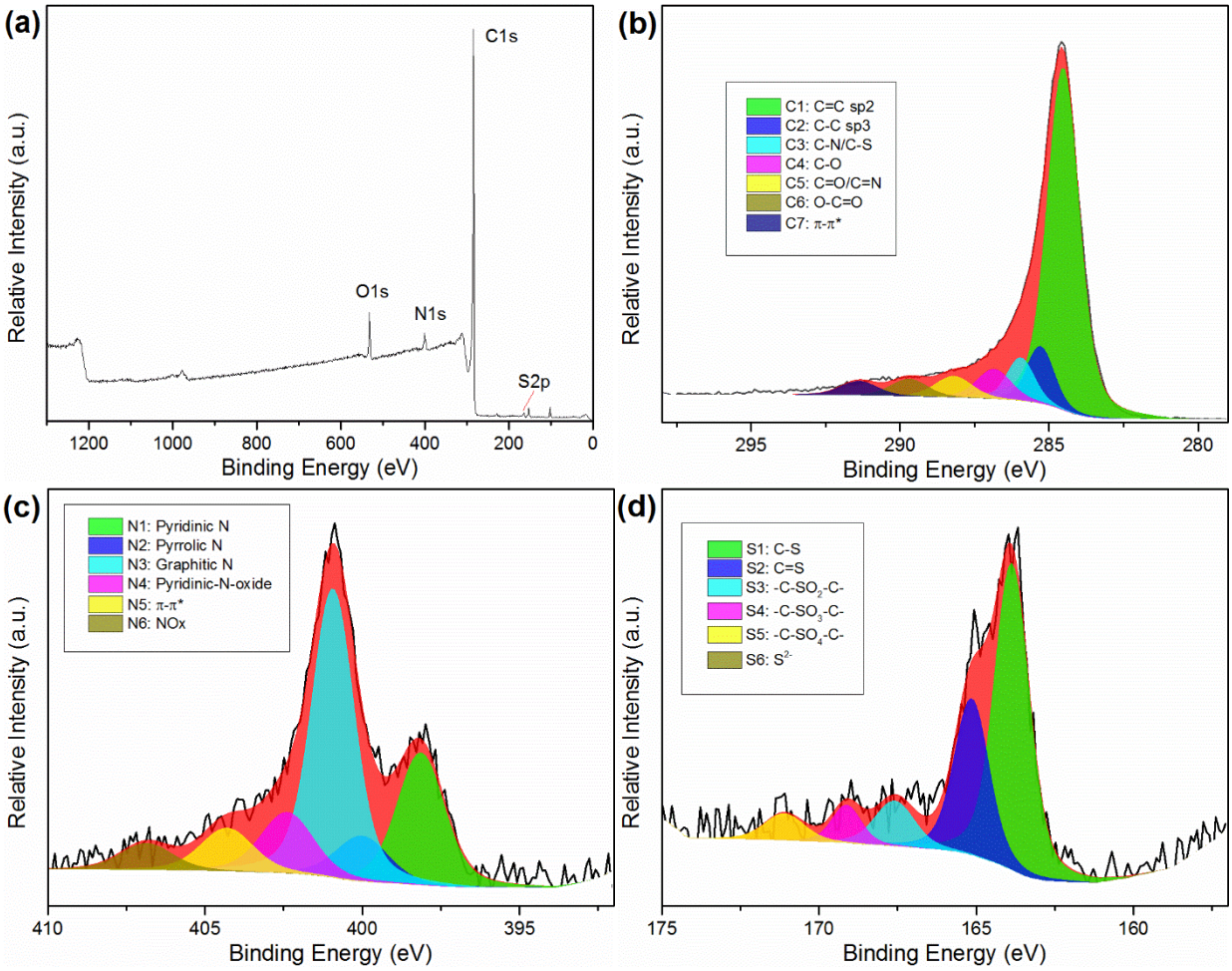

Figure 6.3 (a) XPS survey spectrum and high-resolution scans of (b) C1s (c) N1s and (d) S2p electrons of NSC900

Further analysis on high-resolution XPS spectra of individual elements was utilized to evaluate their chemical states, in which more detailed information are given in Table 6.3. The high-resolution C1s spectrum could be deconvoluted into seven components.[242, 246-249] The sp^2 C=C or aromatic group and sp^3 C-C are centered at 284.5 and 285.1 eV, while carbon atoms connected to N, S, and O heteroatoms are represented by C-N/C-S at 285.8 eV, C-O at 286.7 eV,

C=O/C=N at 288.1 eV, and O-C=O at 289.7 eV. The small peak at 291.5 eV corresponds to π-π shake up. Fitting the N1s signal shows the presence of six nitrogen states denoted by pyridinic-N at 398.3 eV, pyrrolic-N at 399.9 eV, graphitic-N at 401.0 eV, pyridinic N-oxide at 402.4 eV, π-π* satellite at 404.3 eV, and entrapped NO_x at 406.8 eV.[250-252] The chemical states of sulfur in the S2p spectrum contain the covalently bonded S atoms in aromatic carbon network, indicated by $S2p_{3/2}$ and $S2p_{1/2}$ doublet peaks centered at 163.8 and 165.2 eV, and the oxidized species attributed to -C-SO_x-C- with peaks at 167-171 eV. It should be noted that some samples treated at low temperature have polysulfide-like S^{2-} species with a peak centered at 161.6 eV.[253] The O1s signal is fitted into four components: C=O at 530.9 eV, C-O/-O- at 532.1 eV, O=C-OR at 533.2 eV, and NO_x at 534.5 eV.[222, 254-257]

Table 6.3 XPS peak assignments for NSC samples pyrolyzed at different temperature

Peak	Chemical State	Fraction of species (%)					
		NSC	**NSC450**	**NSC600**	**NSC750**	**NSC900**	**NSC1050**
C1s	sp^2 C=C	28.9	46.1	42.4	49.0	65.5	77.2
	sp^3 C-C	21.9	23.5	26.2	17.9	9.4	0.1
	C-N/C-S	14.5	12.8	-	11.7	7.1	8.7
	C-O	25.0	7.0	15.6	8.3	6.2	4.8
	C=O/C=N	7.5	4.5	6.6	5.2	4.8	3.4
	O-C=O	1.5	3.5	5.4	4.4	3.9	3.5
	π-π* shake up	0.7	2.8	3.8	3.4	3.2	2.5
N1s	Pyridinic	33.5	43.2	44.3	30.9	22.6	11.1
	Pyrrolic	51.0	33.5	11.4	6.8	8.7	0.2
	Graphitic	14.2	17.9	33.7	44.5	43.8	60.6
	Pyridinic N-oxide	-	1.5	4.3	8.6	11.6	0.4
	π-π* satellite	0.9	2.0	3.9	5.8	8.3	17.9
	entrapped NO_x	0.4	2.0	2.4	3.5	5.0	9.9
S2p	C-S-C	42.3	41.4	45.1	43.7	44.3	47.9
	C=S	42.3	41.4	45.1	43.7	44.4	48.0
	$C-SO_2-C$	3.2	4.8	3.4	5.9	5.0	0.2
	$C-SO_3-C$	2.0	1.9	3.2	3.7	3.1	1.5
	$C-SO_4-C$	0.7	2.1	2.3	2.5	3.0	1.7
	S^{2-}	9.6	8.4	1.0	0.6	0.1	0.7
O1s	C=O	5.0	24.9	19.1	7.5	7.0	2.3
	C-O/-O-	21.2	51.3	36	70.4	72.4	81.8
	O=C-OR	73.0	19.5	36.5	17.4	16.0	13.0
	NO_x	0.8	4.4	8.4	4.7	4.7	2.9

The high resolution carbon spectrum in Figure 6.3b reveals that the majority fraction of carbon species is sp^2 C=C carbon, while the fitted spectra of nitrogen and sulfur species are dominated with graphitic nitrogen and thiophenic sulfur, as shown in Figure 6.3c,d. It was also

noted that pyrolysis temperature was found to affect the transformation of unstable heteroatoms dopant (pyrrolic nitrogen and S^{2-}) toward more stable structurally-bound heteroatoms (pyridinic/graphitic nitrogen and thiophenic sulfur), as presented in Table 6.3 and Figure 6.4, which is in agreement with the previously reported literature.[242, 258] The appearances of oxidized species are also identified across all samples, which strongly denote the existence of an oxidation reaction due to the presence of residual oxygen species of carbonized CNFs upon solvothermal treatment.

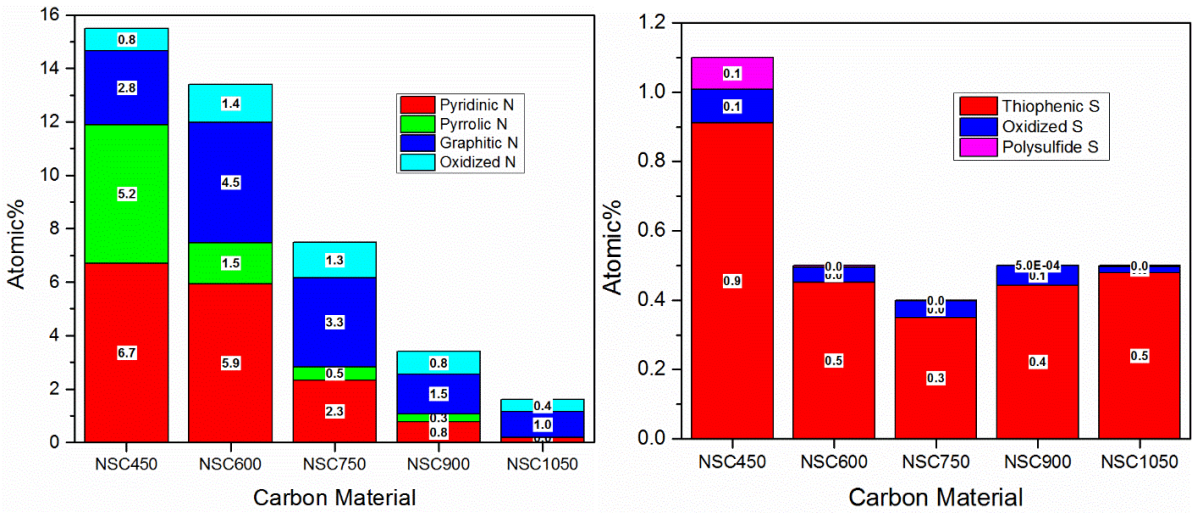

Figure 6.4 Summary of nitrogen and sulfur compositions for NSC samples pyrolyzed at different temperature

The effectiveness of various pyrolyzed NSC as an electrocatalyst material was studied based on their activity toward ORR. The ORR activities of pyrolyzed NSC, pyrolyzed non-doped carbon nanofibers from solvothermal-treated CNFs (C900), and commercial Pt/C were tested using cyclic voltammetry (CV) curve and linear sweep voltammetry (LSV) in 0.1 M KOH as electrolytes. NSC900 has the highest activity compared to the other pyrolyzed NSC samples, as suggested by its lowest onset potential (Figure 6.5). An onset potential of 60 mV lower than that of Pt/C catalyst was recorded. The as-synthesized NSC900 could also reach a cathodic peak potential of 0.66 V

(*vs*. RHE), which is comparable to that of most reported N-doped carbon materials.[29, 217] Indeed, the electrocatalytic performance of NSC900 is well-aligned with both structural and chemical analysis that suggest the as-synthesized NSC900 is the most optimal carbocatalyst among other NSC samples. In this regard, carbonization of NSC at 900°C is confirmed as the best annealing temperature to generate a carbocatalyst with a strong balance between a highly crystalline carbon structure, large surface area, and active catalytic sites. It should be noted, however, that although NSC900 was found to improve both ORR and HER activity compared to C900, the improvement obtained by the N,S-doping toward HER is not significant and the performance is still far from competitive compared with Pt/C electrocatalysts.

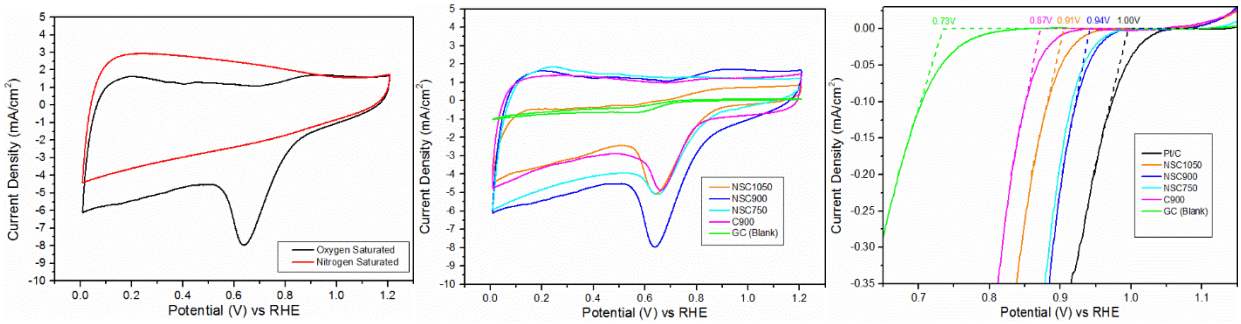

Figure 6.5 CV curves and onset LSV for different electrodes (GC, Commercial 20% Pt/C, C900, NSC750, NSC900, and NSC1050) toward ORR in 0.1 M KOH solution

6.3.2 N,S-doped CNFs carbon nanofibers coated with N,P-doped carbon derived from melamine-phytic acid complex particles (NSC/MPA)

Concerning the limited improvement on HER activities for the as-synthesized NSC900, further functionalization strategies were considered to enhance its activity. An attempt to incorporate an additional doping element of phosphor using a hydrothermal reaction between NSC and phytic acids followed by pyrolysis at 900 °C was performed. The resulting carbon nanofibers were consisted of 3.9 % N, 0.5 % S, 1.9 % P, and 4.9 % O. Still, no significant improvement in HER activity was observed even after the addition of phosphor as a third doping element. It was

believed that the as-prepared N,S- or N,S,P-doped carbon nanofibers derived from the mechanically-treated CNFs were not able to provide sufficient active doping sites to promote good HER activity. In this regard, an alternative approach of coating layers of N,P-doped carbon nanoparticles onto N,S-doped carbon nanofiber network (sample NSC900) was investigated. Both computationally simulated and experimental studies reported in literature have demonstrated that several carbon materials co-doped with N/P heteroatoms are able to induce outstanding HER activities.[123, 221, 227] In this work, the synthesis of N,S-doped carbon nanofibers coated with N,P-doped carbon (as described by the carbon hybrid in this study) was obtained through Figure 6.6. Initially, NSC samples obtained after solvothermal treatment were dispersed with complex particles of melamine-phytic acid (MPA) via the aid of sonication prior to pyrolysis. Owing to the accessible hydrogen bonding and π-π interactions, a relatively well-dispersed mixture was achieved. Subsequently, the dry mixture of NSC/MPA was annealed at 900 °C, a pyrolysis temperature at which optimal N,S-doped carbon nanofiber was exhibited. As carbonization occurred, complex particles of MPA were converted to N,P-doped carbon. At the same time, due to the cooperative interaction between MPA complex particles and solvothermal-treated NSC in their vicinity, the synthesized N,P-doped carbon could be easily integrated with the pyrolyzed NSC and use the nanofibers morphology as a template to form shell-like carbon hybrids.

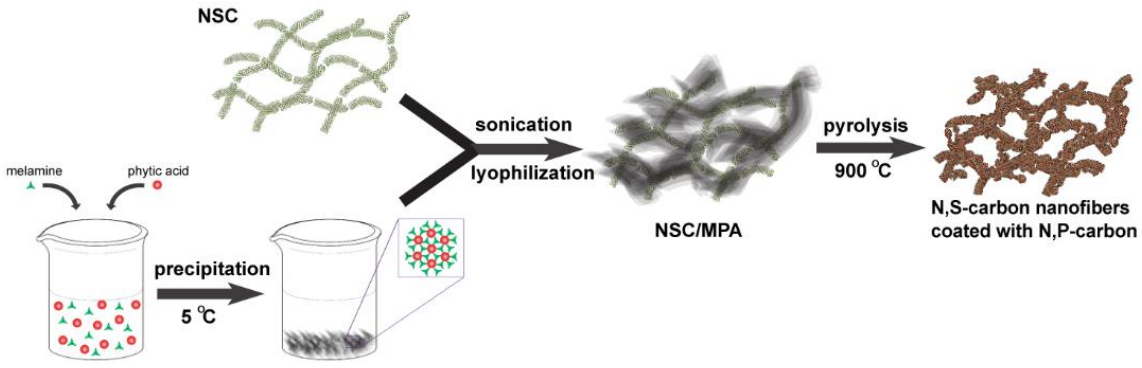

Figure 6.6 Carbon hybrids preparation

Optimization of carbon hybrids was assessed by formulating NSC/MPA composite mixtures with different mass ratios that could give a sensible N,P-doped carbon coverage on the surface of carbon nanofibers while maintaining the 3D nanofiber network. As represented in Figure 6.7a, carbonization of neat MPA complex particles would lead to uniform aggregates of carbonaceous material. In contrast, the carbonization of MPA from the NSC/MPA mixture would lead to the formation of less aggregated carbonaceous material. Figure 6.7c-f reveal that all carbon hybrids may still have the entangled nanofiber network as part of their carbon morphology similar to NSC900, as displayed in Figure 6.7b. However, noticeable changes in the nanofiber morphology of carbon hybrids were identified with the increasing mass loading of MPA complex particles in the NSC/MPA mixture prior to pyrolysis. At a very low loading of MPA, represented by NSC/MPA-1 in Figure 6.7c, the surface of the carbon nanofibers is relatively unchanged from neat NSC900 in Figure 6.7b. As the MPA mass loading increases, the nanofiber surfaces become more uneven and look as if some sections of nanofibers are "swollen" due to the presence of coating layers made from aggregated carbon, which can be represented by NSC/MPA-5 and NSC/MPA-10 in Figure 6.7d,e. It is believed that the coating of aggregated carbon layers on the surface of the nanofiber would closely resemble the characteristic of non-uniform core-shell-like nanofiber. The aggregated carbon shell layers also tend to promote a bridging effect between nearby entangled networks and result in a diminishing amount of pores in the 3D nanofibers network. A further increase of the MPA loading in the mixture would eventually lead to higher carbon shell content in carbon hybrids, as represented in NSC/MPA-20. When the carbon shell layers start to dominate the composition of carbon hybrids, as shown by Figure 6.7f, each individual nanofiber becomes fully covered with a relatively thick and smooth surface assembled from carbon shell layers. Furthermore, excessive carbon shell layers could induce extensive bridging effects. As a result,

the formation of entangled carbon networks from NSC morphology is replaced with formation of continuous aggregated carbon networks, which results in more densely-packed 3D carbon materials.

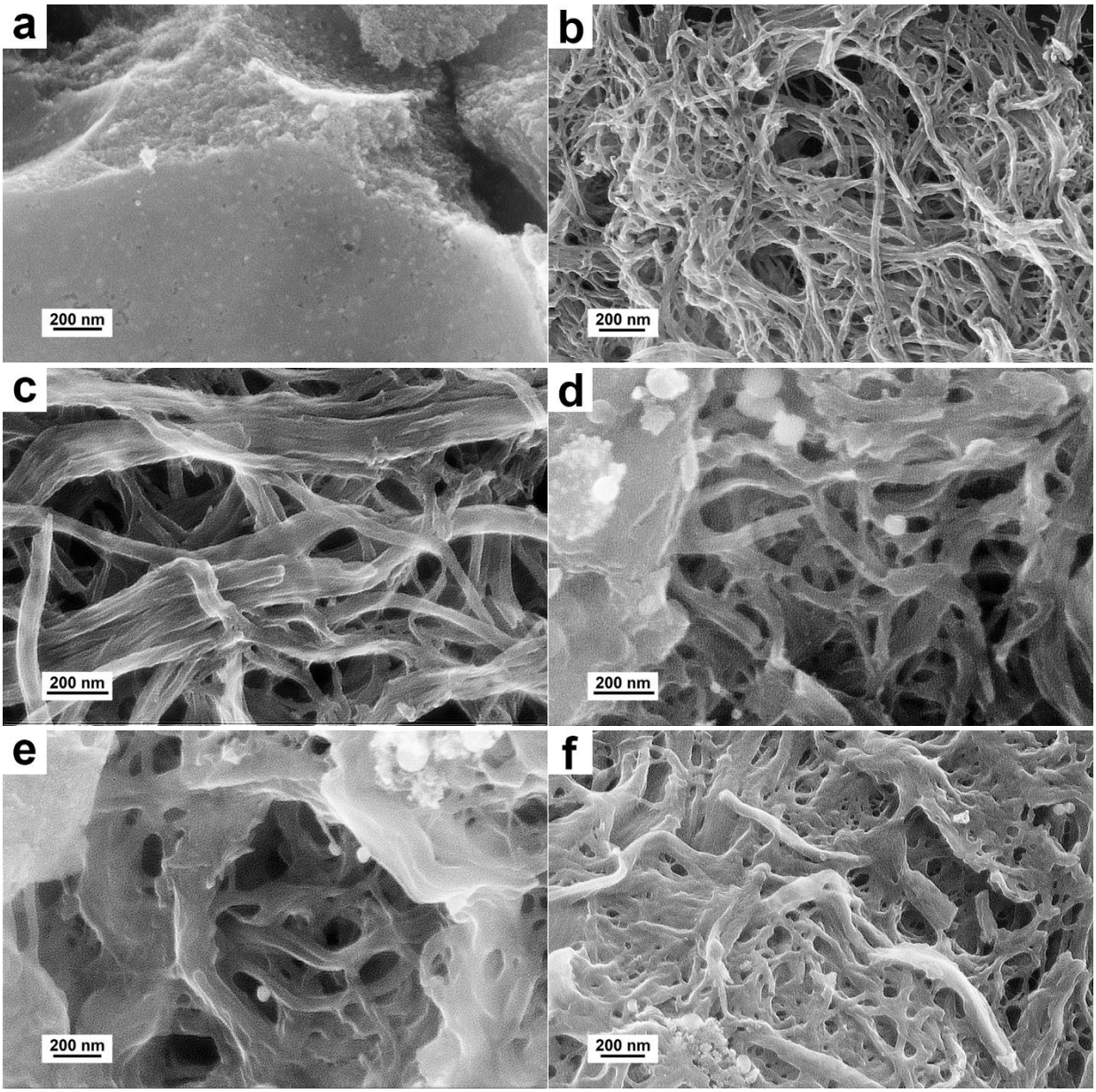

Figure 6.7 SEM images of the as-synthesized (a) N,P-doped carbon from MPA, (b) NSC900, and NSC/MPA hybrids with different loading ratio: (c) NSC/MPA-1, (d) NSC/MPA-5, (e) NSC/MPA-10, and (f) NSC/MPA-20

Compositional mappings for carbon hybrids were also identified using EDS to indicate the distribution of carbon shell layers originated from carbonization of MPA on N,S-doped carbon nanofiber. As shown in Figure 6.8, well-distributed nitrogen and phosphor species are observed for carbon hybrid formulated based on NSC/MPA-5. This result provides supporting evidence that N,P-doped carbon is dispersed along the surface of the nanofibers. Additionally, the dispersion of sulfur atoms is shown across the surface of carbon hybrids. Although the uncoated section of N,S-doped carbon nanofiber is one possible reason for the presence of sulfur atoms, it is also possible that cooperative integration of the carbon framework was obtained during the formation of N,P-doped carbon shell layers and N,S-doped carbon nanofibers as core material.

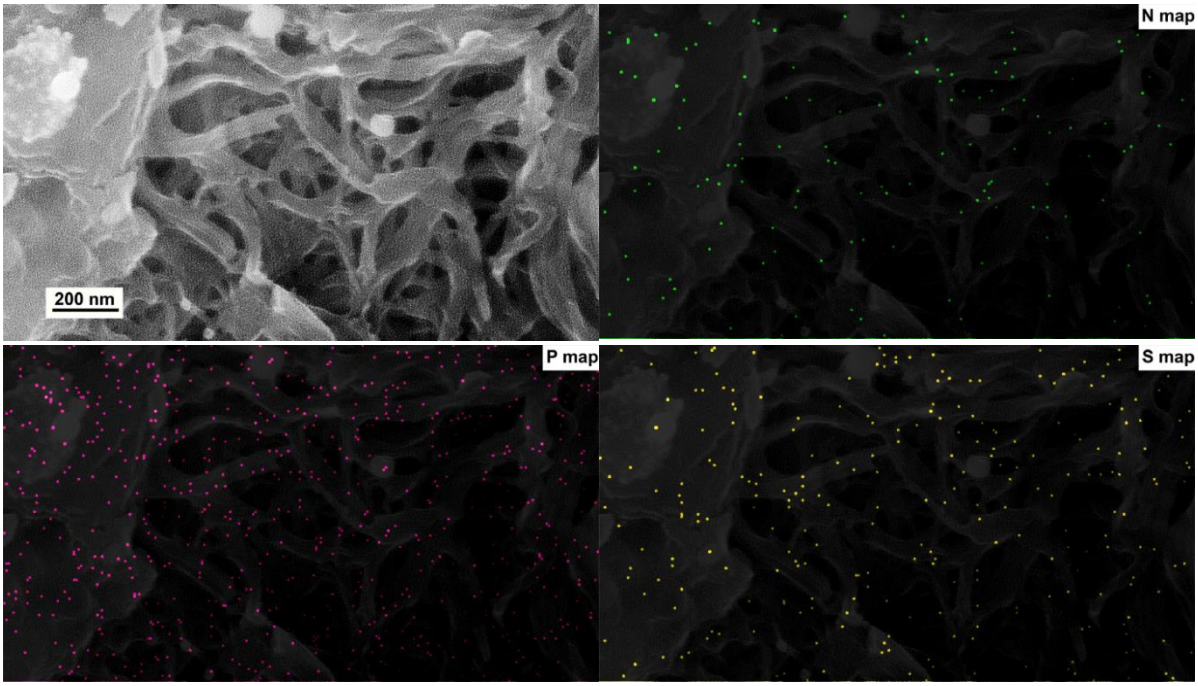

Figure 6.8 The morphology and corresponding N, P, S-heteroatoms distribution of NSC/MPA-5

BET analysis (Figure 6.9a,b) was evaluated to give further insight on the change in morphology of N,S-doped carbon nanofibers coated with N,P-doped carbon prepared from different NSC/MPA mixture formulations. As listed in Table 6.4, the synthesis of N,P-doped carbon from carbonization of neat MPA complex particles typically generates carbon material with

surface area of ~1,000 m^2 g^{-1}. In contrast, the surface area of carbon hybrid networks prepared using mixture formulation varies in the range of ~560 to ~1,220 m^2 g^{-1}. For NSC/MPA-1, the calculated BET surface area of 565 m^2 g^{-1} is relatively close to that of NSC900 (612 m^2 g^{-1}). This insignificant change in the specific surface area implies that carbon nanofiber morphology is still relatively unaltered in the presence of very low amounts of N,P-doped carbon, which is also supported by the previous SEM images in Fig. 4c. By increasing the MPA loading in the NSC/MPA composite mixture prior to pyrolysis, the calculated specific surface area starts to increase due to the large surface area originating from the coating layers of N,P-doped carbon. An increase in the surface area to 682, 1,217, and 954 m^2 g^{-1} was obtained for NSC/MPA-5, NSC/MPA-10, and NSC/MPA-20, respectively. Furthermore, it should also be noted that the surface area of ~1,200 m^2 g^{-1} for NSC/MPA-10, which is even higher than the value for both NSC/MPA-20 and neat MPA (~1,000 m^2 g^{-1}), may imply the synergistic effect between coating layers of N,P-doped carbon and highly porous 3D nanofibers network originating from N,S-doped carbon nanofibers.

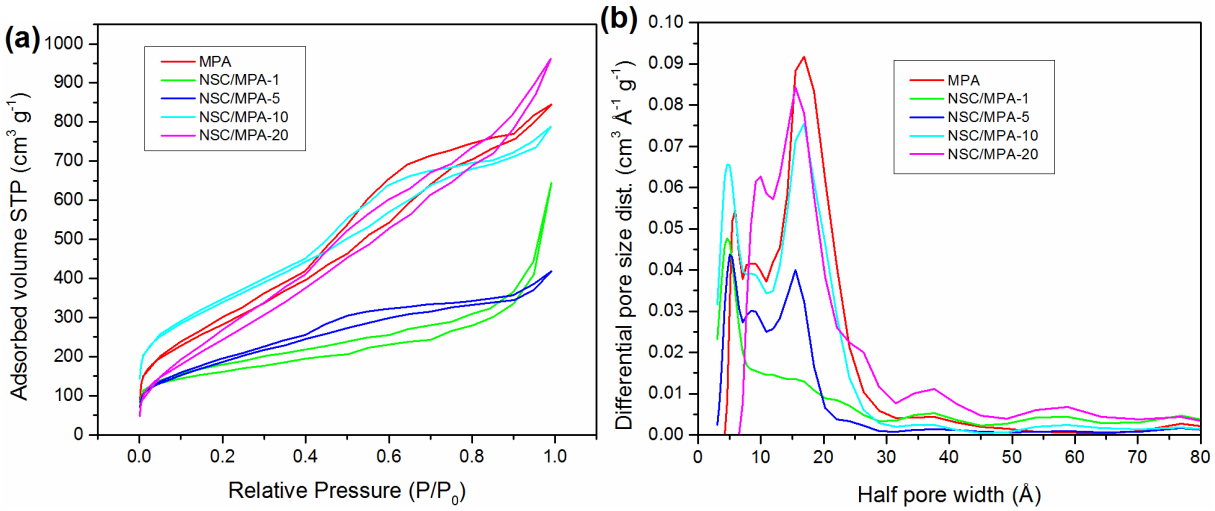

Figure 6.9 (a) N_2 physisorption isotherms and (b) pore size distribution of MPA-derived N,P-graphitic carbon and NSC/MPA carbon hybrids prepared using different mixture formulation

Table 6.4 Surface elemental composition, Raman intensity ratio, BET surface area, and pore volume of various carbon materials

Sample	Elemental Composition (At. %)					Raman I_D/I_G ratio	BET surface area ($m^2 g^{-1}$)
	C	N	P	S	O		
MPA	84.0	4.4	2.8	-	9.0	0.91	1,044
NSC/MPA-1	88.1	2.4	1.6	0.8	7.1	0.83	565
NSC/MPA-5	87.4	3.3	2.5	0.6	6.2	0.88	682
NSC/MPA-10	83.8	4.3	2.7	0.9	8.3	0.87	1,217
NSC/MPA-20	84.2	4.2	2.4	0.8	8.4	0.85	954

XPS measurements on N,S-doped carbon nanofibers coated with N,P-doped carbon were performed to quantitatively evaluate the elemental composition of the samples, as shown in Figure 6.10 and summarized in Table 6.4. As presented in Table 6.4, carbonization of neat MPA complex particles leads to carbonaceous materials consisting of ~4.4 % nitrogen and ~2.8 % phosphor atoms. It is expected that while aromatization and intramolecular condensation occur during pyrolysis to form graphitic carbon, nitrogen and phosphor heteroatoms can be concurrently incorporated into its carbon framework. For N,S-doped carbon nanofibers coated with N,P-doped carbon, Table 6.4 provides evidence that their elemental compositions are relatively close among different formulations of the precursor mixture, in which ~2.5 to 4.3 % nitrogen, ~1.5 to 2.7 % phosphor, and ~0.6 to 0.9 % sulfur are detected. In particular, the relatively consistent sulfur composition at the surface of carbon hybrids reveals that the sulfur atoms originated from N,S-doped carbon nanofibers may be well integrated with N,P-doped carbon upon pyrolysis. In addition, a quantitative increase in the composition of nitrogen and phosphor atoms with increasing mass loading of MPA in the composite precursor supports the evidence on the progress of N,P-doped carbon shell surface coverage. Analogous to the SEM and BET analysis, NSC/MPA-1 has the least amount of nitrogen and phosphor detected, which corresponds well to the fact that only minimal amount of coated N,P-doped carbon layer is expected. With the increasing MPA content in the NSC/MPA mixtures prior to pyrolysis, the formation of more coating layers can be expected

up to a saturation point where extensive coverage of N,P-doped carbon layers on N,S-doped carbon nanofibers generates similar composition to the bulk N,P-doped carbon synthesized from neat MPA. Table 2 points out that the saturation point could be achieved with a mixture formulation between NSC/MPA-5 and NSC/MPA-10. This trend from the XPS results corresponds accordingly with both the SEM and BET analysis.

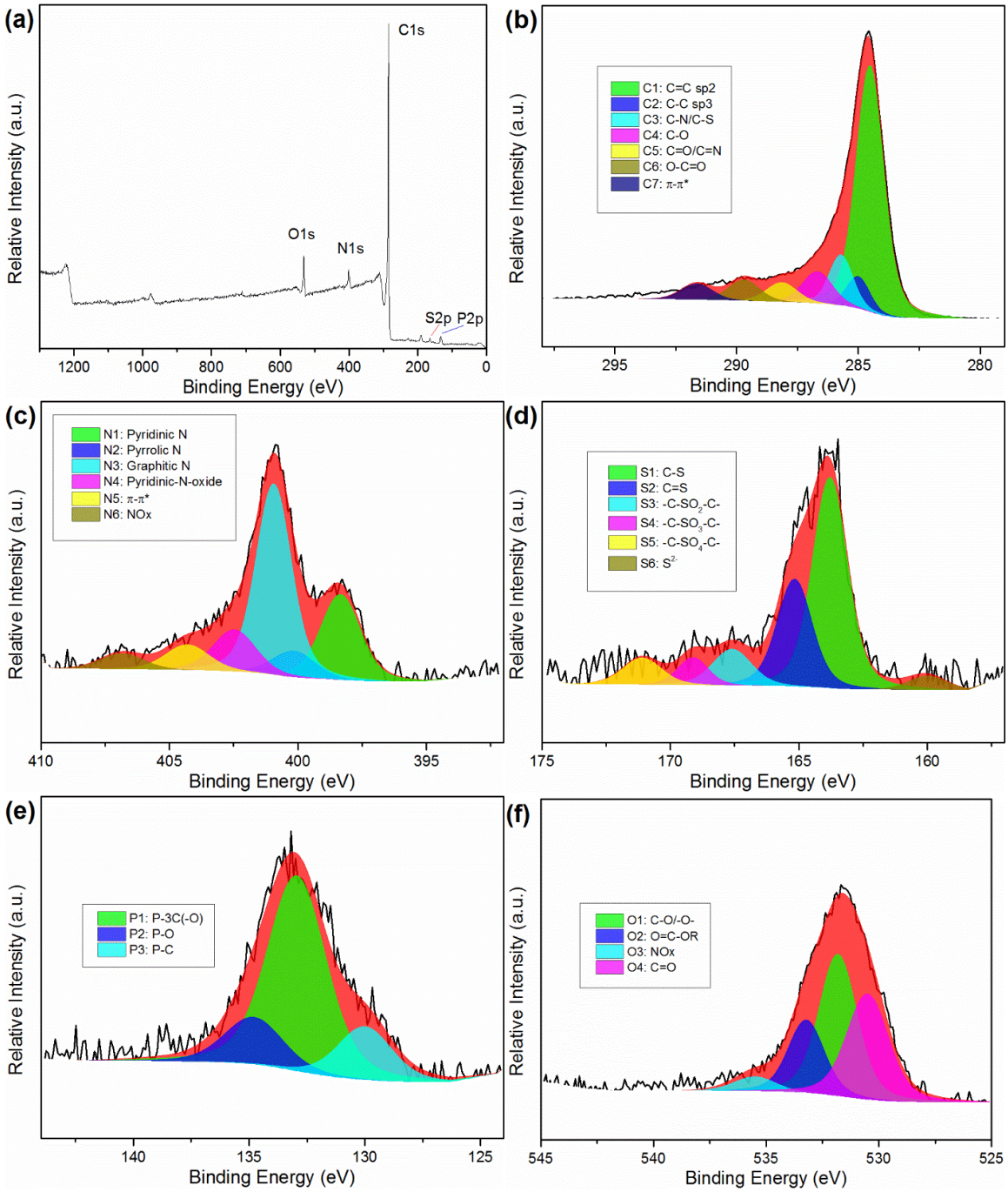

Figure 6.10 (a) XPS survey spectrum and high-resolution scans of (b) C1s (c) N1s (d) S2p (e) P2p and (f) O1s electrons of NSC/MPA-5

Characterization of the carbon structures of N,S-doped carbon nanofibers coated with N,P-doped carbon was conducted with Raman spectra analysis. The spectra (Figure 6.11) reveal that the coupling of N,S-doped carbon nanofibers with N,P-doped carbon bears no significant change

in the carbon structure. The characteristics of broad and weak 2D bands with intensity ratio (I_D/I_G) in the range of 0.83 to 0.88, similar to the carbon characteristics of NSC900, were observed. It should be noted, however, that the I_D/I_G ratio for N,S-doped carbon nanofibers coated with N,P-doped carbon is lower than just N,P-doped carbon synthesized from neat MPA complex particles. The result may imply that the presence of carbon nanofibers does not induce more disordered carbon structure, instead the cooperative integration between N,S-doped carbon nanofibers and N,P-doped carbon may enhance the lack of graphitic carbon structure of N,P-doped carbon from neat MPA.

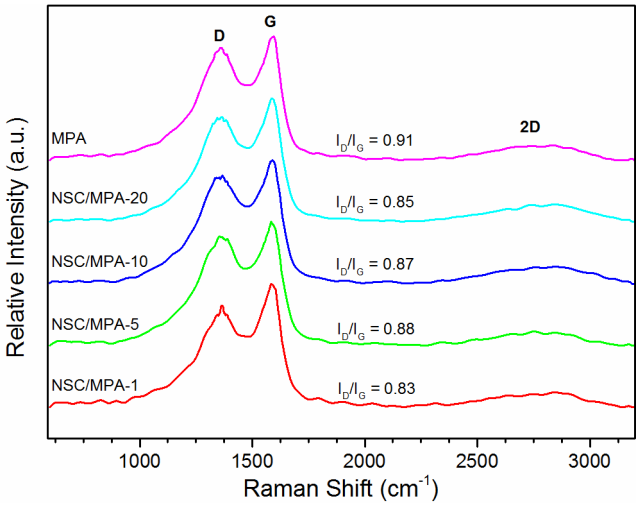

Figure 6.11 Raman spectra of MPA and NSC/MPA hybrids at different mixture formulation

The electrocatalytic functionalities of the as-synthesized N,S-doped carbon nanofibers coated with N,P-doped carbon were investigated toward both HER and ORR. HER measurements were carried out in an acidic solution of 0.5 M H_2SO_4 solution. The N,S-doped carbon nanofibers coated with N,P-doped carbon prepared using different NSC/MPA composite precursors exhibit different catalytic activities, as shown in Figure 6.12a. The optimal HER performance of a hybrid carbocatalyst can be obtained for either NSC/MPA-5 or NSC/MPA-10, which corresponds well with the physiochemical analysis of the carbon material. Given that NSC/MPA-5 could already

provide a high HER activity with a minimal amount of N,P-doped carbon coating layers, a further evaluation of the electrocatalytic properties on N,S-doped carbon nanofibers coated with N,P-doped carbon will be based on NSC/MPA-5. The polarization curve of NSC/MPA-5 shows a potential of 331 mV to achieve a cathodic current density of 10 mA cm^{-2} with an onset potential of 233 mV. Compared to either NSC900 or neat MPA based carbon particles, the HER performance of NSC/MPA-5 is superior. The result provides a good evidence that a synergistic integration between carbon nanofiber architecture and catalytically active graphitic carbon layers on the surface could lead to a more effective electrocatalytic activity.

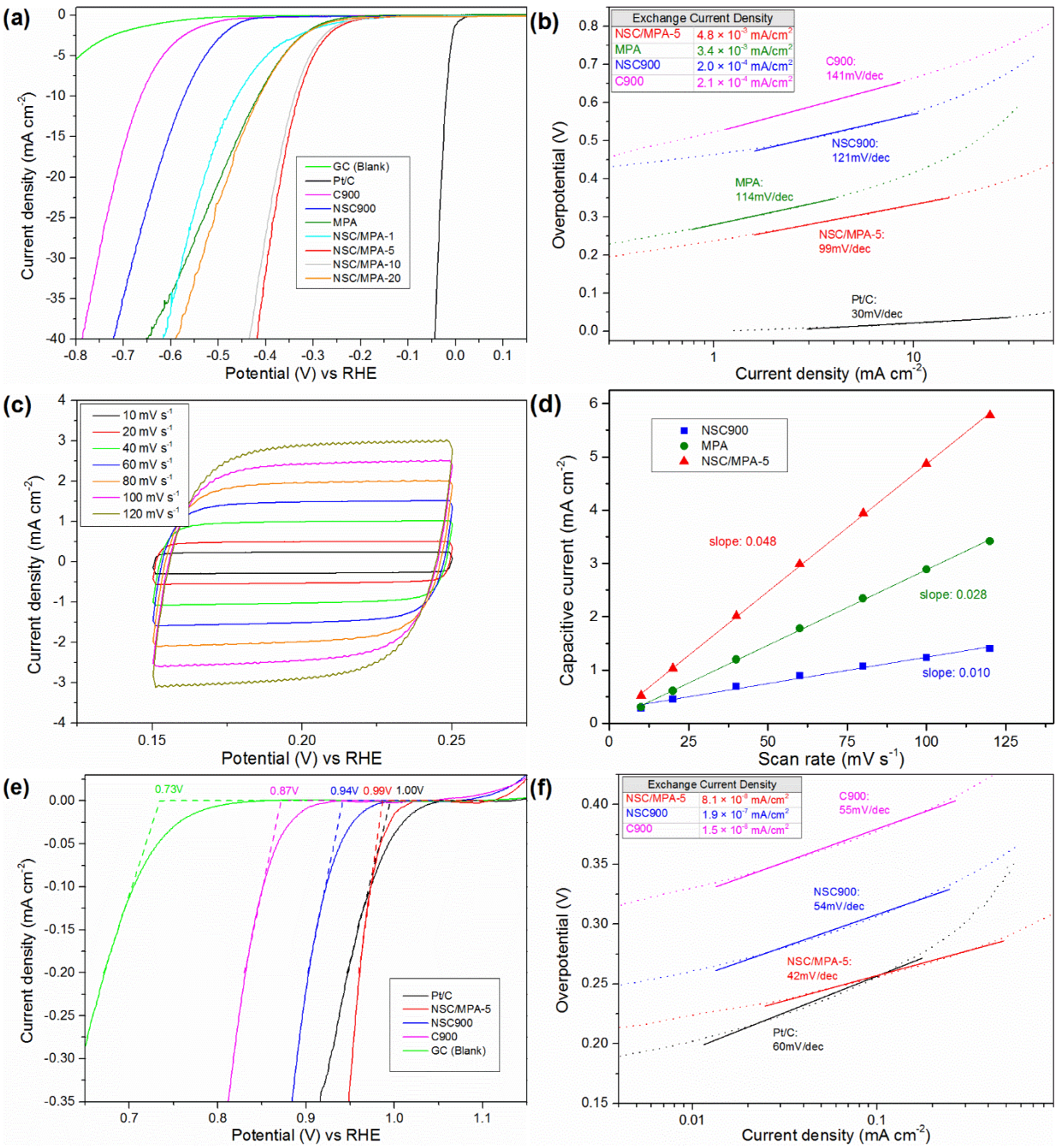

Figure 6.12 (a) HER polarization curves in 0.5 M H_2SO_4 with (b) the corresponding Tafel plot. (c) Cyclic voltammetry curves for NSC/MPA-5 electrode at different scan rates and (d) the extracted capacitive current. (e) ORR polarization curves in 0.1 M KOH with (f) the corresponding Tafel plot

In order to better understand the electrocatalytic enhancement achieved from NSC/MPA-5, quantitative evaluations on both the Tafel slope and the exchange current density (J_0) derived from

Tafel plot were conducted and compared with both NSC900 and MPA-derived N,P-doped carbon. Figure 6.12b shows that the Tafel slopes between these three samples are all in the approximate range of ~90 to ~120 mV decade^{-1}, in which the NSC/MPA-5 displays the lowest slope at 99 mV decade^{-1}. The Tafel slope is a tool often used to determine the rate-determining step involved in electrocatalysis of HER, OER, and ORR. There are three generally accepted steps for the HER mechanism in acidic conditions:[259] the discharge step (Volmer reaction, Equation 6.1), the desorption step (Heyrovsky reaction, Equation 6.2), and the recombination step (Tafel reaction, Equation 6.3).

$$H_3O^+ + e^- \rightarrow H_{ads} + H_2O \quad (6.1)$$

$$H_{ads} + H_3O^+ + e^- \rightarrow H_2 + H_2O \quad (6.2)$$

$$H_{ads} + H_{ads} \rightarrow H_2 \quad (6.3)$$

Based on these mechanisms, it has been reported that Tafel slopes of 120, 40, and 30 mV decade^{-1} are involved when the rate-limiting step is the Volmer, Heyrovsky, and Tafel reaction, respectively. All doped-carbon samples prepared in this work is close to a slope of 120 mV decade^{-1}, which suggests that Volmer reaction is the rate-determining step. Although the detailed HER mechanism for the as-synthesized carbon samples remains unclear, it is believed that higher Tafel slope is often undesirable as it would lead to lower HER rate in the high overpotential region.[225, 259]

The exchange current density (J_0) of N,P-doped carbon from neat MPA, NSC900, and NSC/MPA-5 was evaluated by extrapolating the Tafel plot, as presented in Figure 6.12b and Table 6.5. The highest exchange current density of 4.8×10^{-3} mA cm^{-2} was obtained for the NSC/MPA-5. This relatively high value (see Table 6.6 for comparison with other reported materials) may be attributed to the additive effect of the high intrinsic activity of N,P-doped carbon

shell layers and the mesoporous-rich nanofiber morphology that can provide more accessible active sites and more rapid electron transport to the electrode. In an attempt to further understand these effects, the electrochemical double-layer capacitances (C_{dl}), which are often used as an indicator of the electronically-active surface area, for the as-synthesized carbon samples were measured from Figure 6.12c. Figure 6.12d compares the calculated slopes for N,P-doped carbon from neat MPA, NSC900, and NSC/MPA-5, in which these materials exhibit C_{dl} of 14.5, 5.0, and 24.4 mF cm^{-2}, respectively. These results suggest that NSC/MPA-5 allows ~1.6× and ~4.9× higher exposure of active surface area than that of N,P-doped carbon from neat MPA and NSC900 alone. Furthermore, the normalization of the exchange current density by relative surface area (Table 6.5) suggests that the discrepancy in the intrinsic activity between N,P-doped carbon from neat MPA and NSC/MPA-5 is minimal and that the integrated N,P-doped carbon shell layers on N,S-carbon nanofibers are the driving forces to enable good HER activity for NSC/MPA-5.

Table 6.5 Summary of electrochemical properties of the as-prepared catalysts toward HER

Sample	μ_{onset}, mV	μ @ 10mA cm^{-2}, mV	Tafel slope, mV dec^{-1}	J_0, mA cm^{-2}	C_{dl}, mF cm^{-2}	Relative Surface Area	Normalized J_0, mA cm^{-2}
NSC900	450	572	121	2.0×10^{-4}	5.0	0.2	9.9×10^{-4}
MPA	274	409	114	3.4×10^{-3}	14.5	0.6	5.8×10^{-3}
NSC/MPA-5	233	331	99	4.8×10^{-3}	24.4	1.0	4.8×10^{-3}

Table 6.6 Comparison electrochemical properties of various catalyst materials toward HER

Material	μ_{onset}, mV	$\mu_{10mA\ cm^{-2}}$, mV	Tafel slope, mV dec^{-1}	J_0, mA cm^{-2}	Catalyst loading, μg cm^{-2}	C_{dl}, mF cm^{-2}	C_{dl}, mF μg^{-1}	Normalize factor by mass and surface area	Normalized J_0, mA cm^{-2}	Ref
NSC900	450	572	121	2.0×10^{-4}	250	5.0	0.02	0.2	9.9×10^{-4}	This Work
MPA	274	409	114	3.4×10^{-3}	250	14.5	0.06	0.6	5.8×10^{-3}	This Work
NSC/MPA-5	233	331	99	4.8×10^{-3}	250	24.4	0.10	1.0	4.8×10^{-3}	This Work
N-graphene	331	490	116	7.0×10^{-5}						[123]
P-graphene	374	553	133	9.0×10^{-6}						[123]
N,P-graphene	289	422	91	2.4×10^{-4}	200	10.6	0.05	0.5	4.4×10^{-4}	[123]
N,S-graphene	130	276	81	8.4×10^{-3}						[224]
S-graphene	382	671	124	9.0×10^{-4}	20	13.3	0.67	6.8	1.3×10^{-4}	[226]
g-C_3N_4@NG	160	240	51.5	3.5×10^{-4}	100	5.0	0.05	0.5	6.8×10^{-4}	[225]
g-C_3N_4@G	80	207	54	4.0×10^{-2}	143	13.0	0.09	0.9	4.3×10^{-2}	[233]
g-C_3N_4@SG	132	346	84	5.6×10^{-3}	20	5.8	0.29	2.9	1.9×10^{-3}	[226]
g-C_3N_4@PG	76	340	90	3.3×10^{-3}	20	4.2	0.21	2.2	1.5×10^{-3}	[227]
SA900Z	236	387	80.2	5.4×10^{-4}	152	11.0	0.07	0.7	7.3×10^{-4}	[222]
SA900ZC	76	204	58.4	1.7×10^{-2}	152	12.9	0.08	0.9	2.0×10^{-2}	[222]
HPC-900	12	97	57.4							[223]
MPSA/GO-1000		163	32	1.6×10^{-1}						[221]
g-C_3N_4@S-Se-G	92	300	86	6.3×10^{-3}	20	4.4	0.22	2.2	2.8×10^{-3}	[226]
pBC-N/MoS_2	108	215	61		30	16.5	0.55			[31]
MoS_2/G			42	3.0×10^{-3}	210	10.4	0.05	0.5	5.9×10^{-3}	[260]
MoS_2 nanosheet	120	186	55	1.3×10^{-2}	285	37.7	0.13	1.4	9.3×10^{-3}	[261]
Cu_2MoS_4	135	337	95	4.0×10^{-2}	41.6					[262]

It should be noted that the evaluated electrochemical properties of the as-synthesized NSC/MPA-5 toward HER are better than previously reported N,P-graphene[225] and comparable to some other recently reported carbon catalysts and metallic catalysts such as N,P-doped carbon derived from bacterium strain before cathodic post-treatment[222], g-C_3N_4 at S-graphene[226], g-C_3N_4 at P-graphene[227], and Cu_2MoS_4[262]. However, in comparison to the most current state-of-the-art Pt/C, carbon hybrids based on MPSA/GO[221], or carbon derived from amino acids-rich biowaste from human hair[223], the apparent electrocatalytic activity of the as-prepared carbon hybrids still need to be improved.

The effect of coating N,S-doped carbon nanofibers with N,P-doped carbon layers on the electrochemical activity toward ORR in alkaline solution was also assessed. It was found that ORR activity could be significantly enhanced. Fig. 6.12e shows a more positive shift in the onset potential closer to that of commercial Pt/C for NSC/MPA-5. The onset potential of NSC/MPA-5 is only 10 mV higher than the onset potential of Pt/C. Furthermore, the pronounced cathodic peak of 0.84 V (*vs*. RHE) was demonstrated from CV measurements in O_2-saturated 0.1 M KOH (Figure 6.13). Based on these results, NSC/MPA-5 exceeds the performance of typical N-doped carbon material as ORR carbocatalyst (Table 6.7). The positive improvement of NSC/MPA-5 from NSC900 is assumed to have originated from better exposure of active dopants, which is also in agreement with other reported result.[29, 242] A Tafel plot for ORR in an alkaline medium was also derived from its polarization curves, as depicted in Figure 6.12f. Tafel slopes in the range of ~40 to ~60 mV decade^{-1} were observed in the low overpotential region for the as-synthesized carbon samples and commercial Pt/C. Although the mechanism steps of ORR often vary widely and are still not well-understood,[263] a relatively similar Tafel slope for the as-synthesized carbon samples to that value of Pt/C may imply that the same rate-determining step is highly possible in the low

overpotential region. For comparison, Tafel slopes in the range of 47 to 57 mV decade^{-1} have also been reported for some carbon-supported metal oxides.[264]

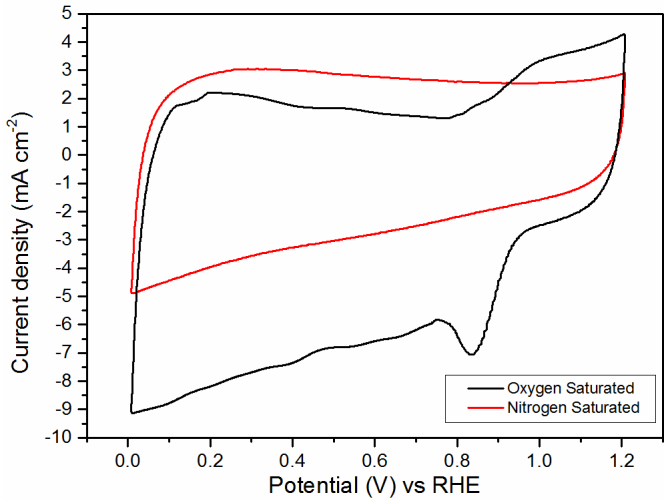

Figure 6.13 CV curves for NSC/MPA-5 carbon hybrid toward ORR in 0.1 M KOH solution

Table 6.7 Comparison onset potential and cathodic peak potential of various catalyst materials toward ORR

Material	Carbon precursor	μ_{onset}, V (*vs*. RHE)	$\mu_{cathodic\ peak}$, V (*vs*. RHE)	Ref
NSC900	CNFs	0.94	0.66	This Work
NSC/MPA-5	CNFs + Melamine + Phytic acid	0.99	0.84	This Work
N-CNF	Bacterial Cellulose		0.85	[29]
N-CNTs	Carbon Nanotube		0.78	[29]
N-RGO	Reduced Graphene Oxide		0.68	[29]
SA-CNF-900	Spider Silk	0.98	0.83	[265]
NGSH	Graphene + Single-walled Carbon Nanotube	0.88	~0.64	[266]
NG	Graphene Oxide	0.86	0.64	[217]
CNT@NCNT	Carbon Nanotube	0.99		[267]
CFO/CNF	Bacterial Cellulose + Co + Fe	0.88		[268]

Besides the electrocatalytic activity, long-term stability is another important feature of electrocatalyst materials. In order to assess this parameter, the as-prepared NSC/MPA-5 sample was exposed to continuous 1,500 cyclic voltammetry tests for continuous HER or ORR process under a constant voltage. Figure 6.14a,b suggest that the carbon material suffers from some degree of degradation during the long-term HER process in an acidic environment since the onset potential after the durability test is shifted to a higher value. In this regard, there is a strong possibility that owing to the characteristic of limited high-ordered, graphitic carbon structures from both N,S-doped carbon nanofibers as the core material and N,P-doped carbon from MPA as shell layers, the as-prepared NSC/MPA-5 is still relatively susceptible to an oxidation or decomposition reaction. In contrast, the NSC/MPA-5 has been found to have better long-term stability toward a long-term ORR process in an alkaline medium. A relatively stable ORR performance before and after the test is shown in Figure 6.14c-e. It is also expected that the as-synthesized NSC/MPA-5 still has a good tolerance toward methanol contamination, which is confirmed in Figure 6.14f. In this regard, although the current HER stability is a concern, it is believed that a further optimization process and incorporation of a highly-ordered, graphitic carbon filler might offer significant enhancement in both carbocatalyst activity and durability.

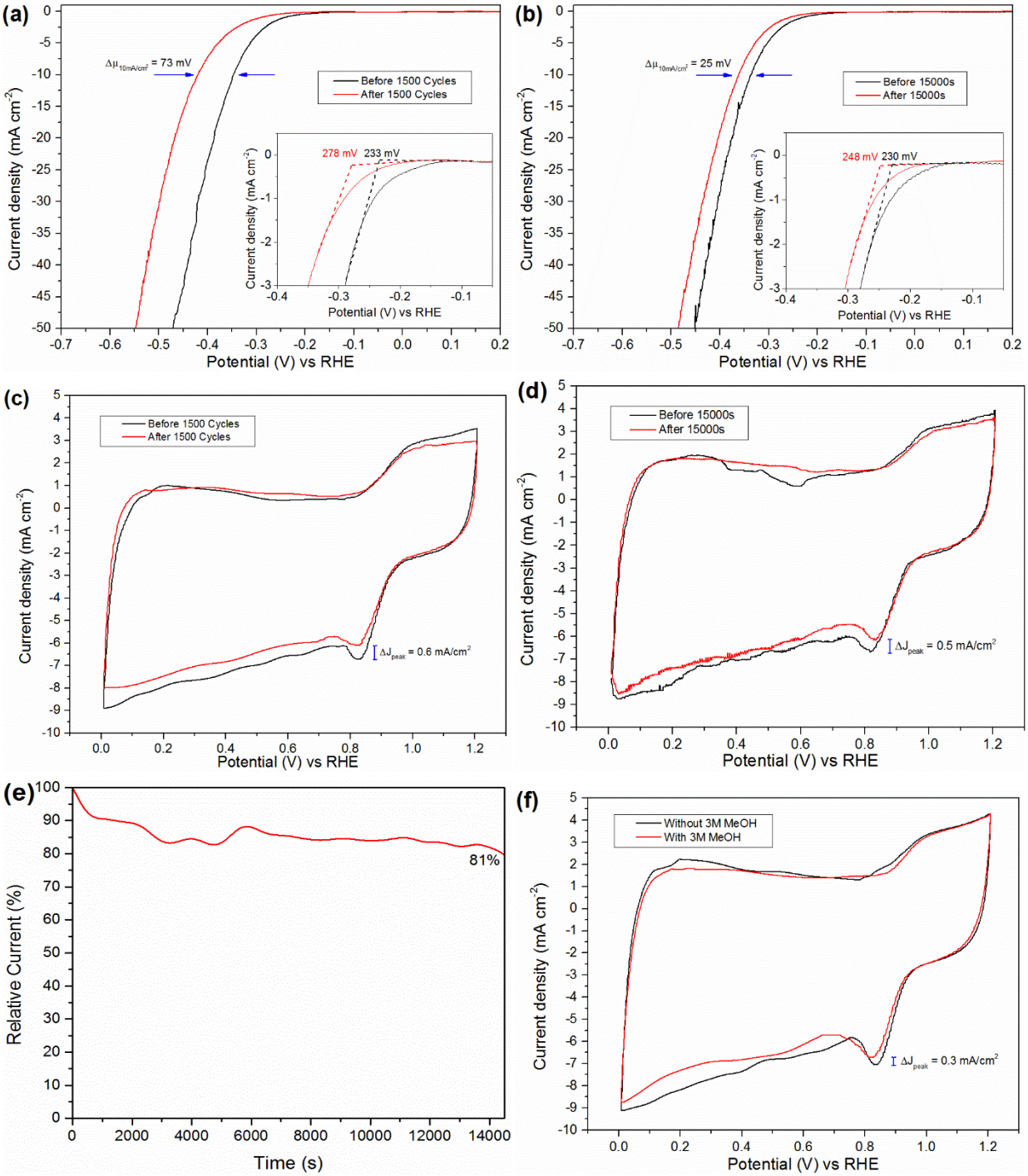

Figure 6.14 Stability of NSC/MPA-5 electrocatalyst: (a,b) Polarization curves toward long-term HER process, (c,d) cyclic voltammetry curves toward long-term ORR process, (e) amperometric curve at constant applied voltage of 0.84 V (*vs*. RHE) and (f) methanol tolerance

6.4 Conclusion

In summary, nitrogen- and sulfur-codoped porous carbon nanofibers were prepared from inexpensive, naturally abundant, and potentially mass-producible cellulose nanofibril precursors for carbon electrocatalyst. The physiochemical properties of samples were thoroughly characterized and the electrochemical properties were tested. Both ORR and HER using pyrolyzed N,S-doped CNFs-derived carbon nanofibers were still not competitive. However, hybridization of N,S-doped CNFs-derived carbon nanofiber network coated with N,P-doped carbon has been found to significantly increase both HER and ORR electrocatalytic activity. The carbon hybrids demonstrated a low onset potential of 233 mV (*vs*. RHE), a current density of 10 mA cm^{-2} at 331 mV (*vs*. RHE), and a Tafel slope of 99 mV $decade^{-1}$ toward HER in an acidic medium. Improvement in ORR performance was also displayed. The electrochemical properties were comparable to that of commercial Pt/C as the onset potential of hybrid carbon was only 10 mV lower than that of commercial Pt/C, and a high cathodic peak at 0.84 V was obtained from hybrid carbon nanofiber network. The high activity of N,S-doped CNFs-derived carbon nanofibers coated with N,P-doped carbon can be attributed to the synergistic effects of heteroatoms-doping, structural morphology, and large accessible active sites. Overall, the results in this study offer a new insight into designing and engineering metal-free carbocatalyst using easily available, affordable, and sustainable material toward a more effective electrocatalytic activity.

CHAPTER VII

OVERALL CONCLUSIONS AND RECOMMENDATIONS

7.1 Conclusions

In this dissertation, we have demonstrated several modification routes of CNFs, the tailored properties after modification CNFs, and fabrication of high value-added applications using the altered CNFs. In all attempted modification methods, the synthesis of homogeneous functionalized CNFs has been very challenging. We designed the processing techniques to meet this requirement and optimized the modification conditions to maximize the functionalization impact while preserving the essential properties of CNFs.

In the first part of the work, coupling agent polymer was employed to exploit a facile route of CNFs surface hydrophobization. The maleic anhydride groups could easily react with the accessible surface hydroxyl groups of CNFs. However, the long chain of the hydrophobic backbone in the coupling agent may provide steric hindrance such that only very limited amount of ester bonding was obtained. Nevertheless, the long hydrophobic backbone of the coupling agent were able to cover most of the surface hydroxyl groups of CNFs as indicated by high water contact angle and low critical surface tension. The characterization study also showed that the inherent CNFs properties remained relatively unchanged. The preparation of polystyrene/CNFs nanocomposite further highlighted the effect of CNFs as excellent reinforcing filler and the important of surface interaction between CNFs filler and hydrophobic polymer matrices. The superior mechanical properties of nanocomposite at very low loading suggest that the inherent amphiphilic surface of CNFs was sufficient to provide a good dispersion and filler-matrix surface

interaction. Nevertheless, as filler loading was increased, surface hydrophobization was necessary to provide the optimal surface interaction.

Following the first part of the work, it has been noted that the modification approach required the use of an organic solvent as the dispersing medium and a dry condition for the grafting reaction. These conditions were unfavorable since potential aggregation tendency could still be present. Since CNFs have a good dispersion in an aqueous medium, the second work adopted suspension (surfactant-free emulsion) polymerization to graft hydrophobic polymer on their surface. By adjusting the monomer mixture, salt content in the solution, and polymerization condition, the optimal hydrophobic CNFs dispersed in water could be accomplished. Since the primary objective of this work is on homogeneous surface hydrophobized CNFs, no attempt was made on optimizing the experiment to control the molecular weight of grafted polymers. The as-obtained hydrophobic CNFs were used to prepare hydrophobic aerogels. It was found that the characteristics of the hydrophobic CNFs aerogels closely resembled those of the neat CNFs aerogels. The main differences were limited only to the surface wetting and the low compression strength. The hydrophobic CNFs aerogels were used to demonstrate oil/water separation and wet-solvent shape recovery capability.

The third part of the work involved both carbonization and its surface functionalization. Carbonization was studied as the technological possibility to obtain bio-based nanocarbon to compete with other recent nanosized carbon materials (i.e. carbon nanotubes and graphene). With the increasing interest in nanocarbon for energy-related materials, the use of bio-based CNFs could offer a competitive material for electrocatalyst application. Simultaneous carbonization and heteroatoms doping were obtained through solvothermal treatment. The as-obtained carbon material exhibited heteroatoms-doped carbon nanofiber with the same morphology as their

precursor CNFs but with higher surface area. An additional step using high temperature pyrolysis was required in order to obtain bio-based carbon nanofibers with good conductivity. Although enhanced surface active site could be detected from the pyrolyzed heteroatoms-doped carbon nanofibers, recombination of heteroatoms-doped CNFs-derived carbon with a more active carbon materials could generate better electrocatalytic performance. The improvement obtained from carbon hybrids may be attributed to the synergistic effect between the architectural templates provided by CNFs-derived carbon, the interactions among heteroatoms dopants, and the mesopore-rich of graphitic carbon hybrids.

Overall, the main objectives of this thesis work were achieved. Several modifications approached for CNFs were reported, and the enhanced properties of highly functionalized CNFs were clearly elucidated. The modification mechanism and the influence of modified CNFs were deduced using various analytical techniques. A broad range of applications for the altered CNFs-based materials was demonstrated and identified as high-performance nanofiber materials that are comparable with other reported advanced materials. Herein, the current study established the promising high value-added products obtained using both CNFs as the building blocks and different modification routes as the pathways.

7.2 Future works

As indicated in Chapter IV and V of this thesis work, the effect of surface hydrophobization for CNFs played significant roles to open new applications. Future attention should focus on the innovative approaches to obtain hydrophobic CNFs using an aqueous medium with better control on grafted material and more robust process to provide greater flexibility on the properties of grafted material. In addition, exploiting different applications of surface hydrophobized CNFs beyond their reinforcing capacity should be considered, especially regarding the gas barrier, light

scattering, and biocompatibility. The result will be valuable to develop CNFs as multifunctional nanofiber materials.

Given the limited technical knowledge on CNFs-derived carbon shown in Chapter VI, an extensive study in a demonstration of CNFs-derived carbon nanofibers could facilitate more technical knowledge to open new potential roadmap toward different applications that are beyond surface functionalized CNFs. The fundamental understanding of the effects of each carbonization parameters on CNFs-based carbon would give better tuning on the properties of the carbon materials and allow the CNFs-based carbon to be more competitive toward other nanocarbon, i.e. carbon nanotubes and graphene. Recombination with another nanomaterial has been found useful to improve the surface functionality of CNFs-based carbon nanofibers significantly. Therefore, it may be of great interest to scientists to further focus on the innovative recombination approach for CNFs-based carbon nanofibers.

APPENDIX A: COPYRIGHT PERMISSION

SPRINGER LICENSE
TERMS AND CONDITIONS

Oct 12, 2016

This Agreement between Arie Mulyadi ("You") and Springer ("Springer") consists of your license details and the terms and conditions provided by Springer and Copyright Clearance Center.

License Number	3966700623763
License date	Oct 12, 2016
Licensed Content Publisher	Springer
Licensed Content Publication	Cellulose
Licensed Content Title	Surface modification of cellulose nanofibrils by maleated styrene block copolymer and their composite reinforcement application
Licensed Content Author	Arie Mulyadi
Licensed Content Date	Jan 1, 2015
Licensed Content Volume Number	23
Licensed Content Issue Number	1
Type of Use	Thesis/Dissertation
Portion	Full text
Number of copies	1
Author of this Springer article	Yes and you are the sole author of the new work
Order reference number	
Title of your thesis / dissertation	FUNCTIONALIZATION AND CARBONIZATION OF CELLULOSE NANOFIBRILS AS HIGH-PERFORMANCE FIBER MATERIALS AND THEIR APPLICATIONS
Expected completion date	Nov 2016
Estimated size (pages)	141
Requestor Location	Arie Mulyadi 500 10th Street NW ATLANTA, GA 30332 United States Attn: Arie Mulyadi
Billing Type	Invoice
Billing Address	Arie Mulyadi 500 10th Street NW

ATLANTA, GA 30332
United States
Attn: Arie Mulyadi

Total **0.00 USD**

Terms and Conditions

Introduction
The publisher for this copyrighted material is Springer. By clicking "accept" in connection with completing this licensing transaction, you agree that the following terms and conditions apply to this transaction (along with the Billing and Payment terms and conditions established by Copyright Clearance Center, Inc. ("CCC"), at the time that you opened your Rightslink account and that are available at any time at http://myaccount.copyright.com).
Limited License
With reference to your request to reuse material on which Springer controls the copyright, permission is granted for the use indicated in your enquiry under the following conditions:
- Licenses are for one-time use only with a maximum distribution equal to the number stated in your request.
- Springer material represents original material which does not carry references to other sources. If the material in question appears with a credit to another source, this permission is not valid and authorization has to be obtained from the original copyright holder.
- This permission
• is non-exclusive
• is only valid if no personal rights, trademarks, or competitive products are infringed.
• explicitly excludes the right for derivatives.
- Springer does not supply original artwork or content.
- According to the format which you have selected, the following conditions apply accordingly:
• **Print and Electronic:** This License include use in electronic form provided it is password protected, on intranet, or CD-Rom/DVD or E-book/E-journal. It may not be republished in electronic open access.
• **Print:** This License excludes use in electronic form.
• **Electronic:** This License only pertains to use in electronic form provided it is password protected, on intranet, or CD-Rom/DVD or E-book/E-journal. It may not be republished in electronic open access.
For any electronic use not mentioned, please contact Springer at permissions.springer@spi-global.com.
- Although Springer controls the copyright to the material and is entitled to negotiate on rights, this license is only valid subject to courtesy information to the author (address is given in the article/chapter).
- If you are an STM Signatory or your work will be published by an STM Signatory and you are requesting to reuse figures/tables/illustrations or single text extracts, permission is granted according to STM Permissions Guidelines: http://www.stm-assoc.org/permissions-guidelines/
For any electronic use not mentioned in the Guidelines, please contact Springer at permissions.springer@spi-global.com. If you request to reuse more content than stipulated in the STM Permissions Guidelines, you will be charged a permission fee for the excess content.
Permission is valid upon payment of the fee as indicated in the licensing process. If permission is granted free of charge on this occasion, that does not prejudice any rights we might have to charge for reproduction of our copyrighted material in the future.
-If your request is for reuse in a Thesis, permission is granted free of charge under the following conditions:
This license is valid for one-time use only for the purpose of defending your thesis and with a maximum of 100 extra copies in paper. If the thesis is going to be published, permission needs to be reobtained.
- includes use in an electronic form, provided it is an author-created version of the thesis on his/her own website and his/her university's repository, including UMI (according to the definition on the Sherpa website: http://www.sherpa.ac.uk/romeo/);
- is subject to courtesy information to the co-author or corresponding author.
Geographic Rights: Scope
Licenses may be exercised anywhere in the world.

Altering/Modifying Material: Not Permitted
Figures, tables, and illustrations may be altered minimally to serve your work. You may not alter or modify text in any manner. Abbreviations, additions, deletions and/or any other alterations shall be made only with prior written authorization of the author(s).
Reservation of Rights
Springer reserves all rights not specifically granted in the combination of (i) the license details provided by you and accepted in the course of this licensing transaction and (ii) these terms and conditions and (iii) CCC's Billing and Payment terms and conditions.
License Contingent on Payment
While you may exercise the rights licensed immediately upon issuance of the license at the end of the licensing process for the transaction, provided that you have disclosed complete and accurate details of your proposed use, no license is finally effective unless and until full payment is received from you (either by Springer or by CCC) as provided in CCC's Billing and Payment terms and conditions. If full payment is not received by the date due, then any license preliminarily granted shall be deemed automatically revoked and shall be void as if never granted. Further, in the event that you breach any of these terms and conditions or any of CCC's Billing and Payment terms and conditions, the license is automatically revoked and shall be void as if never granted. Use of materials as described in a revoked license, as well as any use of the materials beyond the scope of an unrevoked license, may constitute copyright infringement and Springer reserves the right to take any and all action to protect its copyright in the materials.
Copyright Notice: Disclaimer
You must include the following copyright and permission notice in connection with any reproduction of the licensed material:
"Springer book/journal title, chapter/article title, volume, year of publication, page, name(s) of author(s), (original copyright notice as given in the publication in which the material was originally published) "With permission of Springer"
In case of use of a graph or illustration, the caption of the graph or illustration must be included, as it is indicated in the original publication.
Warranties: None
Springer makes no representations or warranties with respect to the licensed material and adopts on its own behalf the limitations and disclaimers established by CCC on its behalf in its Billing and Payment terms and conditions for this licensing transaction.
Indemnity
You hereby indemnify and agree to hold harmless Springer and CCC, and their respective officers, directors, employees and agents, from and against any and all claims arising out of your use of the licensed material other than as specifically authorized pursuant to this license.
No Transfer of License
This license is personal to you and may not be sublicensed, assigned, or transferred by you without Springer's written permission.
No Amendment Except in Writing
This license may not be amended except in a writing signed by both parties (or, in the case of Springer, by CCC on Springer's behalf).
Objection to Contrary Terms
Springer hereby objects to any terms contained in any purchase order, acknowledgment, check endorsement or other writing prepared by you, which terms are inconsistent with these terms and conditions or CCC's Billing and Payment terms and conditions. These terms and conditions, together with CCC's Billing and Payment terms and conditions (which are incorporated herein), comprise the entire agreement between you and Springer (and CCC) concerning this licensing transaction. In the event of any conflict between your obligations established by these terms and conditions and those established by CCC's Billing and Payment terms and conditions, these terms and conditions shall control.
Jurisdiction
All disputes that may arise in connection with this present License, or the breach thereof, shall be settled exclusively by arbitration, to be held in the Federal Republic of Germany, in accordance with German law.

Other conditions:

V 12AUG2015

Title: Fluorine-Free Oil Absorbents Made from Cellulose Nanofibril Aerogels

Author: Arie Mulyadi, Zhe Zhang, Yulin Deng

Publication: Applied Materials

Publisher: American Chemical Society

Date: Feb 1, 2016

PERMISSION/LICENSE IS GRANTED FOR YOUR ORDER AT NO CHARGE

This type of permission/license, instead of the standard Terms & Conditions, is sent to you because no fee is being charged for your order. Please note the following:

- Permission is granted for your request in both print and electronic formats, and translations.
- If figures and/or tables were requested, they may be adapted or used in part.
- Please print this page for your records and send a copy of it to your publisher/graduate school.
- Appropriate credit for the requested material should be given as follows: "Reprinted (adapted) with permission from (COMPLETE REFERENCE CITATION). Copyright (YEAR) American Chemical Society." Insert appropriate information in place of the capitalized words.
- One-time permission is granted only for the use specified in your request. No additional uses are granted (such as derivative works or other editions). For any other uses, please submit a new request.

ROYAL SOCIETY OF CHEMISTRY LICENSE TERMS AND CONDITIONS

Oct 12, 2016

This Agreement between Arie Mulyadi ("You") and Royal Society of Chemistry ("Royal Society of Chemistry") consists of your license details and the terms and conditions provided by Royal Society of Chemistry and Copyright Clearance Center.

License Number	3966701013047
License date	Oct 12, 2016
Licensed Content Publisher	Royal Society of Chemistry
Licensed Content Publication	Chemical Society Reviews
Licensed Content Title	Cellulose nanomaterials review: structure, properties and nanocomposites
Licensed Content Author	Robert J. Moon,Ashlie Martini,John Nairn,John Simonsen,Jeff Youngblood
Licensed Content Date	May 12, 2011
Licensed Content Volume Number	40
Licensed Content Issue Number	7
Type of Use	Thesis/Dissertation
Requestor type	academic/educational
Portion	figures/tables/images
Number of figures/tables/images	1
Format	electronic
Distribution quantity	10
Will you be translating?	no
Order reference number	
Title of the thesis/dissertation	FUNCTIONALIZATION AND CARBONIZATION OF CELLULOSE NANOFIBRILS AS HIGH-PERFORMANCE FIBER MATERIALS AND THEIR APPLICATIONS
Expected completion date	Nov 2016
Estimated size	141
Requestor Location	Arie Mulyadi 500 10th Street NW ATLANTA, GA 30332

	United States Attn: Arie Mulyadi
Billing Type	Invoice
Billing Address	Arie Mulyadi 500 10th Street NW ATLANTA, GA 30332 United States Attn: Arie Mulyadi
Total	**0.00 USD**

Terms and Conditions

This License Agreement is between {Requestor Name} (“You”) and The Royal Society of Chemistry (“RSC”) provided by the Copyright Clearance Center (“CCC”). The license consists of your order details, the terms and conditions provided by the Royal Society of Chemistry, and the payment terms and conditions.

RSC / TERMS AND CONDITIONS

INTRODUCTION

The publisher for this copyrighted material is The Royal Society of Chemistry. By clicking “accept” in connection with completing this licensing transaction, you agree that the following terms and conditions apply to this transaction (along with the Billing and Payment terms and conditions established by CCC, at the time that you opened your RightsLink account and that are available at any time at .

LICENSE GRANTED

The RSC hereby grants you a non-exclusive license to use the aforementioned material anywhere in the world subject to the terms and conditions indicated herein. Reproduction of the material is confined to the purpose and/or media for which permission is hereby given.

RESERVATION OF RIGHTS

The RSC reserves all rights not specifically granted in the combination of (i) the license details provided by your and accepted in the course of this licensing transaction; (ii) these terms and conditions; and (iii) CCC’s Billing and Payment terms and conditions.

REVOCATION

The RSC reserves the right to revoke this license for any reason, including, but not limited to, advertising and promotional uses of RSC content, third party usage, and incorrect source figure attribution.

THIRD-PARTY MATERIAL DISCLAIMER

If part of the material to be used (for example, a figure) has appeared in the RSC publication with credit to another source, permission must also be sought from that source. If the other source is another RSC publication these details should be included in your RightsLink request. If the other source is a third party, permission must be obtained from the third party. The RSC disclaims any responsibility for the reproduction you make of items owned by a third party.

PAYMENT OF FEE

If the permission fee for the requested material is waived in this instance, please be advised that any future requests for the reproduction of RSC materials may attract a fee.

ACKNOWLEDGEMENT

The reproduction of the licensed material must be accompanied by the following acknowledgement:
Reproduced (“Adapted” or “in part”) from {Reference Citation} (or Ref XX) with permission of The Royal Society of Chemistry.

If the licensed material is being reproduced from New Journal of Chemistry (NJC), Photochemical & Photobiological Sciences (PPS) or Physical Chemistry Chemical Physics (PCCP) you must include one of the following acknowledgements:

For figures originally published in NJC:
Reproduced (“Adapted” or “in part”) from {Reference Citation} (or Ref XX) with permission of The Royal Society of Chemistry (RSC) on behalf of the European Society for Photobiology, the European Photochemistry Association and the RSC.

For figures originally published in PPS:

Reproduced (“Adapted” or “in part”) from {Reference Citation} (or Ref XX) with permission of The Royal Society of Chemistry (RSC) on behalf of the Centre National de la Recherche Scientifique (CNRS) and the RSC.
For figures originally published in PCCP:
Reproduced (“Adapted” or “in part”) from {Reference Citation} (or Ref XX) with permission of the PCCP Owner Societies.
HYPERTEXT LINKS
With any material which is being reproduced in electronic form, you must include a hypertext link to the original RSC article on the RSC’s website. The recommended form for the hyperlink is http://dx.doi.org/10.1039/DOI suffix, for example in the link http://dx.doi.org/10.1039/b110420a the DOI suffix is ‘b110420a’. To find the relevant DOI suffix for the RSC article in question, go to the Journals section of the website and locate the article in the list of papers for the volume and issue of your specific journal. You will find the DOI suffix quoted there.
LICENSE CONTINGENT ON PAYMENT
While you may exercise the rights licensed immediately upon issuance of the license at the end of the licensing process for the transaction, provided that you have disclosed complete and accurate details of your proposed use, no license is finally effective unless and until full payment is received from you (by CCC) as provided in CCC's Billing and Payment terms and conditions. If full payment is not received on a timely basis, then any license preliminarily granted shall be deemed automatically revoked and shall be void as if never granted. Further, in the event that you breach any of these terms and conditions or any of CCC's Billing and Payment terms and conditions, the license is automatically revoked and shall be void as if never granted. Use of materials as described in a revoked license, as well as any use of the materials beyond the scope of an unrevoked license, may constitute copyright infringement and the RSC reserves the right to take any and all action to protect its copyright in the materials.
WARRANTIES
The RSC makes no representations or warranties with respect to the licensed material.
INDEMNITY
You hereby indemnify and agree to hold harmless the RSC and the CCC, and their respective officers, directors, trustees, employees and agents, from and against any and all claims arising out of your use of the licensed material other than as specifically authorized pursuant to this licence.
NO TRANSFER OF LICENSE
This license is personal to you or your publisher and may not be sublicensed, assigned, or transferred by you to any other person without the RSC's written permission.
NO AMENDMENT EXCEPT IN WRITING
This license may not be amended except in a writing signed by both parties (or, in the case of “Other Conditions, v1.2”, by CCC on the RSC's behalf).
OBJECTION TO CONTRARY TERMS
You hereby acknowledge and agree that these terms and conditions, together with CCC's Billing and Payment terms and conditions (which are incorporated herein), comprise the entire agreement between you and the RSC (and CCC) concerning this licensing transaction, to the exclusion of all other terms and conditions, written or verbal, express or implied (including any terms contained in any purchase order, acknowledgment, check endorsement or other writing prepared by you). In the event of any conflict between your obligations established by these terms and conditions and those established by CCC's Billing and Payment terms and conditions, these terms and conditions shall control.
JURISDICTION
This license transaction shall be governed by and construed in accordance with the laws of the District of Columbia. You hereby agree to submit to the jurisdiction of the courts located in the District of Columbia for purposes of resolving any disputes that may arise in connection with this licensing transaction.
LIMITED LICENSE
The following terms and conditions apply to specific license types:
Translation
This permission is granted for non-exclusive world English rights only unless your license was granted for translation rights. If you licensed translation rights you may only translate this content into the languages you requested. A professional translator must perform all translations and reproduce the content word for word preserving the integrity of the article.

Title: Cellulose Nanocrystals vs. Cellulose Nanofibrils: A Comparative Study on Their Microstructures and Effects as Polymer Reinforcing Agents

Author: Xuezhu Xu, Fei Liu, Long Jiang, et al

Publication: Applied Materials

Publisher: American Chemical Society

Date: Apr 1, 2013

PERMISSION/LICENSE IS GRANTED FOR YOUR ORDER AT NO CHARGE

This type of permission/license, instead of the standard Terms & Conditions, is sent to you because no fee is being charged for your order. Please note the following:

- Permission is granted for your request in both print and electronic formats, and translations.
- If figures and/or tables were requested, they may be adapted or used in part.
- Please print this page for your records and send a copy of it to your publisher/graduate school.
- Appropriate credit for the requested material should be given as follows: "Reprinted (adapted) with permission from (COMPLETE REFERENCE CITATION). Copyright (YEAR) American Chemical Society." Insert appropriate information in place of the capitalized words.
- One-time permission is granted only for the use specified in your request. No additional uses are granted (such as derivative works or other editions). For any other uses, please submit a new request.

If credit is given to another source for the material you requested, permission must be obtained from that source.

Title: Development of Biochar-Based Functional Materials: Toward a Sustainable Platform Carbon Material

Author: Wu-Jun Liu, Hong Jiang, Han-Qing Yu

Publication: Chemical Reviews

Publisher: American Chemical Society

Date: Nov 1, 2015

PERMISSION/LICENSE IS GRANTED FOR YOUR ORDER AT NO CHARGE

This type of permission/license, instead of the standard Terms & Conditions, is sent to you because no fee is being charged for your order. Please note the following:

- Permission is granted for your request in both print and electronic formats, and translations.
- If figures and/or tables were requested, they may be adapted or used in part.
- Please print this page for your records and send a copy of it to your publisher/graduate school.
- Appropriate credit for the requested material should be given as follows: "Reprinted (adapted) with permission from (COMPLETE REFERENCE CITATION). Copyright (YEAR) American Chemical Society." Insert appropriate information in place of the capitalized words.
- One-time permission is granted only for the use specified in your request. No additional uses are granted (such as derivative works or other editions). For any other uses, please submit a new request.

If credit is given to another source for the material you requested, permission must be obtained from that source.

JOHN WILEY AND SONS LICENSE TERMS AND CONDITIONS

Oct 12, 2016

This Agreement between Arie Mulyadi ("You") and John Wiley and Sons ("John Wiley and Sons") consists of your license details and the terms and conditions provided by John Wiley and Sons and Copyright Clearance Center.

License Number	3966710211880
License date	Oct 12, 2016
Licensed Content Publisher	John Wiley and Sons
Licensed Content Publication	Advanced Materials
Licensed Content Title	Application and Future Challenges of Functional Nanocarbon Hybrids
Licensed Content Author	Cameron J. Shearer,Alexey Cherevan,Dominik Eder
Licensed Content Date	Feb 22, 2014
Licensed Content Pages	24
Type of Use	Dissertation/Thesis
Requestor type	University/Academic
Format	Electronic
Portion	Figure/table
Number of figures/tables	1
Original Wiley figure/table number(s)	Figure 1
Will you be translating?	No
Title of your thesis / dissertation	FUNCTIONALIZATION AND CARBONIZATION OF CELLULOSE NANOFIBRILS AS HIGH-PERFORMANCE FIBER MATERIALS AND THEIR APPLICATIONS
Expected completion date	Nov 2016
Expected size (number of pages)	141
Requestor Location	Arie Mulyadi 500 10th Street NW ATLANTA, GA 30332 United States Attn: Arie Mulyadi
Publisher Tax ID	EU826007151
Billing Type	Invoice

Billing Address	Arie Mulyadi 500 10th Street NW ATLANTA, GA 30332 United States Attn: Arie Mulyadi
Total	**0.00 USD**

Terms and Conditions

TERMS AND CONDITIONS

This copyrighted material is owned by or exclusively licensed to John Wiley & Sons, Inc. or one of its group companies (each a"Wiley Company") or handled on behalf of a society with which a Wiley Company has exclusive publishing rights in relation to a particular work (collectively "WILEY"). By clicking "accept" in connection with completing this licensing transaction, you agree that the following terms and conditions apply to this transaction (along with the billing and payment terms and conditions established by the Copyright Clearance Center Inc., ("CCC's Billing and Payment terms and conditions"), at the time that you opened your RightsLink account (these are available at any time at http://myaccount.copyright.com).

Terms and Conditions

- The materials you have requested permission to reproduce or reuse (the "Wiley Materials") are protected by copyright.

- You are hereby granted a personal, non-exclusive, non-sub licensable (on a stand-alone basis), non-transferable, worldwide, limited license to reproduce the Wiley Materials for the purpose specified in the licensing process. This license, **and any CONTENT (PDF or image file) purchased as part of your order,** is for a one-time use only and limited to any maximum distribution number specified in the license. The first instance of republication or reuse granted by this license must be completed within two years of the date of the grant of this license (although copies prepared before the end date may be distributed thereafter). The Wiley Materials shall not be used in any other manner or for any other purpose, beyond what is granted in the license. Permission is granted subject to an appropriate acknowledgement given to the author, title of the material/book/journal and the publisher. You shall also duplicate the copyright notice that appears in the Wiley publication in your use of the Wiley Material. Permission is also granted on the understanding that nowhere in the text is a previously published source acknowledged for all or part of this Wiley Material. Any third party content is expressly excluded from this permission.

- With respect to the Wiley Materials, all rights are reserved. Except as expressly granted by the terms of the license, no part of the Wiley Materials may be copied, modified, adapted (except for minor reformatting required by the new Publication), translated, reproduced, transferred or distributed, in any form or by any means, and no derivative works may be made based on the Wiley Materials without the prior permission of the respective copyright owner.**For STM Signatory Publishers clearing permission under the terms of the STM Permissions Guidelines only, the terms of the license are extended to include subsequent editions and for editions in other languages, provided such editions are for the work as a whole in situ and does not involve the separate exploitation of the permitted figures or extracts,** You may not alter, remove or suppress in any manner any copyright, trademark or other notices displayed by the Wiley Materials. You may not license, rent, sell, loan, lease, pledge, offer as security, transfer or assign the Wiley Materials on a stand-alone basis, or any of the rights granted to you hereunder to any other person.

- The Wiley Materials and all of the intellectual property rights therein shall at all times remain the exclusive property of John Wiley & Sons Inc, the Wiley Companies, or their respective licensors, and your interest therein is only that of having possession of and the right to reproduce the Wiley Materials

pursuant to Section 2 herein during the continuance of this Agreement. You agree that you own no right, title or interest in or to the Wiley Materials or any of the intellectual property rights therein. You shall have no rights hereunder other than the license as provided for above in Section 2. No right, license or interest to any trademark, trade name, service mark or other branding ("Marks") of WILEY or its licensors is granted hereunder, and you agree that you shall not assert any such right, license or interest with respect thereto

- NEITHER WILEY NOR ITS LICENSORS MAKES ANY WARRANTY OR REPRESENTATION OF ANY KIND TO YOU OR ANY THIRD PARTY, EXPRESS, IMPLIED OR STATUTORY, WITH RESPECT TO THE MATERIALS OR THE ACCURACY OF ANY INFORMATION CONTAINED IN THE MATERIALS, INCLUDING, WITHOUT LIMITATION, ANY IMPLIED WARRANTY OF MERCHANTABILITY, ACCURACY, SATISFACTORY QUALITY, FITNESS FOR A PARTICULAR PURPOSE, USABILITY, INTEGRATION OR NON-INFRINGEMENT AND ALL SUCH WARRANTIES ARE HEREBY EXCLUDED BY WILEY AND ITS LICENSORS AND WAIVED BY YOU.

- WILEY shall have the right to terminate this Agreement immediately upon breach of this Agreement by you.

- You shall indemnify, defend and hold harmless WILEY, its Licensors and their respective directors, officers, agents and employees, from and against any actual or threatened claims, demands, causes of action or proceedings arising from any breach of this Agreement by you.

- IN NO EVENT SHALL WILEY OR ITS LICENSORS BE LIABLE TO YOU OR ANY OTHER PARTY OR ANY OTHER PERSON OR ENTITY FOR ANY SPECIAL, CONSEQUENTIAL, INCIDENTAL, INDIRECT, EXEMPLARY OR PUNITIVE DAMAGES, HOWEVER CAUSED, ARISING OUT OF OR IN CONNECTION WITH THE DOWNLOADING, PROVISIONING, VIEWING OR USE OF THE MATERIALS REGARDLESS OF THE FORM OF ACTION, WHETHER FOR BREACH OF CONTRACT, BREACH OF WARRANTY, TORT, NEGLIGENCE, INFRINGEMENT OR OTHERWISE (INCLUDING, WITHOUT LIMITATION, DAMAGES BASED ON LOSS OF PROFITS, DATA, FILES, USE, BUSINESS OPPORTUNITY OR CLAIMS OF THIRD PARTIES), AND WHETHER OR NOT THE PARTY HAS BEEN ADVISED OF THE POSSIBILITY OF SUCH DAMAGES. THIS LIMITATION SHALL APPLY NOTWITHSTANDING ANY FAILURE OF ESSENTIAL PURPOSE OF ANY LIMITED REMEDY PROVIDED HEREIN.

- Should any provision of this Agreement be held by a court of competent jurisdiction to be illegal, invalid, or unenforceable, that provision shall be deemed amended to achieve as nearly as possible the same economic effect as the original provision, and the legality, validity and enforceability of the remaining provisions of this Agreement shall not be affected or impaired thereby.

- The failure of either party to enforce any term or condition of this Agreement shall not constitute a waiver of either party's right to enforce each and every term and condition of this Agreement. No breach under this agreement shall be deemed waived or excused by either party unless such waiver or consent is in writing signed by the party granting such waiver or consent. The waiver by or consent of a party to a breach of any provision of this Agreement shall not operate or be construed as a waiver of or consent to any other or subsequent breach by such other party.

- This Agreement may not be assigned (including by operation of law or otherwise) by you without WILEY's prior written consent.

- Any fee required for this permission shall be non-refundable after thirty (30) days from receipt by the CCC.

- These terms and conditions together with CCC's Billing and Payment terms and conditions (which are incorporated herein) form the entire agreement between you and WILEY concerning this licensing

transaction and (in the absence of fraud) supersedes all prior agreements and representations of the parties, oral or written. This Agreement may not be amended except in writing signed by both parties. This Agreement shall be binding upon and inure to the benefit of the parties' successors, legal representatives, and authorized assigns.

- In the event of any conflict between your obligations established by these terms and conditions and those established by CCC's Billing and Payment terms and conditions, these terms and conditions shall prevail.

- WILEY expressly reserves all rights not specifically granted in the combination of (i) the license details provided by you and accepted in the course of this licensing transaction, (ii) these terms and conditions and (iii) CCC's Billing and Payment terms and conditions.

- This Agreement will be void if the Type of Use, Format, Circulation, or Requestor Type was misrepresented during the licensing process.

- This Agreement shall be governed by and construed in accordance with the laws of the State of New York, USA, without regards to such state's conflict of law rules. Any legal action, suit or proceeding arising out of or relating to these Terms and Conditions or the breach thereof shall be instituted in a court of competent jurisdiction in New York County in the State of New York in the United States of America and each party hereby consents and submits to the personal jurisdiction of such court, waives any objection to venue in such court and consents to service of process by registered or certified mail, return receipt requested, at the last known address of such party.

WILEY OPEN ACCESS TERMS AND CONDITIONS

Wiley Publishes Open Access Articles in fully Open Access Journals and in Subscription journals offering Online Open. Although most of the fully Open Access journals publish open access articles under the terms of the Creative Commons Attribution (CC BY) License only, the subscription journals and a few of the Open Access Journals offer a choice of Creative Commons Licenses. The license type is clearly identified on the article.

The Creative Commons Attribution License

The Creative Commons Attribution License (CC-BY) allows users to copy, distribute and transmit an article, adapt the article and make commercial use of the article. The CC-BY license permits commercial and non-

Creative Commons Attribution Non-Commercial License

The Creative Commons Attribution Non-Commercial (CC-BY-NC)License permits use, distribution and reproduction in any medium, provided the original work is properly cited and is not used for commercial purposes.(see below)

Creative Commons Attribution-Non-Commercial-NoDerivs License

The Creative Commons Attribution Non-Commercial-NoDerivs License (CC-BY-NC-ND) permits use, distribution and reproduction in any medium, provided the original work is properly cited, is not used for commercial purposes and no modifications or adaptations are made. (see below)

Use by commercial "for-profit" organizations

Use of Wiley Open Access articles for commercial, promotional, or marketing purposes requires further explicit permission from Wiley and will be subject to a fee.

Further details can be found on Wiley Online Library http://olabout.wiley.com/WileyCDA/Section/id-410895.html

Other Terms and Conditions:

v1.10 Last updated September 2015

ELSEVIER LICENSE
TERMS AND CONDITIONS

Oct 12, 2016

This Agreement between Arie Mulyadi ("You") and Elsevier ("Elsevier") consists of your license details and the terms and conditions provided by Elsevier and Copyright Clearance Center.

License Number	3966710359749
License date	Oct 12, 2016
Licensed Content Publisher	Elsevier
Licensed Content Publication	Carbon
Licensed Content Title	Changes in electrical and microstructural properties of microcrystalline cellulose as function of carbonization temperature
Licensed Content Author	Yo-Rhin Rhim,Dajie Zhang,D. Howard Fairbrother,Kevin A. Wepasnick,Kenneth J. Livi,Robert J. Bodnar,Dennis C. Nagle
Licensed Content Date	April 2010
Licensed Content Volume Number	48
Licensed Content Issue Number	4
Licensed Content Pages	13
Start Page	1012
End Page	1024
Type of Use	reuse in a thesis/dissertation
Intended publisher of new work	other
Portion	figures/tables/illustrations
Number of figures/tables/illustrations	2
Format	electronic
Are you the author of this Elsevier article?	No
Will you be translating?	No
Order reference number	
Original figure numbers	Fig.1 and Fig.4
Title of your thesis/dissertation	FUNCTIONALIZATION AND CARBONIZATION OF CELLULOSE NANOFIBRILS AS HIGH-PERFORMANCE FIBER MATERIALS AND THEIR APPLICATIONS
Expected completion date	Nov 2016
Estimated size (number of pages)	141
Elsevier VAT number	GB 494 6272 12
Requestor Location	

Arie Mulyadi
500 10th Street NW

ATLANTA, GA 30332
United States
Attn: Arie Mulyadi

Total **0.00 USD**

Terms and Conditions

INTRODUCTION

1. The publisher for this copyrighted material is Elsevier. By clicking "accept" in connection with completing this licensing transaction, you agree that the following terms and conditions apply to this transaction (along with the Billing and Payment terms and conditions established by Copyright Clearance Center, Inc. ("CCC"), at the time that you opened your Rightslink account and that are available at any time at http://myaccount.copyright.com).

GENERAL TERMS

2. Elsevier hereby grants you permission to reproduce the aforementioned material subject to the terms and conditions indicated.
3. Acknowledgement: If any part of the material to be used (for example, figures) has appeared in our publication with credit or acknowledgement to another source, permission must also be sought from that source. If such permission is not obtained then that material may not be included in your publication/copies. Suitable acknowledgement to the source must be made, either as a footnote or in a reference list at the end of your publication, as follows:
"Reprinted from Publication title, Vol /edition number, Author(s), Title of article / title of chapter, Pages No., Copyright (Year), with permission from Elsevier [OR APPLICABLE SOCIETY COPYRIGHT OWNER]." Also Lancet special credit - "Reprinted from The Lancet, Vol. number, Author(s), Title of article, Pages No., Copyright (Year), with permission from Elsevier."
4. Reproduction of this material is confined to the purpose and/or media for which permission is hereby given.
5. Altering/Modifying Material: Not Permitted. However figures and illustrations may be altered/adapted minimally to serve your work. Any other abbreviations, additions, deletions and/or any other alterations shall be made only with prior written authorization of Elsevier Ltd. (Please contact Elsevier at permissions@elsevier.com)
6. If the permission fee for the requested use of our material is waived in this instance, please be advised that your future requests for Elsevier materials may attract a fee.
7. Reservation of Rights: Publisher reserves all rights not specifically granted in the combination of (i) the license details provided by you and accepted in the course of this licensing transaction, (ii) these terms and conditions and (iii) CCC's Billing and Payment terms and conditions.
8. License Contingent Upon Payment: While you may exercise the rights licensed immediately upon issuance of the license at the end of the licensing process for the transaction, provided that you have disclosed complete and accurate details of your proposed use, no license is finally effective unless and until full payment is received from you (either by publisher or by CCC) as provided in CCC's Billing and Payment terms and conditions. If full payment is not received on a timely basis, then any license preliminarily granted shall be deemed automatically revoked and shall be void as if never granted. Further, in the event that you breach any of these terms and conditions or any of CCC's Billing and Payment terms and conditions, the license is automatically revoked and shall be void as if never granted. Use of materials as described in a revoked license, as well as any use of the materials beyond the scope of an unrevoked license, may constitute copyright infringement and publisher reserves the right to take any and all action to protect its copyright in the materials.
9. Warranties: Publisher makes no representations or warranties with respect to the licensed material.
10. Indemnity: You hereby indemnify and agree to hold harmless publisher and CCC, and their respective officers, directors, employees and agents, from and against any and all claims arising out of your use of the licensed material other than as specifically authorized pursuant to this license.
11. No Transfer of License: This license is personal to you and may not be sublicensed, assigned, or transferred by you to any other person without publisher's written permission.

12. No Amendment Except in Writing: This license may not be amended except in a writing signed by both parties (or, in the case of publisher, by CCC on publisher's behalf).
13. Objection to Contrary Terms: Publisher hereby objects to any terms contained in any purchase order, acknowledgment, check endorsement or other writing prepared by you, which terms are inconsistent with these terms and conditions or CCC's Billing and Payment terms and conditions. These terms and conditions, together with CCC's Billing and Payment terms and conditions (which are incorporated herein), comprise the entire agreement between you and publisher (and CCC) concerning this licensing transaction. In the event of any conflict between your obligations established by these terms and conditions and those established by CCC's Billing and Payment terms and conditions, these terms and conditions shall control.
14. Revocation: Elsevier or Copyright Clearance Center may deny the permissions described in this License at their sole discretion, for any reason or no reason, with a full refund payable to you. Notice of such denial will be made using the contact information provided by you. Failure to receive such notice will not alter or invalidate the denial. In no event will Elsevier or Copyright Clearance Center be responsible or liable for any costs, expenses or damage incurred by you as a result of a denial of your permission request, other than a refund of the amount(s) paid by you to Elsevier and/or Copyright Clearance Center for denied permissions.

LIMITED LICENSE

The following terms and conditions apply only to specific license types:
15. **Translation**: This permission is granted for non-exclusive world **English** rights only unless your license was granted for translation rights. If you licensed translation rights you may only translate this content into the languages you requested. A professional translator must perform all translations and reproduce the content word for word preserving the integrity of the article.
16. **Posting licensed content on any Website**: The following terms and conditions apply as follows: Licensing material from an Elsevier journal: All content posted to the web site must maintain the copyright information line on the bottom of each image; A hyper-text must be included to the Homepage of the journal from which you are licensing at http://www.sciencedirect.com/science/journal/xxxxx or the Elsevier homepage for books at http://www.elsevier.com; Central Storage: This license does not include permission for a scanned version of the material to be stored in a central repository such as that provided by Heron/XanEdu.
Licensing material from an Elsevier book: A hyper-text link must be included to the Elsevier homepage at http://www.elsevier.com . All content posted to the web site must maintain the copyright information line on the bottom of each image.

Posting licensed content on Electronic reserve: In addition to the above the following clauses are applicable: The web site must be password-protected and made available only to bona fide students registered on a relevant course. This permission is granted for 1 year only. You may obtain a new license for future website posting.
17. **For journal authors:** the following clauses are applicable in addition to the above:
Preprints:
A preprint is an author's own write-up of research results and analysis, it has not been peer-reviewed, nor has it had any other value added to it by a publisher (such as formatting, copyright, technical enhancement etc.).
Authors can share their preprints anywhere at any time. Preprints should not be added to or enhanced in any way in order to appear more like, or to substitute for, the final versions of articles however authors can update their preprints on arXiv or RePEc with their Accepted Author Manuscript (see below).
If accepted for publication, we encourage authors to link from the preprint to their formal publication via its DOI. Millions of researchers have access to the formal publications on ScienceDirect, and so links will help users to find, access, cite and use the best available version. Please note that Cell Press, The Lancet and some society-owned have different preprint policies. Information on these policies is available on the journal homepage.
Accepted Author Manuscripts: An accepted author manuscript is the manuscript of an article that has been accepted for publication and which typically includes author-incorporated changes suggested during submission, peer review and editor-author communications.
Authors can share their accepted author manuscript:

- immediately
  via their non-commercial person homepage or blog

- by updating a preprint in arXiv or RePEc with the accepted manuscript
- via their research institute or institutional repository for internal institutional uses or as part of an invitation-only research collaboration work-group
- directly by providing copies to their students or to research collaborators for their personal use
- for private scholarly sharing as part of an invitation-only work group on commercial sites with which Elsevier has an agreement

– after the embargo period
- via non-commercial hosting platforms such as their institutional repository
- via commercial sites with which Elsevier has an agreement

In all cases accepted manuscripts should:

– link to the formal publication via its DOI
– bear a CC-BY-NC-ND license - this is easy to do
– if aggregated with other manuscripts, for example in a repository or other site, be shared in alignment with our hosting policy not be added to or enhanced in any way to appear more like, or to substitute for, the published journal article.

Published journal article (JPA): A published journal article (PJA) is the definitive final record of published research that appears or will appear in the journal and embodies all value-adding publishing activities including peer review co-ordination, copy-editing, formatting, (if relevant) pagination and online enrichment.
Policies for sharing publishing journal articles differ for subscription and gold open access articles:
Subscription Articles: If you are an author, please share a link to your article rather than the full-text. Millions of researchers have access to the formal publications on ScienceDirect, and so links will help your users to find, access, cite, and use the best available version.
Theses and dissertations which contain embedded PJAs as part of the formal submission can be posted publicly by the awarding institution with DOI links back to the formal publications on ScienceDirect.
If you are affiliated with a library that subscribes to ScienceDirect you have additional private sharing rights for others' research accessed under that agreement. This includes use for classroom teaching and internal training at the institution (including use in course packs and courseware programs), and inclusion of the article for grant funding purposes.
Gold Open Access Articles: May be shared according to the author-selected end-user license and should contain a CrossMark logo, the end user license, and a DOI link to the formal publication on ScienceDirect.
Please refer to Elsevier's posting policy for further information.
18. **For book authors** the following clauses are applicable in addition to the above: Authors are permitted to place a brief summary of their work online only. You are not allowed to download and post the published electronic version of your chapter, nor may you scan the printed edition to create an electronic version. **Posting to a repository:** Authors are permitted to post a summary of their chapter only in their institution's repository.
19. **Thesis/Dissertation**: If your license is for use in a thesis/dissertation your thesis may be submitted to your institution in either print or electronic form. Should your thesis be published commercially, please reapply for permission. These requirements include permission for the Library and Archives of Canada to supply single copies, on demand, of the complete thesis and include permission for Proquest/UMI to supply single copies, on demand, of the complete thesis. Should your thesis be published commercially, please reapply for permission. Theses and dissertations which contain embedded PJAs as part of the formal submission can be posted publicly by the awarding institution with DOI links back to the formal publications on ScienceDirect.

Elsevier Open Access Terms and Conditions
You can publish open access with Elsevier in hundreds of open access journals or in nearly 2000 established subscription journals that support open access publishing. Permitted third party re-use of these open access articles is defined by the author's choice of Creative Commons user license. See our open access license policy for more information.
Terms & Conditions applicable to all Open Access articles published with Elsevier:

REFERENCES

[1]. Klemm, D., B. Heublein, H.-P. Fink, and A. Bohn, Cellulose: Fascinating Biopolymer and Sustainable Raw Material. *Angewandte Chemie International Edition.* **2005**, *44*(22), 3358-3393, DOI: 10.1002/anie.200460587.

[2]. Abdul Khalil, H.P.S., A.H. Bhat, and A.F. Ireana Yusra, Green Composites from Sustainable Cellulose Nanofibrils: A Review. *Carbohydrate Polymers.* **2012**, *87*(2), 963-979, DOI: http://dx.doi.org/10.1016/j.carbpol.2011.08.078.

[3]. Nishiyama, Y., G.P. Johnson, A.D. French, V.T. Forsyth, and P. Langan, Neutron Crystallography, Molecular Dynamics, and Quantum Mechanics Studies of the Nature of Hydrogen Bonding in Cellulose Iβ. *Biomacromolecules.* **2008**, *9*(11), 3133-3140, DOI: 10.1021/bm800726v.

[4]. Jarvis, M., Chemistry: Cellulose Stacks Up. *Nature.* **2003**, *426*(6967), 611-612.

[5]. Moon, R.J., A. Martini, J. Nairn, J. Simonsen, and J. Youngblood, Cellulose Nanomaterials Review: Structure, Properties and Nanocomposites. *Chemical Society Reviews.* **2011**, *40*(7), 3941-3994, DOI: 10.1039/C0CS00108B.

[6]. Herrick, F.W., R.L. Casebier, J.K. Hamilton, and K.R. Sandberg, *Microfibrillated Cellulose: Morphology and Accessibility*. *Journal Name: J. Appl. Polym. Sci.: Appl. Polym. Symp.; (United States); Journal Volume: 37; Conference: 9. Cellulose Conference, Syracuse, Ny, USA, 24 May 1982*, 1983: ; ITT Rayonier Inc., Shelton, WA, Medium: X; Size: Pages: 797-813.

[7]. Klemm, D., F. Kramer, S. Moritz, T. Lindström, M. Ankerfors, D. Gray, and A. Dorris, Nanocelluloses: A New Family of Nature-Based Materials. *Angewandte Chemie International Edition.* **2011**, *50*(24), 5438-5466, DOI: 10.1002/anie.201001273.

[8]. Lavoine, N., I. Desloges, A. Dufresne, and J. Bras, Microfibrillated Cellulose – Its Barrier Properties and Applications in Cellulosic Materials: A Review. *Carbohydrate Polymers.* **2012**, *90*(2), 735-764, DOI: http://dx.doi.org/10.1016/j.carbpol.2012.05.026.

[9]. Eichhorn, S.J., A. Dufresne, M. Aranguren, N.E. Marcovich, J.R. Capadona, S.J. Rowan, C. Weder, W. Thielemans, M. Roman, S. Renneckar, W. Gindl, S. Veigel, J. Keckes, H. Yano, K. Abe, M. Nogi, A.N. Nakagaito, A. Mangalam, J. Simonsen, A.S. Benight, A. Bismarck, L.A. Berglund, and T. Peijs, Review: Current International Research into Cellulose Nanofibres and Nanocomposites. *Journal of Materials Science.* **2009**, *45*(1), 1-33, DOI: 10.1007/s10853-009-3874-0.

[10]. Abe, K., S. Iwamoto, and H. Yano, Obtaining Cellulose Nanofibers with a Uniform Width of 15 Nm from Wood. *Biomacromolecules.* **2007**, *8*(10), 3276-3278, DOI: 10.1021/bm700624p.

[11]. Chao, Y.-p., Y. Sugano, T. Kouda, F. Yoshinaga, and M. Shoda, Production of Bacterial Cellulose by Acetobacter Xylinumwith an Air-Lift Reactor. *Biotechnology Techniques.* **1997**, *11*(11), 829-832, DOI: 10.1023/a:1018433526709.

[12]. Steinbuchel, A., R. Jonas, and L.F. Farah, Biodegradable Polymers and Macromoleculesproduction and Application of Microbial Cellulose. *Polymer Degradation and Stability.* **1998**, *59*(1), 101-106, DOI: http://dx.doi.org/10.1016/S0141-3910(97)00197-3.

[13]. Kralisch, D., N. Hessler, D. Klemm, R. Erdmann, and W. Schmidt, White Biotechnology for Cellulose Manufacturing—the Holir Concept. *Biotechnology and Bioengineering.* **2010**, *105*(4), 740-747, DOI: 10.1002/bit.22579.

[14]. Isogai, A., T. Saito, and H. Fukuzumi, Tempo-Oxidized Cellulose Nanofibers. *Nanoscale.* **2011**, *3*(1), 71-85, DOI: 10.1039/C0NR00583E.
[15]. Saito, T., S. Kimura, Y. Nishiyama, and A. Isogai, Cellulose Nanofibers Prepared by Tempo-Mediated Oxidation of Native Cellulose. *Biomacromolecules.* **2007**, *8*(8), 2485-2491, DOI: 10.1021/bm0703970.
[16]. Isogai, T., T. Saito, and A. Isogai, Wood Cellulose Nanofibrils Prepared by Tempo Electro-Mediated Oxidation. *Cellulose.* **2011**, *18*(2), 421-431, DOI: 10.1007/s10570-010-9484-9.
[17]. Wågberg, L., G. Decher, M. Norgren, T. Lindström, M. Ankerfors, and K. Axnäs, The Build-up of Polyelectrolyte Multilayers of Microfibrillated Cellulose and Cationic Polyelectrolytes. *Langmuir.* **2008**, *24*(3), 784-795, DOI: 10.1021/la702481v.
[18]. Okahisa, Y., A. Yoshida, S. Miyaguchi, and H. Yano, Optically Transparent Wood–Cellulose Nanocomposite as a Base Substrate for Flexible Organic Light-Emitting Diode Displays. *Composites Science and Technology.* **2009**, *69*(11–12), 1958-1961, DOI: http://dx.doi.org/10.1016/j.compscitech.2009.04.017.
[19]. Pääkkö, M., M. Ankerfors, H. Kosonen, A. Nykänen, S. Ahola, M. Österberg, J. Ruokolainen, J. Laine, P.T. Larsson, O. Ikkala, and T. Lindström, Enzymatic Hydrolysis Combined with Mechanical Shearing and High-Pressure Homogenization for Nanoscale Cellulose Fibrils and Strong Gels. *Biomacromolecules.* **2007**, *8*(6), 1934-1941, DOI: 10.1021/bm061215p.
[20]. Henriksson, M., G. Henriksson, L.A. Berglund, and T. Lindström, An Environmentally Friendly Method for Enzyme-Assisted Preparation of Microfibrillated Cellulose (Mfc) Nanofibers. *European Polymer Journal.* **2007**, *43*(8), 3434-3441, DOI: http://dx.doi.org/10.1016/j.eurpolymj.2007.05.038.
[21]. Turbak, A.F., F.W. Snyder, and K.R. Sandberg, Microfibrillated Cellulose. 1983, *Google Patents*.
[22]. Chakraborty, A., M. Sain, and M. Kortschot, Cellulose Microfibrils: A Novel Method of Preparation Using High Shear Refining and Cryocrushing, in Holzforschung. 2005, 102.
[23]. Postek, M.T., A. Vladár, J. Dagata, N. Farkas, B. Ming, R. Wagner, A. Raman, R.J. Moon, R. Sabo, and T.H. Wegner, Development of the Metrology and Imaging of Cellulose Nanocrystals. *Measurement Science and Technology.* **2010**, *22*(2), 024005.
[24]. Xu, X., F. Liu, L. Jiang, J.Y. Zhu, D. Haagenson, and D.P. Wiesenborn, Cellulose Nanocrystals Vs. Cellulose Nanofibrils: A Comparative Study on Their Microstructures and Effects as Polymer Reinforcing Agents. *ACS Applied Materials & Interfaces.* **2013**, *5*(8), 2999-3009, DOI: 10.1021/am302624t.
[25]. Hanus, J. and K. Mazeau, The Xyloglucan–Cellulose Assembly at the Atomic Scale. *Biopolymers.* **2006**, *82*(1), 59-73, DOI: 10.1002/bip.20460.
[26]. Goussé, C., H. Chanzy, M.L. Cerrada, and E. Fleury, Surface Silylation of Cellulose Microfibrils: Preparation and Rheological Properties. *Polymer.* **2004**, *45*(5), 1569-1575, DOI: http://dx.doi.org/10.1016/j.polymer.2003.12.028.
[27]. Carlmark, A. and E. Malmström, Atom Transfer Radical Polymerization from Cellulose Fibers at Ambient Temperature. *Journal of the American Chemical Society.* **2002**, *124*(6), 900-901, DOI: 10.1021/ja016582h.
[28]. Chen, Z., L. Ma, S. Li, J. Geng, Q. Song, J. Liu, C. Wang, H. Wang, J. Li, Z. Qin, and S. Li, Simple Approach to Carboxyl-Rich Materials through Low-Temperature Heat

Treatment of Hydrothermal Carbon in Air. *Applied Surface Science.* **2011**, *257*(20), 8686-8691, DOI: http://dx.doi.org/10.1016/j.apsusc.2011.05.048.
[29]. Liang, H.-W., Z.-Y. Wu, L.-F. Chen, C. Li, and S.-H. Yu, Bacterial Cellulose Derived Nitrogen-Doped Carbon Nanofiber Aerogel: An Efficient Metal-Free Oxygen Reduction Electrocatalyst for Zinc-Air Battery. *Nano Energy.* **2015**, *11*, 366-376, DOI: http://dx.doi.org/10.1016/j.nanoen.2014.11.008.
[30]. Wu, Z.-Y., H.-W. Liang, C. Li, B.-C. Hu, X.-X. Xu, Q. Wang, J.-F. Chen, and S.-H. Yu, Dyeing Bacterial Cellulose Pellicles for Energetic Heteroatom Doped Carbon Nanofiber Aerogels. *Nano Research.* **2014**, *7*(12), 1861-1872, DOI: 10.1007/s12274-014-0546-4.
[31]. Lai, F., Y.-E. Miao, Y. Huang, Y. Zhang, and T. Liu, Nitrogen-Doped Carbon Nanofiber/Molybdenum Disulfide Nanocomposites Derived from Bacterial Cellulose for High-Efficiency Electrocatalytic Hydrogen Evolution Reaction. *ACS Applied Materials & Interfaces.* **2016**, *8*(6), 3558-3566, DOI: 10.1021/acsami.5b06274.
[32]. Balu, B., V. Breedveld, and D.W. Hess, Fabrication of "Roll-Off" and "Sticky" Superhydrophobic Cellulose Surfaces Via Plasma Processing. *Langmuir.* **2008**, *24*(9), 4785-4790, DOI: 10.1021/la703766c.
[33]. Sahin, H.T., Rf-Cf4 Plasma Surface Modification of Paper: Chemical Evaluation of Two Sidedness with Xps/Atr-Ftir. *Applied Surface Science.* **2007**, *253*(9), 4367-4373, DOI: http://dx.doi.org/10.1016/j.apsusc.2006.09.052.
[34]. Daoud, W.A., J.H. Xin, Y.H. Zhang, and C.L. Mak, Pulsed Laser Deposition of Superhydrophobic Thin Teflon Films on Cellulosic Fibers. *Thin Solid Films.* **2006**, *515*(2), 835-837, DOI: http://dx.doi.org/10.1016/j.tsf.2005.12.245.
[35]. Bodin, A., L. Ahrenstedt, H. Fink, H. Brumer, B. Risberg, and P. Gatenholm, Modification of Nanocellulose with a Xyloglucan–Rgd Conjugate Enhances Adhesion and Proliferation of Endothelial Cells: Implications for Tissue Engineering. *Biomacromolecules.* **2007**, *8*(12), 3697-3704, DOI: 10.1021/bm070343q.
[36]. Aloulou, F., S. Boufi, N. Belgacem, and A. Gandini, Adsorption of Cationic Surfactants and Subsequent Adsolubilization of Organic Compounds onto Cellulose Fibers. *Colloid and Polymer Science.* **2004**, *283*(3), 344-350, DOI: 10.1007/s00396-004-1143-y.
[37]. Syverud, K., K. Xhanari, G. Chinga-Carrasco, Y. Yu, and P. Stenius, Films Made of Cellulose Nanofibrils: Surface Modification by Adsorption of a Cationic Surfactant and Characterization by Computer-Assisted Electron Microscopy. *Journal of Nanoparticle Research.* **2011**, *13*(2), 773-782, DOI: 10.1007/s11051-010-0077-1.
[38]. Shimizu, M., T. Saito, H. Fukuzumi, and A. Isogai, Hydrophobic, Ductile, and Transparent Nanocellulose Films with Quaternary Alkylammonium Carboxylates on Nanofibril Surfaces. *Biomacromolecules.* **2014**, *15*(11), 4320-4325, DOI: 10.1021/bm501329v.
[39]. Xhanari, K., K. Syverud, G. Chinga-Carrasco, K. Paso, and P. Stenius, Reduction of Water Wettability of Nanofibrillated Cellulose by Adsorption of Cationic Surfactants. *Cellulose.* **2011**, *18*(2), 257-270, DOI: 10.1007/s10570-010-9482-y.
[40]. Larsson, E., C.C. Sanchez, C. Porsch, E. Karabulut, L. Wågberg, and A. Carlmark, Thermo-Responsive Nanofibrillated Cellulose by Polyelectrolyte Adsorption. *European Polymer Journal.* **2013**, *49*(9), 2689-2696, DOI: http://dx.doi.org/10.1016/j.eurpolymj.2013.05.023.
[41]. Aulin, C., A. Shchukarev, J. Lindqvist, E. Malmström, L. Wågberg, and T. Lindström, Wetting Kinetics of Oil Mixtures on Fluorinated Model Cellulose Surfaces. *Journal of*

Colloid and Interface Science. **2008**, *317*(2), 556-567, DOI: http://dx.doi.org/10.1016/j.jcis.2007.09.096.
[42]. Martins, N.C.T., C.S.R. Freire, R.J.B. Pinto, S.C.M. Fernandes, C. Pascoal Neto, A.J.D. Silvestre, J. Causio, G. Baldi, P. Sadocco, and T. Trindade, Electrostatic Assembly of Ag Nanoparticles onto Nanofibrillated Cellulose for Antibacterial Paper Products. *Cellulose.* **2012**, *19*(4), 1425-1436, DOI: 10.1007/s10570-012-9713-5.
[43]. Kim, J., G. Montero, Y. Habibi, J.P. Hinestroza, J. Genzer, D.S. Argyropoulos, and O.J. Rojas, Dispersion of Cellulose Crystallites by Nonionic Surfactants in a Hydrophobic Polymer Matrix. *Polymer Engineering & Science.* **2009**, *49*(10), 2054-2061, DOI: 10.1002/pen.21417.
[44]. Goussé, C., H. Chanzy, G. Excoffier, L. Soubeyrand, and E. Fleury, Stable Suspensions of Partially Silylated Cellulose Whiskers Dispersed in Organic Solvents. *Polymer.* **2002**, *43*(9), 2645-2651, DOI: http://dx.doi.org/10.1016/S0032-3861(02)00051-4.
[45]. Pei, A., Q. Zhou, and L.A. Berglund, Functionalized Cellulose Nanocrystals as Biobased Nucleation Agents in Poly(L-Lactide) (Plla) – Crystallization and Mechanical Property Effects. *Composites Science and Technology.* **2010**, *70*(5), 815-821, DOI: http://dx.doi.org/10.1016/j.compscitech.2010.01.018.
[46]. Andresen, M., L.-S. Johansson, S.B. Tanem, and P. Stenius, Properties and Characterization of Hydrophobized Microfibrillated Cellulose. *Cellulose.* **2006**, *13*(6), 665-677, DOI: 10.1007/s10570-006-9072-1.
[47]. Lu, J., P. Askeland, and L.T. Drzal, Surface Modification of Microfibrillated Cellulose for Epoxy Composite Applications. *Polymer.* **2008**, *49*(5), 1285-1296, DOI: http://dx.doi.org/10.1016/j.polymer.2008.01.028.
[48]. Rodionova, G., M. Lenes, Ø. Eriksen, B. Hoff, and Ø. Gregersen. *Surface Modification of Microfibrillated Cellulose Films by Gas-Phase Esterification: Improvement of Barrier Properties*. in *Proceedings of the 2010 TAPPI International Conference on Nanotechnology for the Forest Product Industry, Espoo, Finland*. 2010.
[49]. Kim, D.-Y., Y. Nishiyama, and S. Kuga, Surface Acetylation of Bacterial Cellulose. *Cellulose.* **2002**, *9*(3), 361-367, DOI: 10.1023/a:1021140726936.
[50]. Tingaut, P., T. Zimmermann, and F. Lopez-Suevos, Synthesis and Characterization of Bionanocomposites with Tunable Properties from Poly (Lactic Acid) and Acetylated Microfibrillated Cellulose. *Biomacromolecules.* **2009**, *11*(2), 454-464.
[51]. Tome, L.C., M.G. Freire, L.P.N. Rebelo, A.J.D. Silvestre, C.P. Neto, I.M. Marrucho, and C.S.R. Freire, Surface Hydrophobization of Bacterial and Vegetable Cellulose Fibers Using Ionic Liquids as Solvent Media and Catalysts. *Green Chemistry.* **2011**, *13*(9), 2464-2470, DOI: 10.1039/C1GC15432J.
[52]. Yoshida, Y., L. Heux, and A. Isogai, Heterogeneous Reaction between Cellulose and Alkyl Ketene Dimer under Solvent-Free Conditions. *Cellulose.* **2012**, *19*(5), 1667-1676, DOI: 10.1007/s10570-012-9747-8.
[53]. Berlioz, S., S. Molina-Boisseau, Y. Nishiyama, and L. Heux, Gas-Phase Surface Esterification of Cellulose Microfibrils and Whiskers. *Biomacromolecules.* **2009**, *10*(8), 2144-2151, DOI: 10.1021/bm900319k.
[54]. Missoum, K., J. Bras, and M.N. Belgacem, Organization of Aliphatic Chains Grafted on Nanofibrillated Cellulose and Influence on Final Properties. *Cellulose.* **2012**, *19*(6), 1957-1973, DOI: 10.1007/s10570-012-9780-7.

[55]. Siqueira, G., J. Bras, and A. Dufresne, New Process of Chemical Grafting of Cellulose Nanoparticles with a Long Chain Isocyanate. *Langmuir.* **2010**, *26*(1), 402-411, DOI: 10.1021/la9028595.
[56]. Rueda, L., B. Fernández d'Arlas, Q. Zhou, L.A. Berglund, M.A. Corcuera, I. Mondragon, and A. Eceiza, Isocyanate-Rich Cellulose Nanocrystals and Their Selective Insertion in Elastomeric Polyurethane. *Composites Science and Technology.* **2011**, *71*(16), 1953-1960, DOI: http://dx.doi.org/10.1016/j.compscitech.2011.09.014.
[57]. Zhang, W., X. Zhang, C. Lu, Y. Wang, and Y. Deng, Flexible and Transparent Paper-Based Ionic Diode Fabricated from Oppositely Charged Microfibrillated Cellulose. *The Journal of Physical Chemistry C.* **2012**, *116*(16), 9227-9234, DOI: 10.1021/jp301924g.
[58]. Hasani, M., E.D. Cranston, G. Westman, and D.G. Gray, Cationic Surface Functionalization of Cellulose Nanocrystals. *Soft Matter.* **2008**, *4*(11), 2238-2244, DOI: 10.1039/B806789A.
[59]. Arola, S., T. Tammelin, H. Setälä, A. Tullila, and M.B. Linder, Immobilization–Stabilization of Proteins on Nanofibrillated Cellulose Derivatives and Their Bioactive Film Formation. *Biomacromolecules.* **2012**, *13*(3), 594-603, DOI: 10.1021/bm201676q.
[60]. Jonoobi, M., J. Harun, A.P. Mathew, M.Z.B. Hussein, and K. Oksman, Preparation of Cellulose Nanofibers with Hydrophobic Surface Characteristics. *Cellulose.* **2010**, *17*(2), 299-307, DOI: 10.1007/s10570-009-9387-9.
[61]. Månsson, P. and L. Westfelt, Grafting of Monodisperse Low-Molecular-Weight Polystyrene onto Cellulose Acetate. *Journal of Polymer Science: Polymer Chemistry Edition.* **1981**, *19*(6), 1509-1515, DOI: 10.1002/pol.1981.170190621.
[62]. Biermann, C.J., J.B. Chung, and R. Narayan, Grafting of Polystyrene onto Cellulose Acetate by Nucleophilic Displacement of Mesylate Groups Using the Polystyrylcarboxylate Anion. *Macromolecules.* **1987**, *20*(5), 954-957, DOI: 10.1021/ma00171a010.
[63]. Harrisson, S., G.L. Drisko, E. Malmström, A. Hult, and K.L. Wooley, Hybrid Rigid/Soft and Biologic/Synthetic Materials: Polymers Grafted onto Cellulose Microcrystals. *Biomacromolecules.* **2011**, *12*(4), 1214-1223, DOI: 10.1021/bm101506j.
[64]. Tsubokawa, N., T. Iida, and T. Takayama, Modification of Cellulose Powder Surface by Grafting of Polymers with Controlled Molecular Weight and Narrow Molecular Weight Distribution. *Journal of Applied Polymer Science.* **2000**, *75*(4), 515-522, DOI: 10.1002/(SICI)1097-4628(20000124)75:4<515::AID-APP6>3.0.CO;2-Q.
[65]. Chen, G., L. Tao, G. Mantovani, V. Ladmiral, D.P. Burt, J.V. Macpherson, and D.M. Haddleton, Synthesis of Azide/Alkyne-Terminal Polymers and Application for Surface Functionalisation through a [2 + 3] Huisgen Cycloaddition Process, "Click Chemistry". *Soft Matter.* **2007**, *3*(6), 732-739, DOI: 10.1039/B618325E.
[66]. Goldmann, A.S., T. Tischer, L. Barner, M. Bruns, and C. Barner-Kowollik, Mild and Modular Surface Modification of Cellulose Via Hetero Diels−Alder (Hda) Cycloaddition. *Biomacromolecules.* **2011**, *12*(4), 1137-1145, DOI: 10.1021/bm101461h.
[67]. Hansson, S., V. Trouillet, T. Tischer, A.S. Goldmann, A. Carlmark, C. Barner-Kowollik, and E. Malmström, Grafting Efficiency of Synthetic Polymers onto Biomaterials: A Comparative Study of Grafting-from Versus Grafting-To. *Biomacromolecules.* **2013**, *14*(1), 64-74, DOI: 10.1021/bm3013132.
[68]. Zhao, G.-L., J. Hafrén, L. Deiana, and A. Córdova, Heterogeneous "Organoclick" Derivatization of Polysaccharides: Photochemical Thiol-Ene Click Modification of Solid

Cellulose. *Macromolecular Rapid Communications.* **2010**, *31*(8), 740-744, DOI: 10.1002/marc.200900764.
[69]. Yang, J.-H. and S.-H. Choi, Comparison Study of a Chiral Stationary Phase Based on Cellulose Derivatives Prepared by "Grafting from" and "Grafting to" Methods. *Journal of Applied Polymer Science.* **2013**, *127*(5), 4122-4128, DOI: 10.1002/app.38028.
[70]. Shukla, S.R. and A.R. Athalye, Graft-Copolymerization of Glycidyl Methacrylate onto Cotton Cellulose. *Journal of Applied Polymer Science.* **1994**, *54*(3), 279-288, DOI: 10.1002/app.1994.070540302.
[71]. Chauhan, G.S., H. Lal, R. Sharma, L. Guleria, and B.D. Sarwade, Grafting of a Styrene–Acrylonitrile Binary Monomer Mixture onto Cellulose Extracted from Pine Needles. *Journal of Applied Polymer Science.* **2002**, *83*(9), 2000-2007, DOI: 10.1002/app.10150.
[72]. Aliouche, D., B. Sid, and H. Ait-Amar. *Graft-Copolymerization of Acrylic Monomers onto Cellulose. Influence on Fibre Swelling and Absorbency*. in *Annales de chimie*. 2006. Lavoisier.
[73]. Ogiwara, Y. and H. Kubota, Comparison of Fe2+□H2o2 and Fe3+□H2o2 Initiation Systems in Graft Copolymerization of Cellulosic Materials. *Journal of Applied Polymer Science.* **1969**, *13*(8), 1613-1620, DOI: 10.1002/app.1969.070130803.
[74]. Littunen, K., U. Hippi, L.-S. Johansson, M. Österberg, T. Tammelin, J. Laine, and J. Seppälä, Free Radical Graft Copolymerization of Nanofibrillated Cellulose with Acrylic Monomers. *Carbohydrate Polymers.* **2011**, *84*(3), 1039-1047, DOI: http://dx.doi.org/10.1016/j.carbpol.2010.12.064.
[75]. McDowall, D.J., B.S. Gupta, and V.T. Stannett, Grafting of Vinyl Monomers to Cellulose by Ceric Ion Initiation. *Progress in Polymer Science.* **1984**, *10*(1), 1-50, DOI: http://dx.doi.org/10.1016/0079-6700(84)90005-4.
[76]. Zahran, M.K., Grafting of Methacrylic Acid and Other Vinyl Monomers onto Cotton Fabric Using Ce (Iv) Ion–Cellulose Thiocarbonate Redox System. *Journal of Polymer Research.* **2006**, *13*(1), 65-71, DOI: 10.1007/s10965-005-9008-8.
[77]. John, G. and C.K.S. Pillai, Grafting of Bio-Monomers. *Polymer Bulletin.* **1989**, *22*(1), 89-94, DOI: 10.1007/bf00283289.
[78]. Feit, B.-A., A. Bar-Nun, M. Lahav, and A. Zilkha, Anionic Graft Polymerization of Vinyl Monomers on Cellulose and Polyvinyl Alcohol. *Journal of Applied Polymer Science.* **1964**, *8*(4), 1869-1888, DOI: 10.1002/app.1964.070080434.
[79]. Mansour, O.Y. and A.H. Basta, Ionic Xanthate Method of Grafting. Ii. *Polymer-Plastics Technology and Engineering.* **1995**, *34*(3), 405-422, DOI: 10.1080/03602559508012191.
[80]. Hafrén, J. and A. Córdova, Direct Organocatalytic Polymerization from Cellulose Fibers. *Macromolecular Rapid Communications.* **2005**, *26*(2), 82-86, DOI: 10.1002/marc.200400470.
[81]. Lönnberg, H., K. Larsson, T. Lindström, A. Hult, and E. Malmström, Synthesis of Polycaprolactone-Grafted Microfibrillated Cellulose for Use in Novel Bionanocomposites–Influence of the Graft Length on the Mechanical Properties. *ACS Applied Materials & Interfaces.* **2011**, *3*(5), 1426-1433, DOI: 10.1021/am2001828.
[82]. Hafrén, J. and A. Córdova, Direct Bronsted Acid-Catalyzed Derivatization of Cellulose with Poly(L-Lactic Acid) and D-Mandelic Acid. *Nordic Pulp and Paper Research Journal.* **2007**, *22*(2), 184-187.
[83]. Lönnberg, H., L. Fogelström, L. Berglund, E. Malmström, and A. Hult, Surface Grafting of Microfibrillated Cellulose with Poly(E-Caprolactone) – Synthesis and

Characterization. *European Polymer Journal.* **2008**, *44*(9), 2991-2997, DOI: http://dx.doi.org/10.1016/j.eurpolymj.2008.06.023.
[84]. Lin, N., G. Chen, J. Huang, A. Dufresne, and P.R. Chang, Effects of Polymer-Grafted Natural Nanocrystals on the Structure and Mechanical Properties of Poly(Lactic Acid): A Case of Cellulose Whisker-Graft-Polycaprolactone. *Journal of Applied Polymer Science.* **2009**, *113*(5), 3417-3425, DOI: 10.1002/app.30308.
[85]. Carlmark, A. and E.E. Malmström, Atrp Grafting from Cellulose Fibers to Create Block-Copolymer Grafts. *Biomacromolecules.* **2003**, *4*(6), 1740-1745, DOI: 10.1021/bm030046v.
[86]. Lindqvist, J. and E. Malmström, Surface Modification of Natural Substrates by Atom Transfer Radical Polymerization. *Journal of Applied Polymer Science.* **2006**, *100*(5), 4155-4162, DOI: 10.1002/app.23457.
[87]. Hansson, S., A. Carlmark, E. Malmström, and L. Fogelström, Toward Industrial Grafting of Cellulosic Substrates Via Arget Atrp. *Journal of Applied Polymer Science.* **2015**, *132*(6), n/a-n/a, DOI: 10.1002/app.41434.
[88]. Daly, W.H., T.S. Evenson †, S.T. Iacono, and R.W. Jones, Recent Developments in Cellulose Grafting Chemistry Utilizing Barton Ester Intermediates and Nitroxide Mediation. *Macromolecular Symposia.* **2001**, *174*(1), 155-164, DOI: 10.1002/1521-3900(200109)174:1<155::AID-MASY155>3.0.CO;2-O.
[89]. Perrier, S., P. Takolpuckdee, J. Westwood, and D.M. Lewis, Versatile Chain Transfer Agents for Reversible Addition Fragmentation Chain Transfer (Raft) Polymerization to Synthesize Functional Polymeric Architectures. *Macromolecules.* **2004**, *37*(8), 2709-2717, DOI: 10.1021/ma035468b.
[90]. Roy, D., J.T. Guthrie, and S. Perrier, Graft Polymerization: Grafting Poly(Styrene) from Cellulose Via Reversible Addition−Fragmentation Chain Transfer (Raft) Polymerization. *Macromolecules.* **2005**, *38*(25), 10363-10372, DOI: 10.1021/ma0515026.
[91]. Roy, D., M. Semsarilar, J.T. Guthrie, and S. Perrier, Cellulose Modification by Polymer Grafting: A Review. *Chemical Society Reviews.* **2009**, *38*(7), 2046-2064, DOI: 10.1039/B808639G.
[92]. Szwarc, M., `Living' Polymers. *Nature.* **1956**, *178*(4543), 1168-1169.
[93]. Otsu, T. and M. Yoshida, Role of Initiator-Transfer Agent-Terminator (Iniferter) in Radical Polymerizations: Polymer Design by Organic Disulfides as Iniferters. *Die Makromolekulare Chemie, Rapid Communications.* **1982**, *3*(2), 127-132, DOI: 10.1002/marc.1982.030030208.
[94]. Li, Y., H. Zhu, F. Shen, J. Wan, S. Lacey, Z. Fang, H. Dai, and L. Hu, Nanocellulose as Green Dispersant for Two-Dimensional Energy Materials. *Nano Energy.* **2015**, *13*, 346-354, DOI: http://dx.doi.org/10.1016/j.nanoen.2015.02.015.
[95]. Jiang, F. and Y.-L. Hsieh, Amphiphilic Superabsorbent Cellulose Nanofibril Aerogels. *Journal of Materials Chemistry A.* **2014**, *2*(18), 6337-6342, DOI: 10.1039/C4TA00743C.
[96]. Rodionova, G., M. Lenes, Ø. Eriksen, and Ø. Gregersen, Surface Chemical Modification of Microfibrillated Cellulose: Improvement of Barrier Properties for Packaging Applications. *Cellulose.* **2011**, *18*(1), 127-134, DOI: 10.1007/s10570-010-9474-y.
[97]. Andresen, M. and P. Stenius, Water-in-Oil Emulsions Stabilized by Hydrophobized Microfibrillated Cellulose. *Journal of Dispersion Science and Technology.* **2007**, *28*(6), 837-844, DOI: 10.1080/01932690701341827.

[98]. Xhanari, K., K. Syverud, and P. Stenius, Emulsions Stabilized by Microfibrillated Cellulose: The Effect of Hydrophobization, Concentration and O/W Ratio. *Journal of Dispersion Science and Technology.* **2011**, *32*(3), 447-452, DOI: 10.1080/01932691003658942.
[99]. Mulyadi, A. and Y. Deng, Surface Modification of Cellulose Nanofibrils by Maleated Styrene Block Copolymer and Their Composite Reinforcement Application. *Cellulose.* **2016**, *23*(1), 519-528, DOI: 10.1007/s10570-015-0787-8.
[100]. Mulyadi, A., Z. Zhang, and Y. Deng, Fluorine-Free Oil Absorbents Made from Cellulose Nanofibril Aerogels. *ACS Applied Materials & Interfaces.* **2016**, *8*(4), 2732-2740, DOI: 10.1021/acsami.5b10985.
[101]. Zhou, X., Z. Zhang, X. Xu, F. Guo, X. Zhu, X. Men, and B. Ge, Robust and Durable Superhydrophobic Cotton Fabrics for Oil/Water Separation. *ACS Applied Materials & Interfaces.* **2013**, *5*(15), 7208-7214, DOI: 10.1021/am4015346.
[102]. Besombes, S. and K. Mazeau, The Cellulose/Lignin Assembly Assessed by Molecular Modeling. Part 1: Adsorption of a Threo Guaiacyl B-O-4 Dimer onto a Iβ Cellulose Whisker. *Plant Physiology and Biochemistry.* **2005**, *43*(3), 299-308, DOI: http://dx.doi.org/10.1016/j.plaphy.2005.02.005.
[103]. Missoum, K., F. Martoïa, M.N. Belgacem, and J. Bras, Effect of Chemically Modified Nanofibrillated Cellulose Addition on the Properties of Fiber-Based Materials. *Industrial Crops and Products.* **2013**, *48*, 98-105, DOI: http://dx.doi.org/10.1016/j.indcrop.2013.04.013.
[104]. Andresen, M., L.-S. Johansson, B.S. Tanem, and P. Stenius, Properties and Characterization of Hydrophobized Microfibrillated Cellulose. *Cellulose.* **2006**, *13*(6), 665-677, DOI: 10.1007/s10570-006-9072-1.
[105]. Nelson, K., T. Retsina, M. Iakovlev, A. van Heiningen, Y. Deng, J.A. Shatkin, and A. Mulyadi, *American Process: Production of Low Cost Nanocellulose for Renewable, Advanced Materials Applications*, in *Materials Research for Manufacturing: An Industrial Perspective of Turning Materials into New Products*, L.D. Madsen and E.B. Svedberg, Editors. **2016**, Springer International Publishing: Cham, 267-302.
[106]. Liu, W.-J., H. Jiang, and H.-Q. Yu, Development of Biochar-Based Functional Materials: Toward a Sustainable Platform Carbon Material. *Chemical Reviews.* **2015**, *115*(22), 12251-12285, DOI: 10.1021/acs.chemrev.5b00195.
[107]. Demirbas, A. and G. Arin, An Overview of Biomass Pyrolysis. *Energy Sources.* **2002**, *24*(5), 471-482, DOI: 10.1080/00908310252889979.
[108]. Toda, M., A. Takagaki, M. Okamura, J.N. Kondo, S. Hayashi, K. Domen, and M. Hara, Green Chemistry: Biodiesel Made with Sugar Catalyst. *Nature.* **2005**, *438*(7065), 178-178, DOI: http://www.nature.com/nature/journal/v438/n7065/suppinfo/438178a_S1.html.
[109]. Tang, M.M. and R. Bacon, Carbonization of Cellulose Fibers—I. Low Temperature Pyrolysis. *Carbon.* **1964**, *2*(3), 211-220, DOI: http://dx.doi.org/10.1016/0008-6223(64)90035-1.
[110]. Liu, Z., F.-S. Zhang, and J. Wu, Characterization and Application of Chars Produced from Pinewood Pyrolysis and Hydrothermal Treatment. *Fuel.* **2010**, *89*(2), 510-514, DOI: http://dx.doi.org/10.1016/j.fuel.2009.08.042.
[111]. Gao, Y., H.-p. Chen, J. Wang, T. Shi, H.-P. Yang, and X.-H. Wang, Characterization of Products from Hydrothermal Liquefaction and Carbonation of Biomass Model

Compounds and Real Biomass. *Journal of Fuel Chemistry and Technology.* **2011**, *39*(12), 893-900, DOI: http://dx.doi.org/10.1016/S1872-5813(12)60001-2.
[112]. Dumanlı, A.G. and A.H. Windle, Carbon Fibres from Cellulosic Precursors: A Review. *Journal of Materials Science.* **2012**, *47*(10), 4236-4250, DOI: 10.1007/s10853-011-6081-8.
[113]. Antal, M.J., K. Mochidzuki, and L.S. Paredes, Flash Carbonization of Biomass. *Industrial & Engineering Chemistry Research.* **2003**, *42*(16), 3690-3699, DOI: 10.1021/ie0301839.
[114]. Sevilla, M. and A.B. Fuertes, The Production of Carbon Materials by Hydrothermal Carbonization of Cellulose. *Carbon.* **2009**, *47*(9), 2281-2289, DOI: http://dx.doi.org/10.1016/j.carbon.2009.04.026.
[115]. Baccile, N., C. Falco, and M.-M. Titirici, Characterization of Biomass and Its Derived Char Using 13c-Solid State Nuclear Magnetic Resonance. *Green Chemistry.* **2014**, *16*(12), 4839-4869, DOI: 10.1039/C3GC42570C.
[116]. Shearer, C.J., A. Cherevan, and D. Eder, Application and Future Challenges of Functional Nanocarbon Hybrids. *Advanced Materials.* **2014**, *26*(15), 2295-2318, DOI: 10.1002/adma.201305254.
[117]. Wang, Z., L. Ci, L. Chen, S. Nayak, P.M. Ajayan, and N. Koratkar, Polarity-Dependent Electrochemically Controlled Transport of Water through Carbon Nanotube Membranes. *Nano Letters.* **2007**, *7*(3), 697-702, DOI: 10.1021/nl062853g.
[118]. Li, Y., H. Zhu, F. Shen, J. Wan, X. Han, J. Dai, H. Dai, and L. Hu, Highly Conductive Microfiber of Graphene Oxide Templated Carbonization of Nanofibrillated Cellulose. *Advanced Functional Materials.* **2014**, *24*(46), 7366-7372, DOI: 10.1002/adfm.201402129.
[119]. Zhao, Y., J. Wei, R. Vajtai, P.M. Ajayan, and E.V. Barrera, Iodine Doped Carbon Nanotube Cables Exceeding Specific Electrical Conductivity of Metals. *Scientific Reports.* **2011**, *1*, 83, DOI: 10.1038/srep00083
[120]. Peigney, A., C. Laurent, E. Flahaut, R.R. Bacsa, and A. Rousset, Specific Surface Area of Carbon Nanotubes and Bundles of Carbon Nanotubes. *Carbon.* **2001**, *39*(4), 507-514, DOI: http://dx.doi.org/10.1016/S0008-6223(00)00155-X.
[121]. Rhim, Y.-R., D. Zhang, D.H. Fairbrother, K.A. Wepasnick, K.J. Livi, R.J. Bodnar, and D.C. Nagle, Changes in Electrical and Microstructural Properties of Microcrystalline Cellulose as Function of Carbonization Temperature. *Carbon.* **2010**, *48*(4), 1012-1024, DOI: http://dx.doi.org/10.1016/j.carbon.2009.11.020.
[122]. Brown, R.A., A.K. Kercher, T.H. Nguyen, D.C. Nagle, and W.P. Ball, Production and Characterization of Synthetic Wood Chars for Use as Surrogates for Natural Sorbents. *Organic Geochemistry.* **2006**, *37*(3), 321-333, DOI: http://dx.doi.org/10.1016/j.orggeochem.2005.10.008.
[123]. Zheng, Y., Y. Jiao, L.H. Li, T. Xing, Y. Chen, M. Jaroniec, and S.Z. Qiao, Toward Design of Synergistically Active Carbon-Based Catalysts for Electrocatalytic Hydrogen Evolution. *ACS Nano.* **2014**, *8*(5), 5290-5296, DOI: 10.1021/nn501434a.
[124]. Azeredo, H.M.C., L.H.C. Mattoso, R.J. Avena-Bustillos, G.C. Filho, M.L. Munford, D. Wood, and T.H. McHugh, Nanocellulose Reinforced Chitosan Composite Films as Affected by Nanofiller Loading and Plasticizer Content. *Journal of Food Science.* **2010**, *75*(1), N1-N7, DOI: 10.1111/j.1750-3841.2009.01386.x.

[125]. Medeiros, E.S., L.H.C. Mattoso, E.N. Ito, K.S. Gregorski, G.H. Robertson, R.D. Offeman, D.F. Wood, W.J. Orts, and S.H. Imam, Electrospun Nanofibers of Poly(Vinyl Alcohol) Reinforced with Cellulose Nanofibrils. *Journal of Biobased Materials and Bioenergy.* **2008**, *2*(3), 231-242, DOI: 10.1166/jbmb.2008.411.
[126]. Trovatti, E., A.J.F. Carvalho, S.J.L. Ribeiro, and A. Gandini, Simple Green Approach to Reinforce Natural Rubber with Bacterial Cellulose Nanofibers. *Biomacromolecules.* **2013**, *14*(8), 2667-2674, DOI: 10.1021/bm400523h.
[127]. Tingaut, P., T. Zimmermann, and F. Lopez-Suevos, Synthesis and Characterization of Bionanocomposites with Tunable Properties from Poly(Lactic Acid) and Acetylated Microfibrillated Cellulose. *Biomacromolecules.* **2010**, *11*(2), 454-464, DOI: 10.1021/bm901186u.
[128]. Iwamoto, S., S. Yamamoto, S.-H. Lee, and T. Endo, Mechanical Properties of Polypropylene Composites Reinforced by Surface-Coated Microfibrillated Cellulose. *Composites Part A: Applied Science and Manufacturing.* **2014**, *59*, 26-29, DOI: http://dx.doi.org/10.1016/j.compositesa.2013.12.011.
[129]. Yeh, J.-t., C.-C. Tsai, C.-K. Wang, J.-W. Shao, M.-Z. Xiao, and S.-c. Chen, Ultradrawing Novel Ultra-High Molecular Weight Polyethylene Fibers Filled with Bacterial Cellulose Nanofibers. *Carbohydrate Polymers.* **2014**, *101*, 1-10, DOI: http://dx.doi.org/10.1016/j.carbpol.2013.08.034.
[130]. Peters, S., T. Rushing, E. Landis, and T. Cummins, Nanocellulose and Microcellulose Fibers for Concrete. *Transportation Research Record: Journal of the Transportation Research Board.* **2010**(2142), 25-28.
[131]. Cervin, N.T., L. Andersson, J.B.S. Ng, P. Olin, L. Bergström, and L. Wågberg, Lightweight and Strong Cellulose Materials Made from Aqueous Foams Stabilized by Nanofibrillated Cellulose. *Biomacromolecules.* **2013**, *14*(2), 503-511, DOI: 10.1021/bm301755u.
[132]. Cai, H., S. Sharma, W. Liu, W. Mu, W. Liu, X. Zhang, and Y. Deng, Aerogel Microspheres from Natural Cellulose Nanofibrils and Their Application as Cell Culture Scaffold. *Biomacromolecules.* **2014**, *15*(7), 2540-2547, DOI: 10.1021/bm5003976.
[133]. Chen, W., Q. Li, Y. Wang, X. Yi, J. Zeng, H. Yu, Y. Liu, and J. Li, Comparative Study of Aerogels Obtained from Differently Prepared Nanocellulose Fibers. *ChemSusChem.* **2014**, *7*(1), 154-161, DOI: 10.1002/cssc.201300950.
[134]. Jiang, F. and Y.-L. Hsieh, Super Water Absorbing and Shape Memory Nanocellulose Aerogels from Tempo-Oxidized Cellulose Nanofibrils Via Cyclic Freezing-Thawing. *Journal of Materials Chemistry A.* **2014**, *2*(2), 350-359, DOI: 10.1039/C3TA13629A.
[135]. Zhang, Z., G. Sèbe, D. Rentsch, T. Zimmermann, and P. Tingaut, Ultralightweight and Flexible Silylated Nanocellulose Sponges for the Selective Removal of Oil from Water. *Chemistry of Materials.* **2014**, *26*(8), 2659-2668, DOI: 10.1021/cm5004164.
[136]. Korhonen, J.T., M. Kettunen, R.H.A. Ras, and O. Ikkala, Hydrophobic Nanocellulose Aerogels as Floating, Sustainable, Reusable, and Recyclable Oil Absorbents. *ACS Applied Materials & Interfaces.* **2011**, *3*(6), 1813-1816, DOI: 10.1021/am200475b.
[137]. Gebald, C., J.A. Wurzbacher, P. Tingaut, T. Zimmermann, and A. Steinfeld, Amine-Based Nanofibrillated Cellulose as Adsorbent for Co2 Capture from Air. *Environmental Science & Technology.* **2011**, *45*(20), 9101-9108, DOI: 10.1021/es202223p.
[138]. Carlsson, D.O., G. Nystrom, Q. Zhou, L.A. Berglund, L. Nyholm, and M. Stromme, Electroactive Nanofibrillated Cellulose Aerogel Composites with Tunable Structural and

Electrochemical Properties. *Journal of Materials Chemistry.* **2012**, *22*(36), 19014-19024, DOI: 10.1039/C2JM33975G.
[139]. Shatkin, J.A., T.H. Wegner, E. Bilek, and J. Cowie, Market Projections of Cellulose Nanomaterial-Enabled Products–Part 1: Applications. *TAPPI Journal.* **2014**, *13*(5), 9-16.
[140]. Turbak, A.F., F.W. Snyder, and K.R. Sandberg. *Microfibrillated Cellulose, a New Cellulose Product: Properties, Uses, and Commercial Potential*. in *J. Appl. Polym. Sci.: Appl. Polym. Symp.;(United States)*. 1983. ITT Rayonier Inc., Shelton, WA.
[141]. Dimic-Misic, K., P.A.C. Gane, and J. Paltakari, Micro- and Nanofibrillated Cellulose as a Rheology Modifier Additive in Cmc-Containing Pigment-Coating Formulations. *Industrial & Engineering Chemistry Research.* **2013**, *52*(45), 16066-16083, DOI: 10.1021/ie4028878.
[142]. Aulin, C., M. Gällstedt, and T. Lindström, Oxygen and Oil Barrier Properties of Microfibrillated Cellulose Films and Coatings. *Cellulose.* **2010**, *17*(3), 559-574, DOI: 10.1007/s10570-009-9393-y.
[143]. Fukuzumi, H., S. Fujisawa, T. Saito, and A. Isogai, Selective Permeation of Hydrogen Gas Using Cellulose Nanofibril Film. *Biomacromolecules.* **2013**, *14*(5), 1705-1709, DOI: 10.1021/bm400377e.
[144]. Meng, Y., T.M. Young, P. Liu, C.I. Contescu, B. Huang, and S. Wang, Ultralight Carbon Aerogel from Nanocellulose as a Highly Selective Oil Absorption Material. *Cellulose.* **2015**, *22*(1), 435-447, DOI: 10.1007/s10570-014-0519-5.
[145]. Wang, H., Y. Gong, and Y. Wang, Cellulose-Based Hydrophobic Carbon Aerogels as Versatile and Superior Adsorbents for Sewage Treatment. *RSC Advances.* **2014**, *4*(86), 45753-45759, DOI: 10.1039/C4RA08446B.
[146]. Wu, X.-L., T. Wen, H.-L. Guo, S. Yang, X. Wang, and A.-W. Xu, Biomass-Derived Sponge-Like Carbonaceous Hydrogels and Aerogels for Supercapacitors. *ACS Nano.* **2013**, *7*(4), 3589-3597, DOI: 10.1021/nn400566d.
[147]. Liang, H.-W., Q.-F. Guan, Z. Zhu, L.-T. Song, H.-B. Yao, X. Lei, and S.-H. Yu, Highly Conductive and Stretchable Conductors Fabricated from Bacterial Cellulose. *NPG Asia Mater.* **2012**, *4*, e19, DOI: http://www.nature.com/am/journal/v4/n6/suppinfo/am201234s1.html.
[148]. Cao, S., X. Feng, Y. Song, H. Liu, M. Miao, J. Fang, and L. Shi, In Situ Carbonized Cellulose-Based Hybrid Film as Flexible Paper Anode for Lithium-Ion Batteries. *ACS Applied Materials & Interfaces.* **2016**, *8*(2), 1073-1079, DOI: 10.1021/acsami.5b10648.
[149]. Long, C., D. Qi, T. Wei, J. Yan, L. Jiang, and Z. Fan, Nitrogen-Doped Carbon Networks for High Energy Density Supercapacitors Derived from Polyaniline Coated Bacterial Cellulose. *Advanced Functional Materials.* **2014**, *24*(25), 3953-3961, DOI: 10.1002/adfm.201304269.
[150]. Chen, L.-F., Z.-H. Huang, H.-W. Liang, Q.-F. Guan, and S.-H. Yu, Bacterial-Cellulose-Derived Carbon Nanofiber@Mno2 and Nitrogen-Doped Carbon Nanofiber Electrode Materials: An Asymmetric Supercapacitor with High Energy and Power Density. *Advanced Materials.* **2013**, *25*(34), 4746-4752, DOI: 10.1002/adma.201204949.
[151]. Cai, J., H. Niu, Z. Li, Y. Du, P. Cizek, Z. Xie, H. Xiong, and T. Lin, High-Performance Supercapacitor Electrode Materials from Cellulose-Derived Carbon Nanofibers. *ACS Applied Materials & Interfaces.* **2015**, *7*(27), 14946-14953, DOI: 10.1021/acsami.5b03757.

[152]. Eichhorn, S.J., A. Dufresne, M. Aranguren, N.E. Marcovich, J.R. Capadona, S.J. Rowan, C. Weder, W. Thielemans, M. Roman, S. Renneckar, W. Gindl, S. Veigel, J. Keckes, H. Yano, K. Abe, M. Nogi, A.N. Nakagaito, A. Mangalam, J. Simonsen, A.S. Benight, A. Bismarck, L.A. Berglund, and T. Peijs, Review: Current International Research into Cellulose Nanofibres and Nanocomposites. *Journal of Materials Science.* **2010**, *45*(1), 1-33, DOI: 10.1007/s10853-009-3874-0.

[153]. Hamad, W., On the Development and Applications of Cellulosic Nanofibrillar and Nanocrystalline Materials. *The Canadian Journal of Chemical Engineering.* **2006**, *84*(5), 513-519, DOI: 10.1002/cjce.5450840501.

[154]. Henry, C.A., *The Incorporation of Nanomaterials into Polymer Media*, in *Polymer Nanocomposites Handbook*. **2009**, CRC Press.

[155]. Missoum, K., J. Bras, and M.N. Belgacem, Water Redispersible Dried Nanofibrillated Cellulose by Adding Sodium Chloride. *Biomacromolecules.* **2012**, *13*(12), 4118-4125, DOI: 10.1021/bm301378n.

[156]. Peng, Y., D. Gardner, and Y. Han, Drying Cellulose Nanofibrils: In Search of a Suitable Method. *Cellulose.* **2012**, *19*(1), 91-102, DOI: 10.1007/s10570-011-9630-z.

[157]. Lai, S.-M., F.-C. Yeh, Y. Wang, H.-C. Chan, and H.-F. Shen, Comparative Study of Maleated Polyolefins as Compatibilizers for Polyethylene/Wood Flour Composites. *Journal of Applied Polymer Science.* **2003**, *87*(3), 487-496, DOI: 10.1002/app.11419.

[158]. Bhattacharya, A. and B.N. Misra, Grafting: A Versatile Means to Modify Polymers: Techniques, Factors and Applications. *Progress in Polymer Science.* **2004**, *29*(8), 767-814, DOI: http://dx.doi.org/10.1016/j.progpolymsci.2004.05.002.

[159]. Oksman, K., Improved Interaction between Wood and Synthetic Polymers in Wood/Polymer Composites. *Wood Sci.Technol.* **1996**, *30*(3), 197-205, DOI: 10.1007/BF00231633.

[160]. Nikfarjam, N., N. Taheri Qazvini, and Y. Deng, Surfactant Free Pickering Emulsion Polymerization of Styrene in W/O/W System Using Cellulose Nanofibrils. *European Polymer Journal.* **2015**, *64*(0), 179-188, DOI: http://dx.doi.org/10.1016/j.eurpolymj.2015.01.007.

[161]. French, A.D., Idealized Powder Diffraction Patterns for Cellulose Polymorphs. *Cellulose.* **2014**, *21*(2), 885-896, DOI: 10.1007/s10570-013-0030-4.

[162]. Ciolacu, D., F. Ciolacu, and V.I. Popa, Amorphous Cellulose—Structure and Characterization. *Cellulose chemistry and technology.* **2011**, *45*(1), 13.

[163]. Park, S., J. Baker, M. Himmel, P. Parilla, and D. Johnson, Cellulose Crystallinity Index: Measurement Techniques and Their Impact on Interpreting Cellulase Performance. *Biotechnol Biofuels.* **2010**, *3*(1), 10, 1-10, DOI: 10.1186/1754-6834-3-10.

[164]. Garvey, C.J., I.H. Parker, and G.P. Simon, On the Interpretation of X-Ray Diffraction Powder Patterns in Terms of the Nanostructure of Cellulose I Fibres. *Macromolecular Chemistry and Physics.* **2005**, *206*(15), 1568-1575, DOI: 10.1002/macp.200500008.

[165]. Morris, V., S. Ring, A. MacDougall, and R. Wilson, *Biophysical Characterization of Plant Cell Walls*, in *The Plant Cell Wall* J.K.C. Rose, Editor. **2003**, Blackwell: Oxford, 55-91.

[166]. Baeza, J. and J. Freer, *Chemical Characterization of Wood and Its Components*, in *Wood and Cellulosic Chemistry, Second Edition, Revised, and Expanded*, D.N.S. Hon and N. Shiraishi, Editors. **2000**, Dekker: New York, 275-384.

[167]. Szymanska-Chargot, M. and A. Zdunek, Use of Ft-Ir Spectra and Pca to the Bulk Characterization of Cell Wall Residues of Fruits and Vegetables Along a Fraction Process. *Food biophysics.* **2013**, *8*(1), 29-42.
[168]. Wang, Q., Q. Chen, H. Niida, N. Mitsumura, and T. Endo, Effect of Water Content on Crystalline Structure of Ionic Liquids Mixture Pretreated Microcrystalline Cellulose (Mcc). *Materials Sciences and Applications.* **2014**, *2014*(5), 183-192.
[169]. Liu, Y., Recent Progress in Fourier Transform Infrared (Ftir) Spectroscopy Study of Compositional, Structural and Physical Attributes of Developmental Cotton Fibers. *Materials.* **2013**, *6*(1), 299-313.
[170]. Popescu, C.-M., M.-C. Popescu, and C. Vasile, Characterization of Fungal Degraded Lime Wood by Ft-Ir and 2d Ir Correlation Spectroscopy. *Microchemical Journal.* **2010**, *95*(2), 377-387.
[171]. Matuana, L.M., J.J. Balatinecz, R.N.S. Sodhi, and C.B. Park, Surface Characterization of Esterified Cellulosic Fibers by Xps and Ftir Spectroscopy. *Wood Sci.Technol.* **2001**, *35*(3), 191-201, DOI: 10.1007/s002260100097.
[172]. Felix, J.M. and P. Gatenholm, The Nature of Adhesion in Composites of Modified Cellulose Fibers and Polypropylene. *Journal of Applied Polymer Science.* **1991**, *42*(3), 609-620, DOI: 10.1002/app.1991.070420307.
[173]. Chen, G., Y. Zhang, X. Zhou, and J. Xu, Synthesis of Styrene–Maleic Anhydride Copolymer Esters and Their Surface Enriched Properties When Blending with Polyethylene. *Applied Surface Science.* **2006**, *253*(3), 1107-1110, DOI: http://dx.doi.org/10.1016/j.apsusc.2006.01.068.
[174]. Henriksson, M., L.A. Berglund, P. Isaksson, T. Lindstrom, and T. Nishino, Cellulose Nanopaper Structures of High Toughness. *Biomacromolecules.* **2008**, *9*(6), 1579-1585.
[175]. Krässig, H.A., *Cellulose: Structure Accessibility and Reactivity*. *Polymer Monographs, 0275-5777 ; V. 11; Polymer Monographs ; 0275-5777 V. 11.*, 1993, Yverdon, Switzerland: Gordon and Breach Science.
[176]. Sannigrahi, P., S.J. Miller, and A.J. Ragauskas, Effects of Organosolv Pretreatment and Enzymatic Hydrolysis on Cellulose Structure and Crystallinity in Loblolly Pine. *Carbohydrate research.* **2010**, *345*(7), 965-970.
[177]. Xu, X., F. Liu, L. Jiang, J. Zhu, D. Haagenson, and D.P. Wiesenborn, Cellulose Nanocrystals Vs. Cellulose Nanofibrils: A Comparative Study on Their Microstructures and Effects as Polymer Reinforcing Agents. *ACS applied materials & interfaces.* **2013**, *5*(8), 2999-3009.
[178]. Dufresne, A., Polysaccharide Nano Crystal Reinforced Nanocomposites. *Canadian Journal of Chemistry.* **2008**, *86*(6), 484-494, DOI: 10.1139/v07-152.
[179]. Wu, Z.-Y., C. Li, H.-W. Liang, Y.-N. Zhang, X. Wang, J.-F. Chen, and S.-H. Yu, Carbon Nanofiber Aerogels for Emergent Cleanup of Oil Spillage and Chemical Leakage under Harsh Conditions. *Scientific Reports.* **2014**, *4*, 4079, 1-6, DOI: 10.1038/srep04079.
[180]. Chen, L., R. Du, J. Zhang, and T. Yi, Density Controlled Oil Uptake and Beyond: From Carbon Nanotube to Graphene Nanoribbon Aerogels. *Journal of Materials Chemistry A.* **2015**, *3*(41), 20547-20553, DOI: 10.1039/C5TA04370K.
[181]. Wu, D., Z. Yu, W. Wu, L. Fang, and H. Zhu, Continuous Oil-Water Separation with Surface Modified Sponge for Cleanup of Oil Spills. *RSC Advances.* **2014**, *4*(96), 53514-53519, DOI: 10.1039/C4RA07583H.

[182]. Zheng, Q., Z. Cai, and S. Gong, Green Synthesis of Polyvinyl Alcohol (Pva)-Cellulose Nanofibril (Cnf) Hybrid Aerogels and Their Use as Superabsorbents. *Journal of Materials Chemistry A.* **2014**, *2*(9), 3110-3118, DOI: 10.1039/C3TA14642A.
[183]. Sehaqui, H., M. Salajkova, Q. Zhou, and L.A. Berglund, Mechanical Performance Tailoring of Tough Ultra-High Porosity Foams Prepared from Cellulose I Nanofiber Suspensions. *Soft Matter.* **2010**, *6*(8), 1824-1832, DOI: 10.1039/B927505C.
[184]. Sehaqui, H., Q. Zhou, and L.A. Berglund, High-Porosity Aerogels of High Specific Surface Area Prepared from Nanofibrillated Cellulose (Nfc). *Composites Science and Technology.* **2011**, *71*(13), 1593-1599, DOI: 10.1016/j.compscitech.2011.07.003.
[185]. Paakko, M., J. Vapaavuori, R. Silvennoinen, H. Kosonen, M. Ankerfors, T. Lindstrom, L.A. Berglund, and O. Ikkala, Long and Entangled Native Cellulose I Nanofibers Allow Flexible Aerogels and Hierarchically Porous Templates for Functionalities. *Soft Matter.* **2008**, *4*(12), 2492-2499, DOI: 10.1039/B810371B.
[186]. Gui, X., H. Li, K. Wang, J. Wei, Y. Jia, Z. Li, L. Fan, A. Cao, H. Zhu, and D. Wu, Recyclable Carbon Nanotube Sponges for Oil Absorption. *Acta Materialia.* **2011**, *59*(12), 4798-4804, DOI: 10.1016/j.actamat.2011.04.022.
[187]. Bi, H., X. Xie, K. Yin, Y. Zhou, S. Wan, L. He, F. Xu, F. Banhart, L. Sun, and R.S. Ruoff, Spongy Graphene as a Highly Efficient and Recyclable Sorbent for Oils and Organic Solvents. *Advanced Functional Materials.* **2012**, *22*(21), 4421-4425, DOI: 10.1002/adfm.201200888.
[188]. Gurav, J.L., I.-K. Jung, H.-H. Park, E.S. Kang, and D.Y. Nadargi, Silica Aerogel: Synthesis and Applications. *Journal of Nanomaterials.* **2010**, *2010*, 409310, 1-11, DOI: 10.1155/2010/409310.
[189]. Venkateswara Rao, A., N.D. Hegde, and H. Hirashima, Absorption and Desorption of Organic Liquids in Elastic Superhydrophobic Silica Aerogels. *Journal of Colloid and Interface Science.* **2007**, *305*(1), 124-132, DOI: 10.1016/j.jcis.2006.09.025.
[190]. Cervin, N., C. Aulin, P. Larsson, and L. Wågberg, Ultra Porous Nanocellulose Aerogels as Separation Medium for Mixtures of Oil/Water Liquids. *Cellulose.* **2012**, *19*(2), 401-410, DOI: 10.1007/s10570-011-9629-5.
[191]. Du, R., N. Zhang, H. Xu, N. Mao, W. Duan, J. Wang, Q. Zhao, Z. Liu, and J. Zhang, Cmp Aerogels: Ultrahigh-Surface-Area Carbon-Based Monolithic Materials with Superb Sorption Performance. *Advanced Materials.* **2014**, *26*(47), 8053-8058, DOI: 10.1002/adma.201403058.
[192]. Daniel, C., S. Longo, R. Ricciardi, E. Reverchon, and G. Guerra, Monolithic Nanoporous Crystalline Aerogels. *Macromolecular Rapid Communications.* **2013**, *34*(15), 1194-1207, DOI: 10.1002/marc.201300260.
[193]. Missoum, K., M. Belgacem, and J. Bras, Nanofibrillated Cellulose Surface Modification: A Review. *Materials.* **2013**, *6*(5), 1745-1766, DOI: 10.3390/ma6051745.
[194]. Casado, R.M., P.A. Lovell, P. Navabpour, and J.L. Stanford, Polymer Encapsulation of Surface-Modified Carbon Blacks Using Surfactant-Free Emulsion Polymerisation. *Polymer.* **2007**, *48*(9), 2554-2563, DOI: 10.1016/j.polymer.2007.02.063.
[195]. Chen, M., L. Wu, S. Zhou, and B. You, Synthesis of Raspberry-Like Pmma/Sio2 Nanocomposite Particles Via a Surfactant-Free Method. *Macromolecules.* **2004**, *37*(25), 9613-9619, DOI: 10.1021/ma048431f.

[196]. Sheibat-Othman, N. and E. Bourgeat-Lami, Use of Silica Particles for the Formation of Organic−Inorganic Particles by Surfactant-Free Emulsion Polymerization. *Langmuir.* **2009**, *25*(17), 10121-10133, DOI: 10.1021/la900895z.
[197]. Fielding, L.A., J. Tonnar, and S.P. Armes, All-Acrylic Film-Forming Colloidal Polymer/Silica Nanocomposite Particles Prepared by Aqueous Emulsion Polymerization. *Langmuir.* **2011**, *27*(17), 11129-11144, DOI: 10.1021/la202066n.
[198]. Schmid, A., P. Scherl, S.P. Armes, C.A.P. Leite, and F. Galembeck, Synthesis and Characterization of Film-Forming Colloidal Nanocomposite Particles Prepared Via Surfactant-Free Aqueous Emulsion Copolymerization. *Macromolecules.* **2009**, *42*(11), 3721-3728, DOI: 10.1021/ma900465k.
[199]. Ramos, J. and J. Forcada, Surfactant-Free Miniemulsion Polymerization as a Simple Synthetic Route to a Successful Encapsulation of Magnetite Nanoparticles. *Langmuir.* **2011**, *27*(11), 7222-7230, DOI: 10.1021/la200786k.
[200]. Telford, A.M., B.T.T. Pham, C. Neto, and B.S. Hawkett, Micron-Sized Polystyrene Particles by Surfactant-Free Emulsion Polymerization in Air: Synthesis and Mechanism. *Journal of Polymer Science Part A: Polymer Chemistry.* **2013**, *51*(19), 3997-4002, DOI: 10.1002/pola.26841.
[201]. Rudin, A. and P. Choi, *Dispersion and Emulsion Polymerizations*, in *The Elements of Polymer Science & Engineering (Third Edition)*, A.R. Choi, Editor. **2013**, Academic Press: Boston, 427-447.
[202]. Liu, S. and G. Sun, Radical Graft Functional Modification of Cellulose with Allyl Monomers: Chemistry and Structure Characterization. *Carbohydrate Polymers.* **2008**, *71*(4), 614-625, DOI: 10.1016/j.carbpol.2007.07.006.
[203]. Annable, T., I. Gray, P. Lovell, S. Richards, and G. Satgurnathan, *Degradation and Grafting of Hydroxyethyl Cellulose During Emulsion Polymerization*, in *Aqueous Polymer Dispersions*, K. Tauer, Editor. **2004**, Springer Berlin Heidelberg, 159-163.
[204]. Hermans, J., Chemical Mechanisms in the Grafting of Cellulose. *Pure and Applied Chemistry.* **1962**, *5*(1-2), 147-164.
[205]. Chapman, R.A., *Chemical Bonding*, in *Handbook of Nonwovens*, S.J. Russell, Editor. **2007**, Woodhead Publishing, 330-367.
[206]. Klein, A. and E. Daniels, *Formulation Components*, in *Emulsion Polymerization and Emulsion Polymers*, P.A. Lovell and M.S. El-Aasser, Editors. **1997**, J. Wiley: New York.
[207]. Baeza, J. and J. Freer, *Chemical Characterization of Wood and Its Components*, in *Wood and Cellulosic Chemistry, 2nd Ed.* , N.S. DNS Hon, Editor. **2000**, Dekker: New York, USA, 275-384.
[208]. Morris, V., S. Ring, A. MacDougall, R. Wilson, and J. Rose, *Biophysical Characterization of Plant Cell Walls*, in *The Plant Cell Wall*, J.K.C. Rose, Editor. **2003**, CRC Press LLC: Boca Raton, FL, USA, 55-65.
[209]. Ning, L.Q., N.K. Xu, R. Wang, and Y. Liu, Fibrous Membranes Electrospun from the Suspension Polymerization Product of Styrene and Butyl Acrylate for Oil-Water Separation. *RSC Advances.* **2015**, *5*(70), 57101-57113, DOI: 10.1039/C5RA08729E.
[210]. Ma, D., R.D. Carter, J. Laine, and P. Stenius, The Influence of Coating Structure and Surface Energy on Gibbs Energy of Ink Oil Imbibition During Ink Setting. *Nordic Pulp & Paper Research Journal.* **2009**, *24*(2), 213-218.
[211]. Peykova, Y., O.V. Lebedeva, A. Diethert, P. Müller-Buschbaum, and N. Willenbacher, Adhesive Properties of Acrylate Copolymers: Effect of the Nature of the Substrate and

Copolymer Functionality. *International Journal of Adhesion and Adhesives.* **2012**, *34*, 107-116, DOI: 10.1016/j.ijadhadh.2011.12.001.
[212]. Eckersley, S.T., R. O'Daiskey, and A. Rudin, Surface Energetics of Films of Surfactant Free Poly(Methyl Methacrylate-Co-Butyl Acrylate) Emulsion Polymers. *Journal of Colloid and Interface Science.* **1992**, *152*(2), 455-464, DOI: 10.1016/0021-9797(92)90046-O.
[213]. Zhang, W., Y. Zhang, C. Lu, and Y. Deng, Aerogels from Crosslinked Cellulose Nano/Micro-Fibrils and Their Fast Shape Recovery Property in Water. *Journal of Materials Chemistry.* **2012**, *22*(23), 11642-11650, DOI: 10.1039/C2JM30688C.
[214]. Goga, V., *New Phenomenological Model for Solid Foams*, in *Computational Modelling and Advanced Simulations*, J. Murín, V. Kompiš, and V. Kutiš, Editors. **2011**, Springer Netherlands, 67-82.
[215]. Clyne, T.W., A.E. Markaki, and J.C. Tan, Mechanical and Magnetic Properties of Metal Fibre Networks, with and without a Polymeric Matrix. *Composites Science and Technology.* **2005**, *65*(15–16), 2492-2499, DOI: 10.1016/j.compscitech.2005.05.037.
[216]. Winter, M. and R.J. Brodd, What Are Batteries, Fuel Cells, and Supercapacitors? *Chemical Reviews.* **2004**, *104*(10), 4245-4270, DOI: 10.1021/cr020730k.
[217]. Lin, Z., G. Waller, Y. Liu, M. Liu, and C.-P. Wong, Facile Synthesis of Nitrogen-Doped Graphene Via Pyrolysis of Graphene Oxide and Urea, and Its Electrocatalytic Activity toward the Oxygen-Reduction Reaction. *Advanced Energy Materials.* **2012**, *2*(7), 884-888, DOI: 10.1002/aenm.201200038.
[218]. Mahmood, N., C. Zhang, H. Yin, and Y. Hou, Graphene-Based Nanocomposites for Energy Storage and Conversion in Lithium Batteries, Supercapacitors and Fuel Cells. *Journal of Materials Chemistry A.* **2014**, *2*(1), 15-32, DOI: 10.1039/C3TA13033A.
[219]. Wood, K.N., R. O'Hayre, and S. Pylypenko, Recent Progress on Nitrogen/Carbon Structures Designed for Use in Energy and Sustainability Applications. *Energy & Environmental Science.* **2014**, *7*(4), 1212-1249, DOI: 10.1039/C3EE44078H.
[220]. Wang, J., R. Ma, Z. Zhou, G. Liu, and Q. Liu, Magnesiothermic Synthesis of Sulfur-Doped Graphene as an Efficient Metal-Free Electrocatalyst for Oxygen Reduction. *Scientific Reports.* **2015**, *5*, 9304, DOI: 10.1038/srep09304.
[221]. Zhang, J., L. Qu, G. Shi, J. Liu, J. Chen, and L. Dai, N,P-Codoped Carbon Networks as Efficient Metal-Free Bifunctional Catalysts for Oxygen Reduction and Hydrogen Evolution Reactions. *Angewandte Chemie International Edition.* **2016**, *55*(6), 2230-2234, DOI: 10.1002/anie.201510495.
[222]. Wei, L., H.E. Karahan, K. Goh, W. Jiang, D. Yu, O. Birer, R. Jiang, and Y. Chen, A High-Performance Metal-Free Hydrogen-Evolution Reaction Electrocatalyst from Bacterium Derived Carbon. *Journal of Materials Chemistry A.* **2015**, *3*(14), 7210-7214, DOI: 10.1039/C5TA00966A.
[223]. Liu, X., W. Zhou, L. Yang, L. Li, Z. Zhang, Y. Ke, and S. Chen, Nitrogen and Sulfur Co-Doped Porous Carbon Derived from Human Hair as Highly Efficient Metal-Free Electrocatalysts for Hydrogen Evolution Reactions. *Journal of Materials Chemistry A.* **2015**, *3*(16), 8840-8846, DOI: 10.1039/C5TA01209K.
[224]. Ito, Y., W. Cong, T. Fujita, Z. Tang, and M. Chen, High Catalytic Activity of Nitrogen and Sulfur Co-Doped Nanoporous Graphene in the Hydrogen Evolution Reaction. *Angewandte Chemie International Edition.* **2015**, *54*(7), 2131-2136, DOI: 10.1002/anie.201410050.

[225]. Zheng, Y., Y. Jiao, Y. Zhu, L.H. Li, Y. Han, Y. Chen, A. Du, M. Jaroniec, and S.Z. Qiao, Hydrogen Evolution by a Metal-Free Electrocatalyst. *Nature Communications.* **2014**, *5*, 3783, DOI: 10.1038/ncomms4783.
[226]. Shinde, S.S., A. Sami, and J.-H. Lee, Electrocatalytic Hydrogen Evolution Using Graphitic Carbon Nitride Coupled with Nanoporous Graphene Co-Doped by S and Se. *Journal of Materials Chemistry A.* **2015**, *3*(24), 12810-12819, DOI: 10.1039/C5TA02656C.
[227]. Shinde, S.S., A. Sami, and J.-H. Lee, Nitrogen- and Phosphorus-Doped Nanoporous Graphene/Graphitic Carbon Nitride Hybrids as Efficient Electrocatalysts for Hydrogen Evolution. *ChemCatChem.* **2015**, *7*(23), 3873-3880, DOI: 10.1002/cctc.201500701.
[228]. Vartiainen, J., T. Pöhler, K. Sirola, L. Pylkkänen, H. Alenius, J. Hokkinen, U. Tapper, P. Lahtinen, A. Kapanen, K. Putkisto, P. Hiekkataipale, P. Eronen, J. Ruokolainen, and A. Laukkanen, Health and Environmental Safety Aspects of Friction Grinding and Spray Drying of Microfibrillated Cellulose. *Cellulose.* **2011**, *18*(3), 775-786, DOI: 10.1007/s10570-011-9501-7.
[229]. Wu, Z.-Y., H.-W. Liang, L.-F. Chen, B.-C. Hu, and S.-H. Yu, Bacterial Cellulose: A Robust Platform for Design of Three Dimensional Carbon-Based Functional Nanomaterials. *Accounts of Chemical Research.* **2016**, *49*(1), 96-105, DOI: 10.1021/acs.accounts.5b00380.
[230]. Yang, X., X. Zhuang, Y. Huang, J. Jiang, H. Tian, D. Wu, F. Zhang, Y. Mai, and X. Feng, Nitrogen-Enriched Hierarchically Porous Carbon Materials Fabricated by Graphene Aerogel Templated Schiff-Base Chemistry for High Performance Electrochemical Capacitors. *Polymer Chemistry.* **2015**, *6*(7), 1088-1095, DOI: 10.1039/C4PY01408A.
[231]. Gong, K., F. Du, Z. Xia, M. Durstock, and L. Dai, Nitrogen-Doped Carbon Nanotube Arrays with High Electrocatalytic Activity for Oxygen Reduction. *Science.* **2009**, *323*(5915), 760-764, DOI: 10.1126/science.1168049.
[232]. Liu, Q., C. Chen, F. Pan, and J. Zhang, Highly Efficient Oxygen Reduction on Porous Nitrogen-Doped Nanocarbons Directly Synthesized from Cellulose Nanocrystals and Urea. *Electrochimica Acta.* **2015**, *170*, 234-241, DOI: http://dx.doi.org/10.1016/j.electacta.2015.04.094.
[233]. Zhao, Y., F. Zhao, X. Wang, C. Xu, Z. Zhang, G. Shi, and L. Qu, Graphitic Carbon Nitride Nanoribbons: Graphene-Assisted Formation and Synergic Function for Highly Efficient Hydrogen Evolution. *Angewandte Chemie International Edition.* **2014**, *53*(50), 13934-13939, DOI: 10.1002/anie.201409080.
[234]. Titirici, M.-M., R.J. White, C. Falco, and M. Sevilla, Black Perspectives for a Green Future: Hydrothermal Carbons for Environment Protection and Energy Storage. *Energy & Environmental Science.* **2012**, *5*(5), 6796-6822, DOI: 10.1039/C2EE21166A.
[235]. Su, Y., Y. Zhang, X. Zhuang, S. Li, D. Wu, F. Zhang, and X. Feng, Low-Temperature Synthesis of Nitrogen/Sulfur Co-Doped Three-Dimensional Graphene Frameworks as Efficient Metal-Free Electrocatalyst for Oxygen Reduction Reaction. *Carbon.* **2013**, *62*, 296-301, DOI: http://dx.doi.org/10.1016/j.carbon.2013.05.067.
[236]. Gao, Y., X.-H. Wang, H.-P. Yang, and H.-P. Chen, Characterization of Products from Hydrothermal Treatments of Cellulose. *Energy.* **2012**, *42*(1), 457-465, DOI: http://dx.doi.org/10.1016/j.energy.2012.03.023.

[237]. Li, J., Y. Zhang, X. Zhang, J. Han, Y. Wang, L. Gu, Z. Zhang, X. Wang, J. Jian, P. Xu, and B. Song, Direct Transformation from Graphitic C3n4 to Nitrogen-Doped Graphene: An Efficient Metal-Free Electrocatalyst for Oxygen Reduction Reaction. *ACS Applied Materials & Interfaces.* **2015**, *7*(35), 19626-19634, DOI: 10.1021/acsami.5b03845.
[238]. Lewandowska, A.E., C. Soutis, L. Savage, and S.J. Eichhorn, Carbon Fibres with Ordered Graphitic-Like Aggregate Structures from a Regenerated Cellulose Fibre Precursor. *Composites Science and Technology.* **2015**, *116*, 50-57, DOI: http://dx.doi.org/10.1016/j.compscitech.2015.05.009.
[239]. Walcarius, A., Mesoporous Materials and Electrochemistry. *Chemical Society Reviews.* **2013**, *42*(9), 4098-4140, DOI: 10.1039/C2CS35322A.
[240]. Chen, L.-F., X.-D. Zhang, H.-W. Liang, M. Kong, Q.-F. Guan, P. Chen, Z.-Y. Wu, and S.-H. Yu, Synthesis of Nitrogen-Doped Porous Carbon Nanofibers as an Efficient Electrode Material for Supercapacitors. *ACS Nano.* **2012**, *6*(8), 7092-7102, DOI: 10.1021/nn302147s.
[241]. Masoudi Soltani, S., S.K. Yazdi, and S. Hosseini, Effects of Pyrolysis Conditions on the Porous Structure Construction of Mesoporous Charred Carbon from Used Cigarette Filters. *Applied Nanoscience.* **2014**, *4*(5), 551-569, DOI: 10.1007/s13204-013-0230-0.
[242]. Wohlgemuth, S.-A., R.J. White, M.-G. Willinger, M.-M. Titirici, and M. Antonietti, A One-Pot Hydrothermal Synthesis of Sulfur and Nitrogen Doped Carbon Aerogels with Enhanced Electrocatalytic Activity in the Oxygen Reduction Reaction. *Green Chemistry.* **2012**, *14*(5), 1515-1523, DOI: 10.1039/C2GC35309A.
[243]. Yang, Z., Z. Yao, G. Li, G. Fang, H. Nie, Z. Liu, X. Zhou, X.a. Chen, and S. Huang, Sulfur-Doped Graphene as an Efficient Metal-Free Cathode Catalyst for Oxygen Reduction. *ACS Nano.* **2012**, *6*(1), 205-211, DOI: 10.1021/nn203393d.
[244]. Jeon, I.-Y., D. Yu, S.-Y. Bae, H.-J. Choi, D.W. Chang, L. Dai, and J.-B. Baek, Formation of Large-Area Nitrogen-Doped Graphene Film Prepared from Simple Solution Casting of Edge-Selectively Functionalized Graphite and Its Electrocatalytic Activity. *Chemistry of Materials.* **2011**, *23*(17), 3987-3992, DOI: 10.1021/cm201542m.
[245]. Qu, L., Y. Liu, J.-B. Baek, and L. Dai, Nitrogen-Doped Graphene as Efficient Metal-Free Electrocatalyst for Oxygen Reduction in Fuel Cells. *ACS Nano.* **2010**, *4*(3), 1321-1326, DOI: 10.1021/nn901850u.
[246]. Chua, C.K. and M. Pumera, Renewal of Sp2 Bonds in Graphene Oxides Via Dehydrobromination. *J. Mater. Chem.* **2012**, *22*(43), 23227-23231, DOI: 10.1039/C2JM34358D.
[247]. Phaner-Goutorbe, M., A. Sartre, and L. Porte, Soft Oxidation of Graphite Studied by Xps and Stm. *Microsc. Microanal. Microstruct.* **1994**, *5*(4-6), 283-290.
[248]. Li, Y. and N. Chopra, Fabrication of Nanoscale Heterostructures Comprised of Graphene-Encapsulated Gold Nanoparticles and Semiconducting Quantum Dots for Photocatalysis. *Phys. Chem. Chem. Phys.* **2015**, *17*(19), 12881-12893, DOI: 10.1039/C5CP00928F.
[249]. Choi, C.H., S.H. Park, and S.I. Woo, Heteroatom Doped Carbons Prepared by the Pyrolysis of Bio-Derived Amino Acids as Highly Active Catalysts for Oxygen Electro-Reduction Reactions. *Green Chem.* **2011**, *13*(2), 406-412, DOI: 10.1039/C0GC00384K.
[250]. Lahaye, J., G. Nans, P. Fioux, A. Bagreev, A. Broshnik, and V. Strelko, Xps Analysis for the Thermal Conversion of a Vinylpyridine Resin into Active Carbon, in ACS 1997 Proceedings. 1997: University Park, PA.

[251]. Liu, H., Y. Zhang, R. Li, X. Sun, S. Désilets, H. Abou-Rachid, M. Jaidann, and L.-S. Lussier, Structural and Morphological Control of Aligned Nitrogen-Doped Carbon Nanotubes. *Carbon.* **2010**, *48*(5), 1498-1507, DOI: http://dx.doi.org/10.1016/j.carbon.2009.12.045.
[252]. Arrigo, R., M. Havecker, R. Schlogl, and D.S. Su, Dynamic Surface Rearrangement and Thermal Stability of Nitrogen Functional Groups on Carbon Nanotubes. *Chem. Commun.* **2008**(40), 4891-4893, DOI: 10.1039/B812769G.
[253]. Ma, Z., S. Dou, A. Shen, L. Tao, L. Dai, and S. Wang, Sulfur-Doped Graphene Derived from Cycled Lithium–Sulfur Batteries as a Metal-Free Electrocatalyst for the Oxygen Reduction Reaction. *Angew. Chem. Int. Ed.* **2015**, *54*(6), 1888-1892, DOI: 10.1002/anie.201410258.
[254]. Puziy, A.M., O.I. Poddubnaya, R.P. Socha, J. Gurgul, and M. Wisniewski, Xps and Nmr Studies of Phosphoric Acid Activated Carbons. *Carbon.* **2008**, *46*(15), 2113-2123, DOI: http://dx.doi.org/10.1016/j.carbon.2008.09.010.
[255]. Burgess, R., C. Buono, P.R. Davies, R.J. Davies, T. Legge, A. Lai, R. Lewis, D.J. Morgan, N. Robinson, and D.J. Willock, The Functionalisation of Graphite Surfaces with Nitric Acid: Identification of Functional Groups and Their Effects on Gold Deposition. *J. Catal.* **2015**, *323*, 10-18, DOI: http://dx.doi.org/10.1016/j.jcat.2014.12.021.
[256]. Cui, W., Q. Liu, N. Cheng, A.M. Asiri, and X. Sun, Activated Carbon Nanotubes: A Highly-Active Metal-Free Electrocatalyst for Hydrogen Evolution Reaction. *Chem. Commun.* **2014**, *50*(66), 9340-9342, DOI: 10.1039/C4CC02713B.
[257]. Gonzalez-Julian, J., P. Miranzo, M.I. Osendi, and M. Belmonte, Carbon Nanotubes Functionalization Process for Developing Ceramic Matrix Nanocomposites. *J. Mater. Chem.* **2011**, *21*(16), 6063-6071, DOI: 10.1039/C0JM03885G.
[258]. White, R.J., N. Yoshizawa, M. Antonietti, and M.-M. Titirici, A Sustainable Synthesis of Nitrogen-Doped Carbon Aerogels. *Green Chemistry.* **2011**, *13*(9), 2428-2434, DOI: 10.1039/C1GC15349H.
[259]. Shinagawa, T., A.T. Garcia-Esparza, and K. Takanabe, Insight on Tafel Slopes from a Microkinetic Analysis of Aqueous Electrocatalysis for Energy Conversion. *Scientific Reports.* **2015**, *5*, 13801, DOI: 10.1038/srep13801.
[260]. Liao, L., J. Zhu, X. Bian, L. Zhu, M.D. Scanlon, H.H. Girault, and B. Liu, Mos2 Formed on Mesoporous Graphene as a Highly Active Catalyst for Hydrogen Evolution. *Adv. Funct. Mater.* **2013**, *23*(42), 5326-5333, DOI: 10.1002/adfm.201300318.
[261]. Xie, J., J. Zhang, S. Li, F. Grote, X. Zhang, H. Zhang, R. Wang, Y. Lei, B. Pan, and Y. Xie, Controllable Disorder Engineering in Oxygen-Incorporated Mos2 Ultrathin Nanosheets for Efficient Hydrogen Evolution. *JACS.* **2013**, *135*(47), 17881-17888, DOI: 10.1021/ja408329q.
[262]. Tran, P.D., M. Nguyen, S.S. Pramana, A. Bhattacharjee, S.Y. Chiam, J. Fize, M.J. Field, V. Artero, L.H. Wong, J. Loo, and J. Barber, Copper Molybdenum Sulfide: A New Efficient Electrocatalyst for Hydrogen Production from Water. *Energy & Environmental Science.* **2012**, *5*(10), 8912-8916, DOI: 10.1039/C2EE22611A.
[263]. Song, C. and J. Zhang, *Electrocatalytic Oxygen Reduction Reaction*, in *Pem Fuel Cell Electrocatalysts and Catalyst Layers: Fundamentals and Applications*, J. Zhang, Editor. **2008**, Springer London: London, 89-134.
[264]. Roche, I., E. Chaînet, M. Chatenet, and J. Vondrák, Carbon-Supported Manganese Oxide Nanoparticles as Electrocatalysts for the Oxygen Reduction Reaction (Orr) in Alkaline

Medium: Physical Characterizations and Orr Mechanism. *The Journal of Physical Chemistry C.* **2007**, *111*(3), 1434-1443, DOI: 10.1021/jp0647986.
[265]. Zhou, L., P. Fu, X. Cai, S. Zhou, and Y. Yuan, Naturally Derived Carbon Nanofibers as Sustainable Electrocatalysts for Microbial Energy Harvesting: A New Application of Spider Silk. *Appl. Catal., B.* **2016**, *188*, 31-38, DOI: http://dx.doi.org/10.1016/j.apcatb.2016.01.063.
[266]. Tian, G.-L., M.-Q. Zhao, D. Yu, X.-Y. Kong, J.-Q. Huang, Q. Zhang, and F. Wei, Nitrogen-Doped Graphene/Carbon Nanotube Hybrids: In Situ Formation on Bifunctional Catalysts and Their Superior Electrocatalytic Activity for Oxygen Evolution/Reduction Reaction. *Small.* **2014**, *10*(11), 2251-2259, DOI: 10.1002/smll.201303715.
[267]. Tian, G.-L., Q. Zhang, B. Zhang, Y.-G. Jin, J.-Q. Huang, D.S. Su, and F. Wei, Toward Full Exposure of "Active Sites": Nanocarbon Electrocatalyst with Surface Enriched Nitrogen for Superior Oxygen Reduction and Evolution Reactivity. *Adv. Funct. Mater.* **2014**, *24*(38), 5956-5961, DOI: 10.1002/adfm.201401264.
[268]. Liu, S., W. Yan, X. Cao, Z. Zhou, and R. Yang, Bacterial-Cellulose-Derived Carbon Nanofiber-Supported Cofe2o4 as Efficient Electrocatalyst for Oxygen Reduction and Evolution Reactions. *Int. J. Hydrogen Energy.* **2016**, *41*(11), 5351-5360, DOI: http://dx.doi.org/10.1016/j.ijhydene.2016.01.121.